



LUND UNIVERSITY

Myocardium at risk. Validation and practical applications

Nordlund, David

2017

Document Version:

Publisher's PDF, also known as Version of record

[Link to publication](#)

Citation for published version (APA):

Nordlund, D. (2017). *Myocardium at risk. Validation and practical applications*. [Doctoral Thesis (compilation), Department of Clinical Sciences, Lund]. Lund University: Faculty of Medicine.

Total number of authors:

1

General rights

Unless other specific re-use rights are stated the following general rights apply:

Copyright and moral rights for the publications made accessible in the public portal are retained by the authors and/or other copyright owners and it is a condition of accessing publications that users recognise and abide by the legal requirements associated with these rights.

- Users may download and print one copy of any publication from the public portal for the purpose of private study or research.
- You may not further distribute the material or use it for any profit-making activity or commercial gain
- You may freely distribute the URL identifying the publication in the public portal

Read more about Creative commons licenses: <https://creativecommons.org/licenses/>

Take down policy

If you believe that this document breaches copyright please contact us providing details, and we will remove access to the work immediately and investigate your claim.

LUND UNIVERSITY

PO Box 117
221 00 Lund
+46 46-222 00 00



Myocardium at risk

Validation and practical applications

DAVID NORDLUND

DEPARTMENT OF CLINICAL PHYSIOLOGY | LUND UNIVERSITY



Myocardium at risk

Validation and practical applications

Myocardium at risk

Validation and practical applications

David Nordlund



LUND
UNIVERSITY

Thesis for the degree of Doctor of Philosophy
Thesis advisors: Prof. Håkan Arheden, Assoc. Prof. Henrik Engblom
Faculty opponent: Dr. Raymond Y. Kwong

To be presented for public criticism in Föreläsningssal 2, Blocket, Skånes
Universitetssjukhus i Lund on Friday, November 3 2017 at 13:00.

Organization LUND UNIVERSITY	Document name DOCTORAL DISSERTATION			
	Date of issue			
	Sponsoring organization			
Author(s) David Nordlund				
Title and subtitle Myocardium at risk - Validation and practical applications				
<p>Abstract</p> <p>Ischemic heart disease is one of the greatest causes of death in the world today. The advent of reperfusion therapy has seen a marked decrease in mortality and new cardioprotective therapies are being researched continuously. To evaluate these therapies, accurate and precise measures of the injured area is necessary.</p> <p>Following occlusion of a coronary artery the area supplied by this artery becomes ischemic and is known as myocardium at risk (MaR). Persisting ischemia leads to myocardial cell death (myocardial infarction) which gradually develops until the entire MaR is infarcted. If reperfusion therapy is applied, however, the infarct progression can be halted and an area of MaR will be saved. This area is known as myocardial salvage and it is an important measure of the efficacy of cardioprotective treatment.</p> <p>Cardiovascular magnetic resonance (CMR) can be used to measure the size of the infarcted area and has, more recently, been used to measure MaR CMR sequences such as T2-STIR and CE-SSFP. There has been a need to evaluate these techniques. Additionally the use of CMR to measure MaR, infarct, and salvage offers potential to investigate coronary supply areas and investigate factors associated with different rates of infarct development. To these ends the following projects have been undertaken:</p> <p>Paper I - Validating the use of CE-SSFP to measure MaR in an experimental model, showing that CE-SSFP can be used to measure MaR with good accuracy and precision over the first 30 min after contrast injection</p> <p>Paper II - Comparing performance of CE-SSFP and T2-STIR to measure MaR in a multi-vendor, multicentre setting. The paper shows that CE-SSFP and T2-STIR provide similar estimates of MaR in images of diagnostic quality and that CE-SSFP had a higher degree of diagnostic images</p> <p>Paper III - Mapping the extent of coronary supply areas in patients after ST-elevation myocardial infarction</p> <p>Paper IV - Testing the association between gender, smoking, hypertension, and diabetes and infarct development in patients after ST-elevation myocardial infarction, showing that female gender is associated with smaller infarcts and higher myocardial salvage.</p>				
Key words: Myocardium at risk, Area at risk, Magnetic resonance, Myocardial ischemia, Cardioprotection, Myocardial infarction				
Classification system and/or index terms (if any):				
Supplementary bibliographical information:		Language English		
ISSN and key title: 1652-8220		ISBN 978-91-7619-528-4		
Recipient's notes	Number of pages	Price		
	Security classification			

Distribution by (name and address)

I, the undersigned, being the copyright owner of the abstract of the above-mentioned dissertation, hereby grant to all reference sources permission to publish and disseminate the abstract of the above-mentioned dissertation.

Signature D. Nordlund

Date 2017-09-06

Myocardium at risk

Validation and practical applications

David Nordlund



LUND
UNIVERSITY

Faculty Opponent

Dr. Raymond Y. Kwong
Brigham and Women's Hospital
Boston, USA

Evaluation Committee

Prof. Tomas Jernberg
Karolinska Institutet
Stockholm, Sweden

Assoc. Prof. Sandra Lindstedt Ingemansson
Lund University
Lund, Sweden

Assoc. Prof. Christoph Varenhorst
Uppsala University
Uppsala, Sweden

Cover: *Ex-vivo* short-axis slice of a porcine heart acquired through CE-SSFP CMR imaging. The hyperenhanced area or myocardium depicts the myocardium at risk after acute ischemia-reperfusion injury.

© David Nordlund 2017

Typeset in L^AT_EX using a template by Berry Holl with modifications from Daniel Carrera

Faculty of Medicine, Department of Clinical Physiology

ISBN: 978-91-7619-528-4 (print)

ISSN: 1652-8220

Printed in Sweden by Media-Tryck, Lund University, Lund 2017



We have not succeeded in answering all our problems, indeed we sometimes feel we have not completely answered any of them. The answers we have found have only served to raise a whole set of new questions. In some ways we feel that we are as confused as ever, but we think we are confused on a higher level and about more important things.

Earl C. Kelley, *The Workshop Way of Learning*

Contents

List of publications	iii
Abstract	v
Populärvetenskaplig sammanfattning	vii
Abbreviations	ix
Acknowledgements	xi

I Research context

1 Introduction	1
1.1 Ischemic heart disease	3
1.2 Ischemia/reperfusion injury	9
1.3 Magnetic resonance imaging	15
1.4 Methods of determining MaR	28
2 Aims	33
3 Materials and methods	35
3.1 Experimental model	35
3.2 Patient data	36
3.3 Magnetic resonance imaging	38
3.4 Coronary angiography	40
3.5 Statistical methods	41
4 Results and discussion	45
4.1 Introduction	45
4.2 CE-SSFP for measuring MaR	45
4.3 Extent of coronary perfusion	49

4.4 The evolution of myocardial infarction	52
5 Conclusions	55
References	57
 II Research papers	
Author contributions	81
Paper I: Experimental validation of contrast-enhanced SSFP cine CMR for quantification of myocardium at risk in acute myocardial infarction	83
Paper II: Multi-vendor, multicentre comparison of contrast-enhanced SSFP and T2-STIR CMR for determining myocardium at risk in ST-elevation myocardial infarction	95
Paper III: Extent of myocardium at risk for left anterior descending artery, right coronary artery, and left circumflex artery occlusion depicted by contrast-enhanced steady state free precession and T2-weighted short tau inversion recovery magnetic resonance imaging	109
Paper IV: Gender but not diabetes, hypertension or smoking affects infarct evolution in ST-elevation myocardial infarction patients - Data from the CHILL-MI, MITOCARE, and SOCCER trials	121

List of publications

- I **Experimental validation of contrast-enhanced SSFP cine CMR for quantification of myocardium at risk in acute myocardial infarction**
D. Nordlund, M. Kanski, R. Jablonowski, S. Koul, D. Erlinge, M. Carlsson, H. Engblom, A. H. Aletras, H. Arheden
Journal of Cardiovascular Magnetic Resonance, 19:12 (2017).

- II **Multi-vendor, multicentre comparison of contrast-enhanced SSFP and T2-STIR CMR for determining myocardium at risk in ST-elevation myocardial infarction**
D. Nordlund, G. Klug, E. Heiberg, S. Koul, T. H. Larsen, P. Hoffmann, B. Metzler, D. Erlinge, D. Atar, A. H. Aletras, M. Carlsson, H. Engblom, H. Arheden
European Heart Journal - Cardiovascular Imaging, 17(7): 744-753 (2016).

- III **Extent of myocardium at risk for left anterior descending artery, right coronary artery, and left circumflex artery occlusion depicted by contrast-enhanced steady state free precession and T2-weighted short tau inversion recovery magnetic resonance imaging**
D. Nordlund, E. Heiberg, M. Carlsson, E-T. Fründ, P. Hoffmann, S. Koul, D. Atar, A. H. Aletras, D. Erlinge, H. Engblom, H. Arheden
Circulation: Cardiovascular Imaging, 9(7), pii: e004376 (2016).

- IV **Gender but not diabetes, hypertension or smoking affects infarct evolution in ST-elevation myocardial infarction patients**
– Data from the CHILL-MI, MITOCARE and SOCCER trials
D. Nordlund, H. Engblom, J-L. Bonnet, H. S. Hansen, D. Atar, D. Erlinge, U. Ekelund, E. Heiberg, M. Carlsson, H. Arheden
Submitted manuscript.

Abstract

Ischemic heart disease is one of the greatest causes of death in the world today. The advent of reperfusion therapy has seen a marked decrease in mortality and new cardioprotective therapies are being researched continuously. To evaluate these therapies, accurate and precise measures of the injured area is necessary. Following occlusion of a coronary artery the area supplied by this artery becomes ischemic and is known as myocardium at risk (MaR). Persisting ischemia leads to myocardial cell death (myocardial infarction) which gradually develops until the entire MaR is infarcted. If reperfusion therapy is applied, however, the infarct progression can be halted and an part of the MaR will be saved. This area is known as myocardial salvage and it is an important measure of the efficacy of cardioprotective treatment. Cardiovascular magnetic resonance (CMR) can be used to measure the size of the infarcted area and has, more recently, been used to measure MaR using CMR sequences such as T2-STIR and CE-SSFP. While T2-STIR has been validated both experimentally and in patients, there has been a lack of experimental validation using CE-SSFP. Also, it has not been known which of the techniques are most suitable for implementation in cardioprotection trials. In addition to evaluating treatment effect, the use of CMR to measure MaR, infarct, and salvage offers potential to investigate coronary supply areas and investigate factors associated with different rates of infarct development. To these ends the following projects have been undertaken:

Paper I - Validating the use of CE-SSFP to measure MaR in an experimental model, showing that CE-SSFP can be used to measure MaR with good accuracy and precision over the first 30 min after contrast injection

Paper II - Comparing performance of CE-SSFP and T2-STIR to measure MaR in a multi-vendor, multicentre setting. The paper shows that CE-SSFP and T2-STIR provide similar estimates of MaR in images of diagnostic quality and that CE-SSFP had a higher degree of diagnostic images

Paper III - Mapping the extent of coronary supply areas in patients after ST-elevation myocardial infarction

Paper IV - Testing the association between gender, smoking, hypertension, and diabetes

versus infarct development in patients after ST-elevation myocardial infarction, showing that female gender is associated with smaller infarcts and higher myocardial salvage.

Populärvetenskaplig sammanfattning

Hjärtattack, hjärtinfarkt och hjärtstopp nämns ofta i sammanhang som handlar om det som kallas ischemisk hjärtsjukdom. Ischemi betyder otillräcklig blodförsörjning, och när det drabbar hjärtat beror det ofta på att det uppstått en propp i ett av kärlen som försörjer hjärtat med blod (kranskärl). Om ischemin får fortgå kommer hjärtmuskel (myokard) gradvis att dö, det vill säga utveckla hjärtinfarkt.

För bara några decennier sedan fanns ingen bra behandling för att rädda hjärtmuskel när ett stopp i kranskärlen uppstod men sedan dess har reperforationsbehandling, då man löser stoppet och släpper på blodflödet igen, revolutionerat vården av dessa patienter och idag kan utvecklingen av infarkt ofta stoppas innan stora hjärtinfarkter uppstått. Det finns dock fortfarande potential att förbättra behandlingen, rädda mer hjärtmuskel och därmed förbättra överlevnaden och välmåendet hos patienter med hjärtinfarkt. För att göra det behövs metoder att kunna mäta och utvärdera dels infarkten och dels det område som hade skadats om ischemin fått fortsätta, det vill säga hur stort det ischemiska området var innan blodförsörjningen återställdes. Det sistnämnda kallas för myokardiellt riskområde, "myocardium at risk (MaR)". Har man information om infarktstorlek och riskområde så kan man räkna ut mängden räddat myokard, "myocardial salvage", vilket används som effektmått i studier som testar effekten av nya behandlingar.

Med magnetisk resonans(MR)-teknik har infarktstorlek kunnat mätas sedan början av 2000-talet. Det har också tagits fram metoder för att mäta riskområde med MR som förenklat bygger på avbildning av ödem (svullnad) i hjärtmuskeln vilket kan mätas upp till en vecka efter hjärtinfarkt. Betänk ett stort skrapår, efter ett tag kommer det att bulta, smärta och svullna upp. Den svullnaden kan sägas motsvara ödemet som uppstår i den del av hjärtmuskel som varit ischemisk och som därmed kan mätas med MR. En av de vanligaste MR-metoderna för att mäta riskområde är T2-STIR medan en nyare metod är CE-SSFP. Det finns utmaningar med T2-STIR som gör att den inte alltid producerar bilder av bra kvalitet där CE-SSFP verkar vara ett lovande alternativ. Därför behövs studier som testar att CE-SSFP verkligen mäter riskområde (delarbete I) samt som jämför prestandan mellan T2-STIR och CE-SSFP (delarbete II).

Att mäta riskområde erbjuder också möjligheter att få kunskap om hur hjärtinfarkt utvecklas och vad som påverkar utvecklingen (delarbete IV) samt att det går att kartlägga områden som varit ischemiska i ett stort antal patienter och därmed se vilka områden som

försörjs av respektive kranskärl (III).

Delarbete I - CE-SSFP testas i en experimentell modell där det visas att CE-SSFP kan användas för att mäta riskområde jämfört med så kallad myokardscintigrafi som referensmetod.

Delarbete II - T2-STIR och CE-SSFP jämförs i en population av ca 200 patienter från olika center i Europa och avbildade med MR-kameror från olika tillverkare. Det visar sig att CE-SSFP producerar bilder av diagnostisk kvalitet i 98% av fall oberoende av vilket center som avbildat patienten eller vilken MR-kamera som använts. T2-STIR däremot producerar bara diagnostiska bilder i 65% av fallen och är beroende av vilket center som skött avbildningen samt av vilken MR-kamera som använts.

Delarbete III - Riskområde och hjärtinfarkt avbildas i ca 200 patienter och används för att kartlägga vilka områden av hjärtmuskel som försörjs av respektive kranskärl.

Delarbete IV - Genom att avbilda riskområde och hjärtinfarkt i ca 300 patienter undersöks hur utvecklingen av hjärtinfarkt sett ut beroende på kön, om patienten röker, om patienten har högt blodtryck och om patienten har diabetes. Delarbetet visar att kvinnor utvecklar mindre hjärtinfarkter än män och att behandlingen har räddat mer myokard hos dem.

Abbreviations

PCI	Percutaneous coronary intervention
CMR	Cardiovascular magnetic resonance
MR	Magnetic resonance
SPECT	Single photon emission computed tomography
MPS	Myocardial perfusion SPECT
MaR	Myocardium at risk
MI	Myocardial infarction
MS	Myocardial salvage
MSI	Myocardial salvage index
LAD	Left anterior descending artery
LCx	Left circumflex artery
RCA	Right coronary artery
PDA	Posterior descending artery
LV	Left ventricle
RV	Right ventricle
STEMI	ST-elevation myocardial infarction
NSTEMI	non-ST-elevation myocardial infarction
ECG	Electrocardiogram
ATP	Adenosine triphosphate
mPTP	Mitochondrial permeability transition pores
RF	Radiofrequency
TE	Echo time
TR	Repetition time
TI	Inversion time
T2-STIR	T2-weighted short tau inversion recovery
SSFP	Steady state free precession
CE-SSFP	Contrast-enhanced SSFP
DTPA	Diethylenetriaminepentaacetic acid
LGE	Late gadolinium enhancement
EGE	Early gadolinium enhancement

Acknowledgements

The process involved in creating this thesis has been rewarding, challenging, and bearable because of the people who were involved, directly or indirectly. For this, I am grateful. Some special words of gratitude go to the following:

Håkan Arheden, for expecting more, not accepting excuses and for treating mistakes like a lesson to learn from. Barring my parents, no other person has provoked as many new thoughts in me, and for this I am grateful. **Henrik Engblom**, I found the cardiac MR group after one of your lectures and you have been a role-model in showing joy, competence, and humility in what you do. **Anthony Aletras**, for being a patient and great teacher.

Joey Ubachs for introducing me to experimental science, **Mikael Kanski** for being the most dependable person i know, **Robert Jablonowski** for always putting in extra effort, **Sascha Kopic** for honesty with a side of sarcastic humour, **Sebastian Bidhult** for never saying no (though sometimes you should!), **Christos Xanthis** for showing character through frustration and happiness alike, and **Sasha Koul** for teaching me interventional procedures and some things about classical music. Thank you all for long days and nights of experiments, they have been extraordinary and unforgettable. Thank you also **David Erlinge** for making it possible for me to be part of the current experimental model.

Thank you **Marcus Carlsson** for showing me there can be joy in efficiency and completing tasks and **Einar Heiberg**, for being genuinely excited about most projects brought to your attention.

Per Arvidsson, for discussing life, cardiac physiology and for showing me how to write a thesis. **Ellen Ostenfeld** for expertly navigating conferences and for dancing. **Tom Gyllenhammar** for wild ideas and a willingness to share them. **Felicia Seemann** for pumpkins, gossip, and for tolerating the clutter on my desk. **Pia Sjöberg**, for having the lowest "tönt-faktor" of anyone I've encountered. Thank you and the rest of the **cardiac MR group** for making research a team sport.

Kerstin Brauer and **Karin Larsson**, for preventing and solving problems. I imagine getting to a PhD without you would be considerably different and much more difficult. Thank you to the **technologists** involved in MR-research, for investing personally in each project and going beyond what is required of you.

Thank you to all the **colleagues** working at the department of Clinical Physiology in Lund who are creating the best work environment I have ever experienced, inside or outside the hospital. **Bo Hedén** and **Henrik Mosén**, you always made time for questions. **Christina Christoffersen** and **Carina Ljungberg**, you cared and gave feedback. **Jonas Jögi**, you have always been straight with me and others.

For all **students** going through the department, in PBL-groups, and in lectures. It has been a privilege to teach and be taught with you. Going into research I wanted to teach and it turned out to be more rewarding than I had imagined.

Thank you **Syntach**, the researchers at the **department of Cardiology** in Lund, and other collaborators over the years.

I am grateful to all friends who have remained through the writing of this thesis. A special thanks to **Mia Stiernman** who lent her artistic skills to the creation of the illustration of coronary anatomy in the introduction chapter. Thank you **Anna Saarvanto** for sharing in this part of my life.

Thank you **Thomas Nordlund**, for being curious about life, reality, and how everything comes together and for sharing your thoughts despite occasional stubborn resistance. **Karin Nordlund**, for always putting family first and for transitioning from a mother into a friend.

Lund, 13 September 2017

Part I

Research context

Chapter 1

Introduction

This organ deserves to be styled the starting point of life and the sun of our microcosm just as much as the sun deserves to be styled the heart of the world. For it is by the hearts' vigorous beat that the blood is moved, perfected, activated, and protected from injury and coagulation.

W. Harvey, *De Motu Cordis*, 1628

Translation by Kenneth J. Franklin

The cell is the common denominator for life as we know it. Cells can reproduce and perform a number of different tasks which increase in complexity when more cells are added to an organism, thus providing the means for life-forms such as humans to evolve. A prerequisite to supporting an organism as large and complicated as a human is the ability to transport nutrients and oxygen into close enough proximity of the cell to allow for uptake by means of diffusion or active transport over the cell membrane. Most cells need to be within tens of micrometers from the closest blood vessel to sustain life [1]. Our circulatory system can be seen as an elegant solution to this challenge which, in its most elementary parts, consists of a pump which circulates blood through vessels to pick up the nutrients and oxygen and deliver them to the tissues of the body [2].

The human heart does not only deliver blood to the rest of the body but also sustains itself by pumping blood via the aorta into the coronary arteries. **Myocardial ischemia** is an inability to supply the heart with enough blood to cover the demand and, if severe and prolonged enough, inevitably leads to cell death which is commonly referred to as myocardial infarction. While a greater demand of blood may certainly cause or worsen ischemia, ischemic heart disease is usually associated with impaired supply. In fact, myocardial ischemia and infarction was probably first understood as a consequence of investigating coronary arteries and finding that they can narrow or even become occluded, thus decreasing the supply of blood to the heart. In this, as in so much else, Leonardo da Vinci was a pioneer who is responsible for the first known account of coronary artery disease. From the writings of da Vinci as translated in Keele 1973 [3]:

“And this old man, a few hours before his death told me that he had lived one hundred years and that he did not feel any bodily ailment other than weakness; and thus while sitting on a bed in the hospital of Santa Maria Nuova at Florence, without any movement or sign of anything amiss he passed from this life. And I made an anatomy in order to see the cause of so sweet a death which I found to proceed from debility through lack of blood and failure of the artery which feeds the heart and the other lower organs, which I found to be very dried, shrunken and withered”

Later, in the 18th century and after much work by key individuals such as William Harvey, Friedrich Hoffmann, and Giovanni Morgagni, Edward Jenner wrote to his teacher William Heberden about an autopsy after a case of sudden death.

“...a kind of firm, fleshy tube, formed within the vessel, with a considerable quantity of ossific matter dispersed irregularly through it. This tube did not appear to have any vascular connection with the coats of the artery, but seemed to lie merely in simple contact with it.” [4]

This autopsy revealed what today may be understood as an arterial thrombus having occluded a coronary artery that had been “ossified” by atherosclerosis and caused the death of the patient via myocardial ischemia.

It would take until the later part of the 20th century for treatments that would remove the offending occlusion to appear with the advent of thrombolytic therapy and percutaneous transluminal coronary angioplasty, also commonly referred to as percutaneous coronary intervention (PCI) [5, 6]. With reperfusion strategies available the situation for these patients changed drastically as mortality numbers plummeted [7–9]. It also, however, brought with it a clinical conundrum hitherto not researched. It became apparent that opening a previously occluded vessel and thus reperfusing ischemic myocardium brought danger in the form of arrhythmias and possibly increased upon the already established injury of the myocardium [10, 11]. The term **reperfusion injury** was coined and great amount of research resources has since been devoted to decreasing reperfusion injury with, as of yet, limited success [12–21]. It is worth noting here that, as the development of myocardial infarction in ischemic myocardium is happening over a relatively short time span and that reperfusion therapy is urgently applied in patients, the separation of what is injured due to the original ischemic period or from reperfusion is not easily performed. Therefore, as we shall see, it is more common to measure and refer to the combined effects of ischemia-reperfusion injury.

In parallel to the expanding use of reperfusion therapy, the field of magnetic resonance imaging began to appear based on discoveries such as tissue relaxation constants by Odeblad and Lindström, spin echoes by Erwin Hahn, and the utilization of magnetic field gradients for spatial localization attributed to Paul Lauterbur [22–24]. Magnetic resonance imaging of the heart, henceforth referred to as **cardiovascular magnetic resonance imaging** (CMR),

allowed for characterization of the cardiac muscle *in-vivo* in a manner that was unparalleled by any other technique. Recall that the discussion on ischemic heart disease so far has concerned examining the coronary arteries and that while autopsy has long been available it does not lend itself to studies of *in-vivo* pathophysiology.

Of particular interest with regards to ischemia-reperfusion injury, CMR techniques were shown to accurately depict irreversibly damaged myocardium [25]. Additionally, earlier studies had looked at myocardial edema following myocardial ischemia [26]. The study of myocardial edema led to the development of techniques to quantify the extent of edema in patients who had suffered myocardial ischemia and then been subjected to reperfusion therapy. The edematous area was shown to closely agree with the area of myocardium that had been ischemic [27–29]. This meant that there was a way to measure not only the size of the actually infarcted myocardium but also the size of the ischemic myocardium that would inevitably have become infarcted if reperfusion therapy had not occurred, so called **myocardium at risk** (MaR), and that this could be done in the relatively tranquil period after the culprit occlusion had been removed.

The difference between myocardial infarct size and MaR is myocardial salvage. This new measure, often normalized to MaR which results in myocardial salvage index (MSI), could now be used to evaluate the efficacy of therapies to minimize myocardial infarct size. One of the main focuses for therapies such as these are, as previously alluded to, to reduce reperfusion injury. Two of the studies testing such therapies, MITOCARE and CHILL-MI, provided the patient data used in this thesis along with patients from the SOCCER trial which tested the effect of oxygen therapy on MSI after myocardial infarction. Apart from providing a measure on the efficacy of therapy, measuring MaR can offer pathophysiological insights in its own right. For example, Paper III of this thesis utilizes the fact that MaR is a reflection of the distribution area of the occluded culprit artery in patients reperfused following myocardial ischemia while Paper IV looks at the factors affecting development of infarction based on its relation to myocardium at risk.

This thesis concerns quantification of MaR in ischemic heart disease by using CMR techniques and applying those techniques to better understand the coronary artery distribution areas and to find which factors affect the development of myocardial infarction.

1.1 Ischemic heart disease

Understanding MaR and its implications requires understanding the underlying disease, here referred to as ischemic heart disease. This section will seek to introduce definitions and subclassifications pertaining to ischemic heart disease and to discuss its' pathophysiology and relevant anatomy.

1.1.1 Definitions

Ischemia refers to an inadequate blood supply to an organ or part of the body. Inadequate blood supply to the heart could stem from a systemically decreased blood supply, such as from bleeding or cardiogenic shock, but is most commonly discussed in the context of decreased flow in one or several parts of the coronary circulation. In this thesis the term ischemic heart disease is limited to ischemia caused by an obstruction of flow through the coronary arteries.

Myocardial cell death is called **myocardial infarction** (MI) which usually refers to injury due to prolonged myocardial ischemia [30]. All myocardium does not become infarcted instantaneously when subjected to ischemia, it is rather a process that can be interrupted by reperfusion (Figure 1.1). Myocardium which is saved by reperfusion therapy is termed **myocardial salvage** (MS, Equation 1.1) while the entirety of the area that was ischemic is referred to as the **myocardium at risk** (MaR).

$$MaR = MI + MS \quad (1.1)$$

In studies, myocardial salvage is often normalized to myocardium at risk to calculate **myocardial salvage index** (MSI, Equation 1.2).

$$MSI = \frac{MS}{MaR} \quad (1.2)$$

1.1.2 Epicardial disease and presentation

Coronary blood flow can either be reduced due to an incomplete blockage of the epicardial coronary artery (coronary stenosis) or it can be halted due to a complete blockage (coronary occlusion). Coronary stenosis is thought to be the result of progressive atherosclerosis starting with thickening of the vessel intima and progressing into fibroatheromas with necrotic cores [31]. At any point in this progression, when coronary flow is insufficient to meet increasing demand, symptoms such as chest pain or dyspnea during exertion may appear and progress with the atherosclerotic lesion. The current understanding of occlusive lesions is that a thrombus suddenly develops [32]. The thrombus is commonly catalyzed by either rupture of a plaque which exposes the thrombogenic core, or by erosion of vessel endothelium exposing the intima and thus triggering thrombocyte aggregation [31, 33, 34]. The degree to which a plaque obstructs blood flow has little bearing on the risk of rupture or erosion which means it is entirely possible, and even common, for coronary occlusion to occur without preceding symptoms [35, 36]. The acute symptoms of coronary occlusion include acute persisting chest pain, dyspnea, unconsciousness and sudden death.

1.1.3 Coronary anatomy

This text will be limited to describing the most common coronary artery layouts. Please refer to Figure 1.2 for visualization.

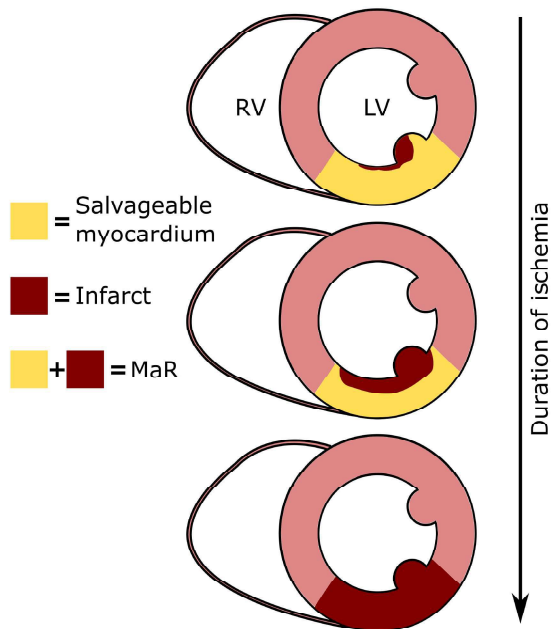


Figure 1.1: Showing the subendocardial to transmural development of infarct due to prolonged myocardial ischemia, also known as the wavefront phenomenon. Myocardium shown in yellow is potentially salvageable by reperfusion. If that were to happen it would be known as myocardial salvage. Dark red myocardium is irreversibly injured. LV=left ventricle, RV=right ventricle

The location of myocardial ischemia is often categorized by which epicardial vessel is affected where the left anterior descending artery (LAD), left circumflex artery (LCx), and right coronary artery (RCA) are the ones most commonly specified. The left coronary artery, also referred to as the left main, is in the majority of cases present to branch into the LAD and LCx after arising from the left anterior sinus of Valsalva in the aorta [37]. The LAD courses through the anterior interventricular groove to supply the anterior aspect of the left ventricle and terminates before, at, or after wrapping around the apex. Thereby it sometimes supplies part of the territory usually attributed to the posterior descending artery (PDA) [38]. The two main types of branches of the LAD are (1) diagonals which travel laterally along the epicardial surface of the left ventricle with the first diagonal being the most proximal to the LAD origin, and (2) septal branches which penetrates into the septal myocardium to supply the anterior interventricular septum. The LCx initially runs in the left atrioventricular groove around the lateral aspect of the heart towards *crux cordis*. If the LCx supplies the PDA the variant is known as a left-dominant system, if it supplies a posterolateral branch but not the PDA the variant is known as a co-dominant system and otherwise it is known as a right-dominant system. Branches arising from the LCx and supplying the left ventricle are termed marginals where the first margin is the one most proximal to the LCx origin. The LCx also supplies part of the left atrium and not infrequently the sinus node [39]. The RCA, instead, arises from the right anterior sinus of Valsalva and travels through the right atrioventricular groove to run around the right ventricle and frequently to supply the PDA. Similar to the branches of the LCx, the early branches of the RCA are called marginals and they supply the lateral wall of the right ventricle. The atrioventricular node, and to a lesser degree the sinus node, is also commonly supplied by the RCA [39].

1.1.4 Infarct development

It has been shown that sustained myocardial ischemia in dogs will progress into myocardial infarction which starts at the endocardial surface and spreads towards the epicardium. This is called the wavefront phenomenon of ischemic cell death (Figure 1.1) [40, 41]. The effect is thought to result from the epicardial to endocardial direction of blood flow in collateral vessels. As intramyocardial tension is highest in the subendocardial myocardium the collaterals are unable to supply these parts to the same degree as the subepicardial myocardium [42]. The subepicardial-subendocardial difference could be further accentuated since it seems that the subendocardium consumes more energy than the subepicardium, possibly due to the increased intramyocardial tension [43]. It should be noted that while the wavefront phenomenon is found in dogs it was not found in a sheep model where it was speculated that the collateral-deficient hearts of sheep would be more similar to humans [44]. Experience from pig experiments also tells us that they do not regularly develop infarct according to the wavefront phenomenon. Clinical experience in humans seems consistent with the wavefront pattern which is corroborated in a small study by Hedström *et*

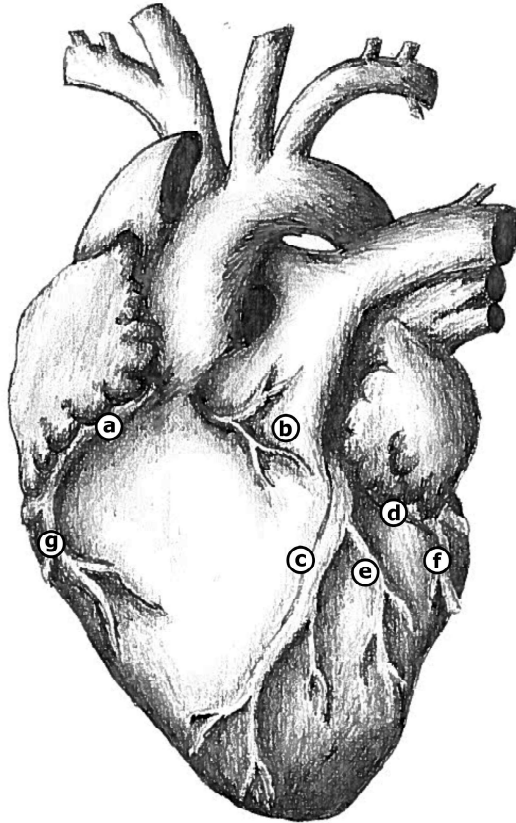


Figure 1.2: Coronary anatomy. a: the right coronary artery (RCA) running in the right atrioventricular groove, b: the position of the left coronary artery hidden behind the pulmonary trunk, c: the left anterior descending artery (LAD) running through the anterior interventricular groove, d: the left circumflex artery (LCx) running in the left atrioventricular groove, e: the first diagonal of the LAD (D1), f: a marginal of the LCx, g: a marginal of the RCA. Drawing provided by courtesy of dr. Mia Stiernman.

al. [45].

The time-scale over which acute myocardial infarction develops has been the subject of some controversy. Early data from dogs showed that it takes an average of 180 minutes for 50% of MaR to become infarcted after acute coronary occlusion, while for pigs and rats the development was substantially quicker at around 40 minutes [46–51]. In 2009 Hedström *et al.* published a study on human patients admitted for acute ST-elevation myocardial infarction (STEMI). Myocardium at risk was measured using myocardial perfusion SPECT (MPS) and myocardial infarct size was measured using CMR. They found that in a highly selected, previously healthy population with coronary occlusion of a single vessel and no visible collaterals, the time for 50% of MaR to become infarcted was 290 minutes from pain onset [45]. In interpreting this result one should remember that most patient populations are not as selected. In other populations there is not always a good correlation between the duration of pain and infarct size, even for populations of exclusively STEMI-patients. This could be because of sometimes incomplete occlusion, collateral flow, or intermittent brief bouts of reperfusion during ischemia. Thus, it is reasonable to suspect that for most patient populations infarct would develop at a slower rate [52]. The difference in rate of infarct development seen between the species could at least partly be attributed to a difference in how well-developed the coronary collateral circulation is [53].

1.1.5 Subclassification

One of the first tests used when myocardial ischemia is suspected is the electrocardiogram (ECG), due to its' accessibility and ability to determine if immediate interventional treatment is appropriate [32, 54–56]. It should therefore not come as a surprise that one of the major subclassifications of ischemic heart disease is based on the ECG.

- **ST-elevation myocardial infarction (STEMI)** is so called because it is seen as a relative "rise" in the ST-segment of the ECG. ST-elevation is a sign of transmural myocardial ischemia caused by coronary occlusion. This will cause myocardial infarction to develop over time unless flow is restored, either spontaneously or by intervention [57].
- **Non ST-elevation myocardial infarction (NSTEMI)** is defined as ischemic myocardial cell death in the absence of ST-elevation on the ECG. Naturally this definition contains a broad spectrum of conditions ranging from small injuries without any ongoing ischemia to severe ischemia [58].
- Myocardial ischemia which causes symptoms but not cell death is termed either stable or unstable angina. Clinically, the difference between angina and NSTEMI is often based on a blood sample showing whether there are markers of cell death in the blood while the difference between stable or unstable angina is based on the character of the symptoms [58].

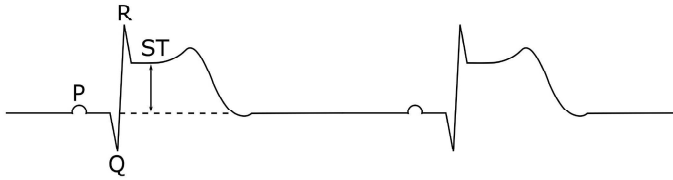


Figure 1.3: ECG showing ST-elevation, a sign of transmural myocardial ischemia.

As STEMI is a clearly defined group compared to NSTEMI, stable angina, and unstable angina it lends itself well to studies aiming to understand what we see using CMR. The patient data in this thesis comes from patients in the STEMI group while the experimental setup used could arguably be said to mimic the STEMI situation.

1.2 Ischemia/reperfusion injury

Where the previous section discussed the macroscopic events of ischemic heart disease the following section will seek to summarize some of what is known about the pathophysiology of ischemia/reperfusion injury on a cellular level, starting with a cursory overview of normal cellular respiration.

1.2.1 Normal physiology of cellular respiration

Consider a collection of cells supplied by an artery. The cells will, among other things, take up glucose and oxygen from the blood while metabolic rest products will be exported from the cells via the blood (Figure 1.4). Glucose is broken down in the cell plasma through glycolysis to generate pyruvate and a small amount of adenosine tri-phosphate (ATP), a molecule which is used to fuel energy demanding processes in the cell [59]. Pyruvate is then metabolised to generate NADH and acetyl coenzyme A which in turn is metabolized in the process known as Krebs's cycle into more NADH as well as an additional small amount of ATP [60, 61]. The main production of ATP, however, happens in the mitochondria, whereby NADH via the proton it carries causes the generation of a proton gradient over the mitochondrial inner membrane which in turn fuels the generation of ATP by passive movement of protons along this gradient. This is a process known as the mitochondrial electron transport chain and it is key to the following discussion that the electron transport chain requires oxygen to generate a proton gradient [62, 63]. It is also worth noting that the proton gradient drives not only the passive movement of protons but also affects the movement of strong anions such as sodium, potassium, calcium and chloride over the mitochondrial membranes.

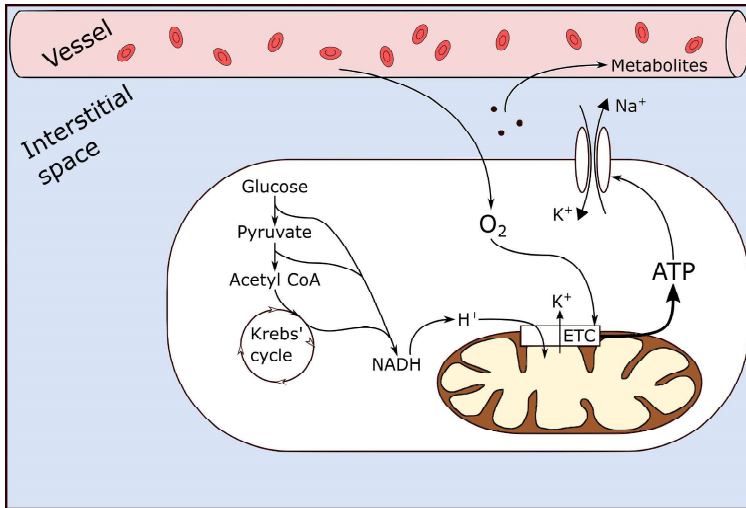


Figure 1.4: Showing the metabolism of a cardiomyocyte supplied by a blood vessel. Glucose is metabolized through a series of steps resulting in NADH which provides the process known as the electron transport chain (ETC) with protons (H^+). The ETC also requires oxygen and is the main source of ATP in the cardiomyocyte. ATP in turn is used to fuel the Na^+/K^+ antiporters.

1.2.2 Ischemia

A sudden occlusion of the artery will suspend the cellular functions described in the previous section and cause compensatory mechanisms to be activated (Figure 1.5). Oxygen will no longer be available and thus the electron transport chain is discontinued and can no longer uphold the proton gradient over the mitochondrial membrane [64]. As a consequence ATP production is impaired leading to a cell-wide deficiency in available energy, eventually accentuated by a depletion of the available glycogen deposits [64, 65]. Additionally, data suggests that the loss of the proton gradient shifts the balance of potassium/proton antiporters towards an influx of potassium into the mitochondrial matrix, causing net movement of water and thus swelling of the mitochondria, initially at the expense of cristae which would then shrink, and eventually by expanding the outer membrane [66–68]. This occurs as mitochondrial permeability transition pores (mPTP) are opening in the inner mitochondrial membrane which intensifies the influx of ions and may trigger oncosis [69]. The swelling is associated with release of cytochrome c, a substance involved in apoptotic/oncotic cell death, and may thus play a part in the eventual ischemic demise of the cell though there is some controversy surrounding the causality of cytochrome c and swelling [67, 70, 71]. On the other hand, there is data to suggest that potassium influx into the mitochondrial matrix may be cardioprotective which lends itself to speculation that maybe some degree of swelling could be functional in the ischemia-reperfusion situation [72].

As discussed, ischemia causes a decrease in the ATP-production of the mitochondria. From this follows that the protons, carried as NADH, that were being utilized in the electron transport chain start accumulating in the plasma [73]. A shift in the metabolism of glucose and glycogen to lactate instead of pyruvate mitigates the resulting acidosis but the result is still a net decrease in ATP production as well as intracellular acidosis [74]. In the cardiomyocyte, ATP is crucial for muscle relaxation and to fuel the sodium/potassium antiporters sustaining the polarization over the cell membrane, both directly and by driving other membrane transporters. The ischemic cell is therefore unable to uphold electrical stability and it will accumulate strong ions, maybe most importantly sodium and chloride, to thus shift the osmotic gradient more into the cell [75]. This shift is further accentuated by transporters which compensate the intracellular acidosis such as the sodium/proton antiporter and sodium/bicarbonate cotransporter, both of which will shift the sodium balance into the cell [76–78].

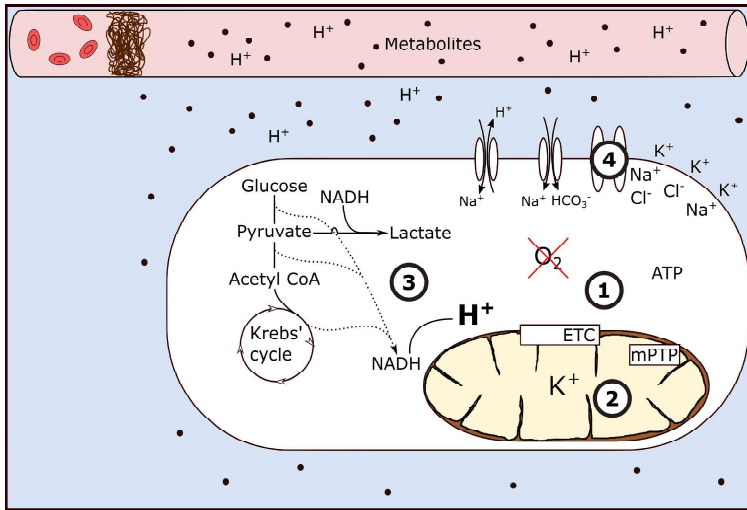


Figure 1.5: Cell metabolism during coronary occlusion. (1) Oxygen is no longer available, the electron transport chain (ETC) is discontinued and as a result far less energy/ATP is available. (2) Increased K^+ concentration in the mitochondria and opening of mitochondrial permeability transition pores (mPTP) initially causes swelling of the mitochondrial matrix and eventually the outer membrane. (3) Intracellular H^+ concentration increases as H^+ is no longer used in the ETC. This effect is mitigated by a shift in metabolism toward lactate. (4) The lack of ATP disrupts the activity of Na^+/K^+ antiporters and the increased H^+ concentration causes activation of transporters such as the Na^+/H^+ antiporter and the Na^+/HCO_3^- cotransporter. Overall Na^+ and Cl^- accumulates in the cell.

1.2.3 Reperfusion

During myocardial ischemia due to coronary occlusion the ischemic area is effectively cut off from the rest of the circulation. Suddenly restoring coronary flow, for example by revascularization therapy, can therefore be a dramatic event where the conditions for the previously ischemic cells change rapidly (Figure 1.6) [79]. This is further accentuated by the effect known as reactive hyperemia referring to that blood flow increases to more than baseline levels for several minutes following ischemia-reperfusion [80–82]. The mechanism for this is incompletely understood but involves regulation of substances such as adrenaline, ADP and ATP, adenosine, substance P, and bradykinin [83–86]. The hyperemic reperfusion is a mechanical stressor on the myocardial tissue and on the blood vessel walls. This likely contributes to hemorrhage in myocardial infarction, where the vessel walls are already injured by ischemia [87]. It also increases the hydrostatic pressure in the capillaries, favouring movement of water into the interstitial space [88].

During ischemia, the metabolites created in the myocytes diffuse into both the interstitial and intravascular spaces and thereby equilibrate the osmotic gradient over these membranes. Come reperfusion the hyperosmotic solution in the blood vessel is flushed away by isotonic blood, causing an osmotic gradient into the interstitial space and the intracellular space, further accentuating swelling of the cell [79, 89]. The movement of water across the vascular endothelium is thought to be facilitated by an increased capillary permeability due to endothelial damage caused by the ischemia/reperfusion injury [90]. Also, movement of water into myocytes is possibly increased by up-regulation of channels such as aquaporins, connexins, and pannexins [79, 91–93]. Restoration of physiological pH outside of the myocytes also cause the compensatory mechanisms previously mentioned to accentuate the movement of sodium into the cell, thus exacerbating cell swelling. In the mitochondria, ischemia causes the cessation of the electron transport chain which creates a pent up potential for creation of oxygen free radicals come restoration of blood flow. This in combination with an inflow of calcium into the mitochondria may stimulate further opening of mPTP which decreases mitochondrial function and facilitates swelling [64, 69, 70, 94].

In conclusion, there is a mechanical stress and an osmotic stress on the reperfused myocardium which may activate cell death by oncosis. In addition to the already mentioned mechanisms there has also been data suggesting that calcium overload, and inflammatory response through neutrophil activation could play a role in reperfusion injury by, for example, causing endothelial damage, impairing perfusion, and activating apoptotic/oncotic pathways [95–97].

1.2.4 Myocardial edema

As the previous discussion on ischemia/reperfusion injury alluded to, it seems that during ischemia there is an increase in intracellular space due to mitochondrial swelling, and an increase in cell plasma [65, 79]. Since the ischemic area is not connected to the circulation this swelling of myocytes needs to happen at the expense of interstitial space [89]. After

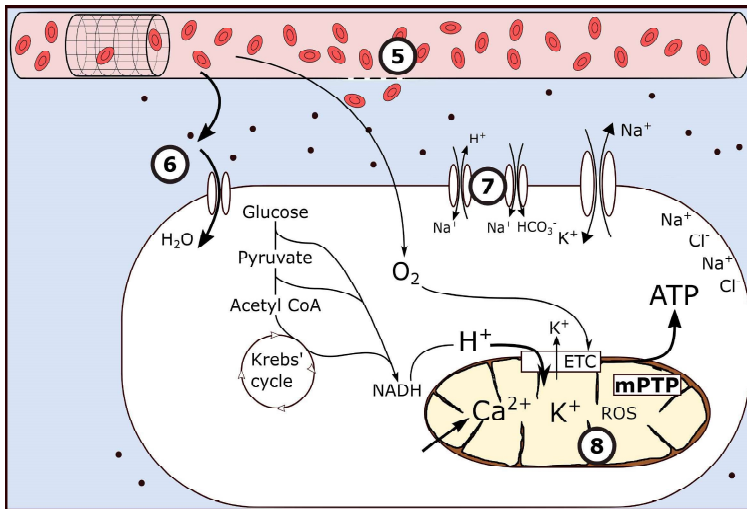


Figure 1.6: Effects of acute reperfusion. (5) Reactive hyperemia and endothelial damage contribute to movement of plasma into the interstitial space and to hemorrhage. (6) Flush-out of metabolites cause an osmotic gradient into the interstitium and further into the cell. Movement of plasma into the cell is facilitated by up-regulation of channels such as aquaporins, connexins, and pannexins. (7) Sudden restoration of extracellular pH causes an increased H⁺ gradient which in turn increases transport of sodium into the cell. (8) Sudden return of oxygen increases creation of reactive oxygen species (ROS) to supernormal levels. Along with an influx of Ca²⁺, this further causes opening of mPTP.

reperfusion, however, it seems that not only swelling of the myocytes but also interstitial edema plays a part in myocardial injury [89, 98, 99]. Indeed data shows that the extracellular volume of myocardium is increased following reperfusion, both in infarcted regions and non-infarcted regions [46, 100, 101]. The increase is greatest in infarcted regions which is explained by a breakdown of cellular membranes to create space where there were cells previously [100]. In the non-infarcted regions, salvaged by reperfusion, most cells are intact and the increase in extracellular volume can instead be attributed mainly to interstitial edema [46]. Apart from possibly playing a role in reperfusion injury, myocardial edema may negatively affect systolic and diastolic function of the myocardium, may impair perfusion of the myocardium, and could cause electrical instability of the heart [98, 102, 103]. All of these effects make it a potential target for treatment or prevention, something that has been studied in the context of cardioplegia for thoracic surgery as well as experimentally but where there currently seems to be a lack of patient data for epicardial coronary artery occlusion/reperfusion [104–106].

1.2.5 Cell death

The subject of cell death in general is incompletely understood and there seems to be many different mechanisms and variations causing cell death who often have common denominators. Ischemic cell death is relatively extensively researched and the pathways of importance are often divided into three categories (1) oncosis, (2) apoptosis, and (3) autophagy [107–109]. The historic background for the division between the first two is in the microscopic appearance where oncosis is associated with swelling of the cell and apoptosis with cell shrinkage [110]. Apoptosis has been called programmed cell death, a felicitous name since in many ways it seems to result in a more ordered, albeit ATP-dependent, destruction of the cell through several defined pathways [111]. One of these pathways includes making the mitochondrial membranes permeable to cytochrome c which can then combine with factors in the cell plasma to form an apoptosome. The apoptosome then triggers caspases that, through several steps, cause DNA in the cell nucleus to fragment [112, 113]. Oncosis, on the other hand, is associated with an ATP-depleted state and bears connotations of a less ordered process in that it has been associated with more inflammation and could be the result of more severe ischemia. Like apoptosis, oncosis is associated with an increased mitochondrial membrane permeability, in this case mediated by opening of mPTP, but is not associated with release of cytochrome c. Thus, instead of activating the apoptotic pathway, the resulting loss of membrane integrity causes mitochondria and the cell to swell (see the sections on ischemia and reperfusion) without fragmentation of the nucleus DNA. One way of interpreting the resulting cell death is that the cells “burst” from the oncotic pressure, keeping in mind though that the mechanism is still not fully elucidated. True to its perhaps less ordered nature, oncosis has been associated with higher degrees of inflammation than apoptosis though widespread apoptosis has also been shown to attract inflammatory cells [114–116]. Autophagy is a more recent discovery wherein organelles and proteins are in-

cluded into vacuoles and fused with lysosomes which degrades the contents of the resulting autophagolysosome and could cause cell death. It may have a modulating role on ischemic injury and could promote survival of hibernating myocardium [117].

1.3 Magnetic resonance imaging

As Magnetic resonance (MR) imaging of the heart is used throughout all projects of the thesis this section will introduce a simplified model of understanding the method and seek to provide a background to the discussions that follow in the separate projects.

1.3.1 Introduction

Figure 1.7 shows an image of a corn cob acquired through MR imaging. For us to be able to correctly interpret this image as a cob of corn we need to identify defining attributes such as the stem and the corn. In order to do so there is some information that needs to be conveyed through the image.

- **Contrast** - In order to identify different tissue types there needs to be a difference in intensities between them, such as the difference in intensity between surrounding air and corn in Figure 1.7. Contrast in MR images is acquired through differences in how much "signal" tissues generate and understanding the generation of contrast thus comes down to understanding how signal is generated.
- **Location in-plane** - The image needs to provide information on where the attributes of the imaged object are in relation to each other. Imagine the image of the cob of corn where all the corn is scattered randomly across the image and this becomes apparent.
- **Location through-plane** - Not shown in Figure 1.7 per se is the fact that the two-dimensional image we see was selected from a three-dimensional volume and there therefore needs to be a way to determine location in the through-plane as well as in the two-dimensional plane.

The following explanation will begin by examining generation of signal, and thus contrast, to then delve into how information on in-plane and through-plane location is acquired. After this, CMR imaging will be specifically addressed.

1.3.2 Signal generation

A proton can be considered to have a property called spin, observed by the magnetic moment it induces [118]. For our purposes this could be said to turn some of the protons in a cob of corn (or indeed in a human body) into small magnets. Normally, the poles of these small magnets would be randomly directed in space and would thus, on a big scale,

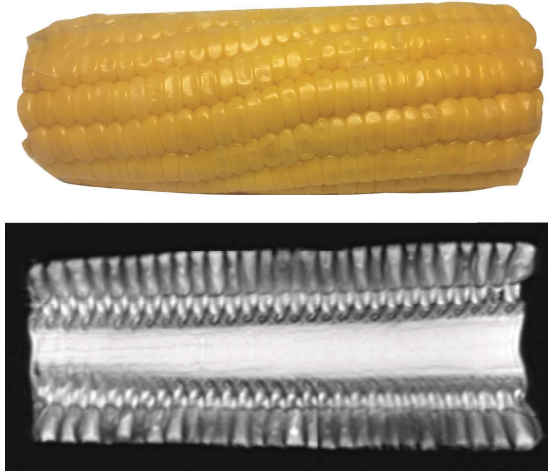


Figure 1.7: A photo of a cob of corn (above) and an MRI image of the same cob (below).

cancel each other out. If the cob were to be put inside a strong magnetic field (B_0), such as in an MR scanner for example, it would introduce a bias in the direction of the small magnets along the B_0 as they would start to precess around B_0 . This bias causes coherence in the given direction and the resulting vector will be used to generate signal. There is a challenge in measuring this vector however, the strength of the magnetic vector in the cob of corn is only a small fraction of B_0 . Therefore, a second magnetic field (B_1) is added for a short amount of time which turns the resultant vector of magnetization at an angle from B_0 thus allowing the measurement of magnetization in a direction where B_0 does not interfere [119]. Applying B_1 causes spins to precesses around this new magnetic field. Thus a B_1 applied along the y-axis will cause magnetization to "flip" towards the x-axis.

B_1 is always played out at a certain frequency for any given nucleus, dependent on the strength of the B_0 . This is because it turns out that precession happens at a rate that is dependent on the magnetic field which causes it, according to Equation (1.3) where w is the rate of precession, γ denotes inherent properties of the protons and B_0 the strength of the magnetic field.

$$w = \gamma * B_0 \quad (1.3)$$

Thus, in order to affect the direction of the magnetization vector, B_1 needs to be played out at the frequency that the precession around B_0 happens. This frequency is called the Larmor frequency and Equation (1.3) is called the Larmor equation after Joseph Larmor [120]. As the Larmor frequency at the field strengths regularly used in MR imaging are within the radiofrequency (RF) spectrum ($3 * 10^3$ to $3 * 10^{11}$ Hz), the B_1 pulses applied are termed RF pulses.

Frame of reference

Imagine the MR scanner as consisting of a tube along which there is a magnetic field, B_0 . The axis of B_0 will be called z . Further imagine there are sensors perpendicular to this field that sense the component of magnetization aimed towards them. These sensors exist in the x -, and y -axes. As the magnetization vector is always precessing about B_0 it will always be rotating on the xy -plane after excitation by B_1 , thus giving rise to an oscillating sinusoidal waveform pattern of signal (Figure 1.8). For simplicity, we introduce the rotating frame where the xy -plane rotates at the Larmor frequency and thus "keeps pace" with the rotating magnetization vector making it appear still (Figure 1.8). In the rest of this thesis reference will be made to z' , x' , and y' which denote the z , x , and y axes in the rotating frame. The direction of the RF-pulse will be defined as x' and thus the direction along which the magnetization vector 'flips' will be y' .

1.3.3 Phase

Before going into magnetization relaxation and spatial encoding it will be important to consider the concept of phase. A magnetization vector has two basic properties, magnitude and direction. As signal is measured in the $x'y'$ plane the angle of magnetization in this plane will affect signal and is known as phase. Additionally spins can be described as being in phase, resulting in higher amplitude of the signal, or out of phase, resulting in lower amplitude of the signal.

Frequency is a closely related concept to phase which can be described as the rate of phase change. This becomes important when discussing spatial encoding as the information about the phase of magnetization can be used in parallel to information about the frequency of precession.

T_1 and T_2

The previous sections can be summarized in that we have a magnetic field, B_0 , which results in a magnetization vector along the z' axis, by affecting protons in the tissue we are interested in, that can then be brought to the y' -plane by playing a RF-pulse along the x' -plane. The resulting transversal magnetization can be measured as voltage which constitutes the MR signal. We shall now consider what happens over time after the RF-pulse flips the magnetization to the y' -axis, namely two things. (1) the magnetization along the y' starts to decay, and (2) the magnetization along z' starts to recover (Figure 1.9).

Magnetization decay is happening due to so called spin-spin interactions, where the spin properties of the protons interact, and because of small inhomogeneities in the magnetic field [119]. Both these effects affect the rate and phase of precession and therefore decrease coherence which in turn decreases the signal. While spin-spin interactions reflect properties of the tissue, magnet field inhomogeneities are dependent on outside factors such as MR scanner hardware (though is also sensitive to tissue properties, notably iron

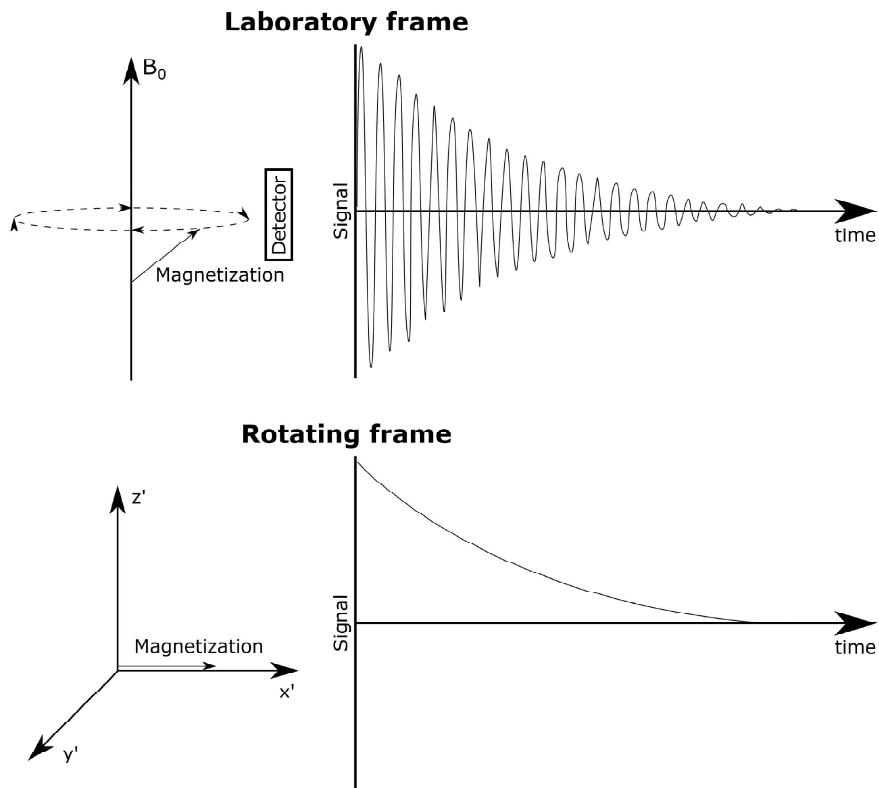


Figure 1.8: Following excitation of the magnetization vector by B_1 a signal will be generated which decays over time. A detector placed perpendicular to B_0 will measure signal in the so called laboratory frame wherein it will follow a sinusoidal shape as the magnetization vector precesses towards or away from the detector. In the rotating frame the xy -plane is rotated at the same speed as the magnetization vector, thereby canceling the waveform pattern of the signal that is generated and allowing simpler visualization. Axes in the rotating frame are called z' , x' , and y' .

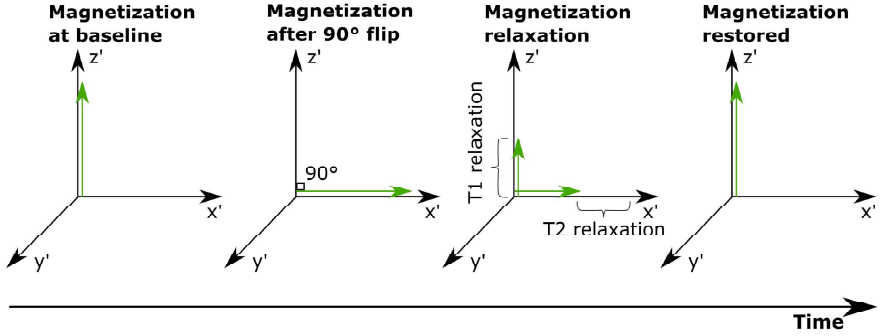


Figure 1.9: Showing the relaxation of magnetization after a 90° flip. Baseline magnetization on the z' axis is flipped entirely to the x' axis. As time elapses both T_1 -relaxation causes regrowth of magnetization along z' while T_2 -relaxation causes magnetization along the x' axis to diminish. Eventually the magnetization vector will be restored to the z' axis, in line with B_0 .

content used to diagnose hemochromatosis) [121]. Therefore it is desirable to be able to separate the effects into T_2 -time reflecting the effect of spin-spin interactions and T_2^* -time reflecting the combined effects of spin-spin interaction and magnet field inhomogeneities. These times then govern the signal decay according to Equations (1.4) and (1.5) where $M_{y'}$ is the magnetization along the y' -axis, M_0 is the initial magnetization immediately after the RF pulse, t is the time from bringing the magnetization to the y' -axis, and $\gamma\Delta B_0$ is the difference in rate of precession caused by magnet field inhomogeneities.

$$M_{y'} = M_0 * e^{\frac{-t}{T_2}} \quad (1.4)$$

$$\frac{1}{T_2^*} = \frac{1}{T_2} + \gamma\Delta B_0 \quad (1.5)$$

Simultaneously, magnetization recovery occurs. When the RF-pulse was applied to flip magnetization onto the y' -axis it deposited energy into the spins. Subsequently the spins start dispersing this energy onto their surroundings, lattice, in what is known as spin-lattice interactions which leads to a regrowth of magnetization along the z' -axis [119]. The rate at which this happens is dependent on the strength of B_0 , the tissue characteristics and on what constitutes the lattice. If gadolinium-based contrast agent is present, for example, it facilitates the dispersion of spin energy and thus accelerates the regrowth of z' magnetization [122, 123]. The rate of regrowth is governed by the time-constant T_1 according to Equation (1.6) where $M_{z'}$ is the magnetization in the z' axis, M_0 is the remaining magnetization in the z' axis immediately after the RF-pulse, and t is the time from the RF-pulse flipping the magnetization.

$$M_{z'} = M_0 * (1 - e^{\frac{-t}{T_1}}) \quad (1.6)$$

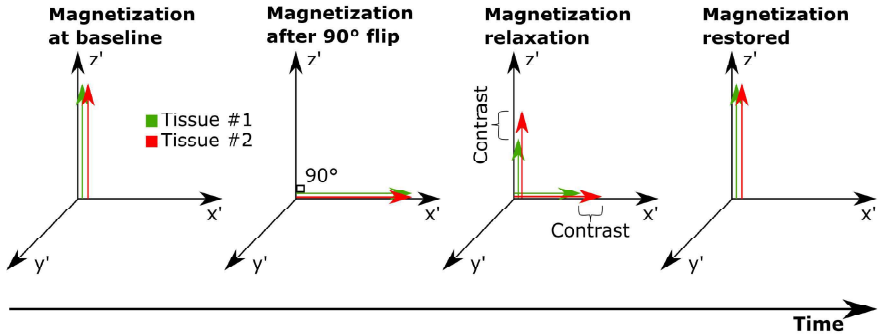


Figure 1.10: Showing the magnetization vector of two different tissue types, Tissue #1 and Tissue #2. As the two tissues have an equally large magnetization vector at baseline they will also have an equally large magnetization vector in the x' axis immediately after the 90° flip. Since these particular tissues have different T_1 and T_2 properties however, it will be possible to distinguish them based on the differences that develop over time as z' and x' magnetization is allowed to relax. If too long time is allowed to pass magnetization is once again restored to baseline and no more contrast between the tissues can be seen.

The reason T_1 and T_2 are important for this discussion has to do with the difference in T_1 and T_2 in different tissues. Playing out an RF-pulse to flip the magnetization and then waiting allows for those differences to manifest as difference in signal (Figure 1.10). Note that for the effect of T_1 to become apparent it is necessary to play an additional pulse to once again bring the z' magnetization to the y' -axis in order to measure it. Sequences of RF-pulses that mostly make apparent the differences between tissues caused by T_1 are called T_1 -weighted sequences while those that mostly bring out differences in T_2 are called T_2 -weighted sequences.

1.3.4 Spatial encoding

As was alluded to in the introduction, the relative location of any element that should be visualized needs to be recorded in order to form a comprehensive image. For MR imaging this is performed through so called *spatial encoding* by using magnetic field gradients and repeated experiments to calculate the origin of the signal. Since there are three spatial dimensions to consider, three encoding strategies are commonly used; (1) slice selection, (2) frequency encoding, and (3) phase encoding.

Slice selection

Remember that an RF-pulse needs to be played at the same frequency as the rate of precession of the spins in any given system to flip the magnetization. Also remember that the rate of precession is dependent on the strength of the magnetic field that the spins are in. These facts are utilized to select a slice of tissue wherein spins are flipped, thereby allowing signal

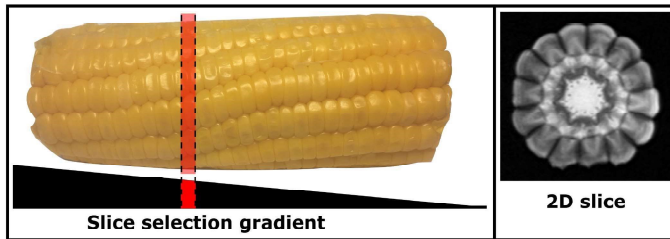


Figure 1.11: Slice selection in a cob of corn. A static field gradient is applied while the RF-pulse is played out. As the gradient changes the precession rate only the spins in a thin slice of the cob precess at the rate which is excited by the RF-pulse. In the image this is visualized by a 2-dimensional MR image of the cob despite the fact that both frequency encoding and phase encoding are also needed to create this image.

recording from this slice selectively without interference from other slices [124]. This is performed by applying a magnetic gradient during the application of the RF-pulse which changes the strength of the field in one axis, thereby causing the spins to precess at different rates over the gradient, so that only a thin band of the object that is imaged resonates with the RF-pulse (Figure 1.11). Slice selection solves the problem of determining positioning in one dimension, effectively turning our 3-dimensional problem into a 2-dimensional problem.

Frequency encoding

Frequency encoding utilizes the same principles as slice selection in that a gradient is applied which changes the frequency of precession for different points in space in one dimension [24]. This gradient, however, is not applied during application of the RF-pulse as this would interfere with (and would by definition be) the slice selection gradient. Rather, the frequency encoding gradient is played out during readout. Since the effect of the gradient is present during readout the signal that is acquired will originate from spins precessing at different rates depending on their position in the frequency encoding direction. The waveform of this combined signal can then be separated into the original signals, and thus positions, using Fourier transform (Figure 1.12).

Phase encoding

Taking slice selection and frequency encoding into account, there is still a need to encode for a third dimension. Phase encoding solves this elegantly by using information about the phase, or angle, of the magnetization vector at different positions [125]. First, a gradient is applied along the phase encoding direction after slice selection but before readout. This speeds up or slows down the spins for a short amount of time, thus affecting the phase of the spins.

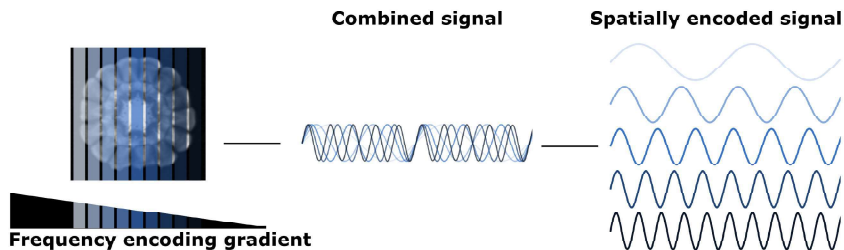


Figure 1.12: Frequency encoding of the slice selected in Figure 1.11. By adding a magnetic gradient during the readout the excited spins will precess at different frequencies, thereby creating a signal consisting of the combined waveforms of spins from all across the gradient. Using Fourier transform these waveforms can be separated based on frequency and, thus, the signal components can be tracked to their position along the frequency encoding direction.

The phase encoding gradient affects the phase of spins over the entire spectrum of the frequency encoding direction meaning that, in order to separate the spatial origin of the signals, the acquisition needs to be repeated as many times as the desired number of picture elements in the phase encoding direction (Figure 1.13). A consequence of this is that the time it takes to acquire an MR image is dependent on the resolution in the phase encoding direction but not in the frequency encoding direction.

1.3.5 Spin echo and gradient echo

It is possible to generate signal by only applying a single RF-pulse which flips the magnetization to the $x'y'$ plane. There is, however, a challenge when trying to interpret this signal in that it will not only be dependent on the tissue properties we may be interested in but also on magnet field inhomogeneities (see the discussion on T_2 and T_2^*). One solution to this challenge is the spin echo [23].

Imagine that magnetization is flipped onto the $x'y'$ plane and time is allowed to pass. The magnetization vector will start to dephase due to spin-spin interactions and due to magnet field inhomogeneities. Now imagine flipping the magnetization 180° and allowing an equal amount of time to pass. The same inhomogeneities which caused dephasing will now work in the opposite direction to rephase spins, effectively canceling the effect of inhomogeneities on the acquired signal. If we now acquire signal immediately following the 180° flip it will increase until the spins are entirely rephased and then start abating again in a pattern that is called an "echo" (Figure 1.14).

Another way of creating an echo would be by using a magnetic gradient, like the ones used for spatial encoding. The gradients are by design dephasing spins and so if a gradient was played in one direction and then at equal strength and for an equal amount of time in the opposite direction it would also generate an echo. This second kind of echo is often referred to as a gradient echo [126].

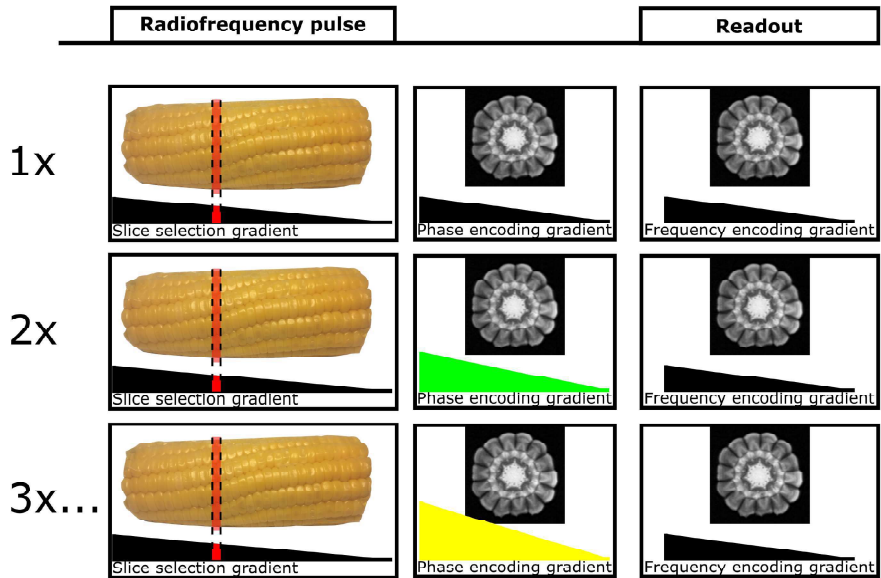


Figure 1.13: Schematic overview of spatial encoding. The slice selection gradient is played during the RF-pulse which flips magnetization onto the $x'y'$ plane while the frequency encoding gradient is played during readout. The phase encoding gradient is played in between the RF-pulse and readout to affect the phase of the precessing spins depending on their location in the phase encoding direction. To solve the resulting equation of what phase corresponds to each respective position requires one experiment per pixel of resolution in the phase encoding direction. Therefore the entire sequence is repeated while changing the strength of the phase encoding gradient for as many times as required.

1.3.6 Pulse sequences

So far the discussion has been focused on the principles and tools available to create an image from an MR acquisition. In practice the RF-pulse, or indeed several RF-pulses, and gradients are played out as pulse sequences which can be varied depending on which result is sought. Some of the parameters that are varied will be listed below.

- **Flip angle** - The angle from z' with which the magnetization is flipped by an RF-pulse
- **Echo time (TE)** - The time from the center of an RF-pulse and the peak of the consequent signal (echo)
- **Repetition time (TR)** - The time from one RF pulse to the corresponding one in the subsequent acquisition
- **Preparation pulses** - Additional RF pulses can be played before the one that flips magnetization for readout. These pulses could affect weighting of the sequence or

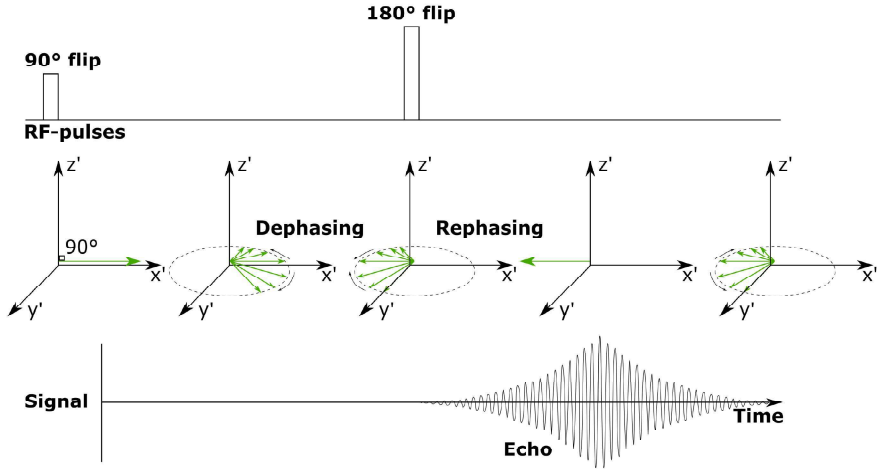


Figure 1.14: Showing the principles of a spin echo. After flipping magnetization 90° to the x' axis the magnetization starts dephasing due to T_2^* effects. By flipping magnetization by 180° the inhomogeneities previously causing the dephasing instead work in the opposite way to rephase spins. Measuring the signal after the 180° flip therefore shows an increasing signal which peaks as magnetization is completely rephased and then diminishes again as dephasing occurs in the other direction.

be used null the signal from, for example, fat or blood or could be used to enhance signal contrast

- **Inversion time (TI)** - When an 180° pulse is played before the RF-pulse used to bring magnetization to the transversal plane, this creates an inversion recovery. The TI is the time from the 180° pulse to the RF-pulse
- **Gradients** - Gradients may be applied for spatial encoding as discussed and may also be used to modify the signal

Together these parameters form a protocol for a pulse sequence. The sequences mentioned below have been selected due to their relevance for this thesis.

SSFP

Balanced steady state free precession (SSFP) is a fast imaging technique [127]. In cardiac imaging it is, for example, used to acquire cinematic images over the cardiac cycle [128]. Imaging is performed by flipping the magnetization back and forth around the z' axis using RF-pulses of the same magnitude but alternating polar signs, thus eventually creating a steady state where each readout yields identical results. Readout is performed around $\frac{TR}{2}$ to capture the resulting spin echo while a balanced frequency encoding gradient is timed to

allow refocusing of the transversal magnetization at the peak of the spin-echo. Thus, SSFP is technically a gradient-echo sequence but displays the properties of a spin-echo sequence [129]. Apart from refocusing the transversal magnetization at readout it is also necessary to refocus it at the RF-pulse in order to ensure that residual magnetization does not affect the following pulses. To this end, the effects of all the spatial encoding gradients are canceled out by making sure that for any gradient that is applied another gradient of equal size in the negative direction is also applied (Figure 1.15) [130]. This is the reason balanced SSFP is referred to as "balanced".

The SSFP signal is dependent on both T_2 and T_1 which can be realized when considering that the signal is directly proportional to the amount of transversal magnetization present during readout. The effect of T_2 , then, can be seen as straightforward where higher T_2 means that the decay of transversal magnetization is slower and thus signal increases with higher T_2 -values (Figure 1.15). To understand the effect of T_1 , consider that a faster recovery of magnetization in the z' axis leads to a larger transversal component in subsequent pulse iterations where this magnetization is brought down to the $x'y'$ plane. Larger T_1 -values result in slower magnetization recovery and therefore less signal. At flip angles of around $50-80^\circ$ both T_2 and T_1 effects are relevant, thus making the SSFP-signal $\frac{T_2}{T_1}$ dependent [131].

T_2 -STIR

The T_2 -weighted short tau inversion recovery (T_2 -STIR) sequence is a sequence designed to be T_2 -weighted with the additional properties of showing no signal from blood or fat [132]. This is potentially useful when imaging myocardium to visualize edema as edema, blood, and fat are all shown as hyper-intense in standard T_2 -weighted images. The STIR part of the name refers to preparatory pulses that are added before flipping magnetization to the transverse plane [133, 134]. First a non-selective 180° pulse is used to flip all magnetization almost immediately followed by a second, selective 180° which returns magnetization to baseline in all stationary tissue. In the time between pulses, however, blood has had time to flow through the plane of interest and magnetization is therefore not restored in blood which is "nulled" and will not contribute any signal in the subsequent imaging. After the blood-nulling pulses, but still before flipping magnetization to the transverse plane, another 180° pulse is played at a timing which allows the magnetization of fat to "grow" back to zero. Since fat has short T_1 compared to other tissues of interest, such as myocardium, these will still retain magnetization at the time of imaging (Figure 1.16).

1.3.7 Contrast agent

Another way of affecting image contrast which is not directly related to the pulse sequence is by introducing intravenously injected contrast agent. Contrast agents are commonly based on gadolinium, a metal with very large magnetic moment. As mentioned before,

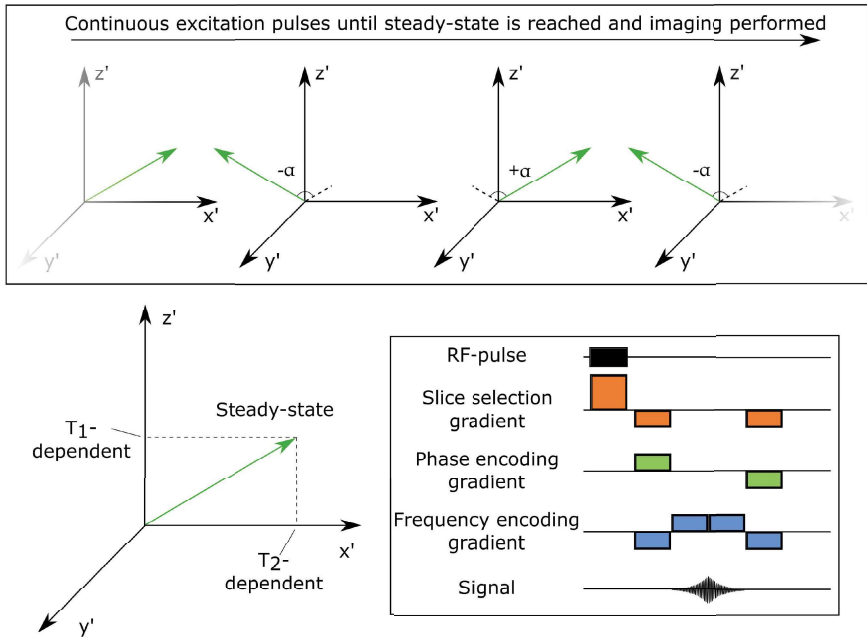


Figure 1.15: In SSFP imaging, steady-state is achieved by flipping magnetization back and forth around z' . This causes a steady state which is dependent on the flip angle (α), T_1 , and T_2 . Longer T_1 will result in slower regrowth of magnetization along the z' axis and thereby a smaller magnetization vector while longer T_2 will result in slower decay of magnetization in the x' axis. The box in the lower right of the figure portrays space encoding gradients in relation to RF-pulse and signal acquired. All gradients are balanced, meaning that for any gradient played in one direction an equal amount is played in the opposite direction.

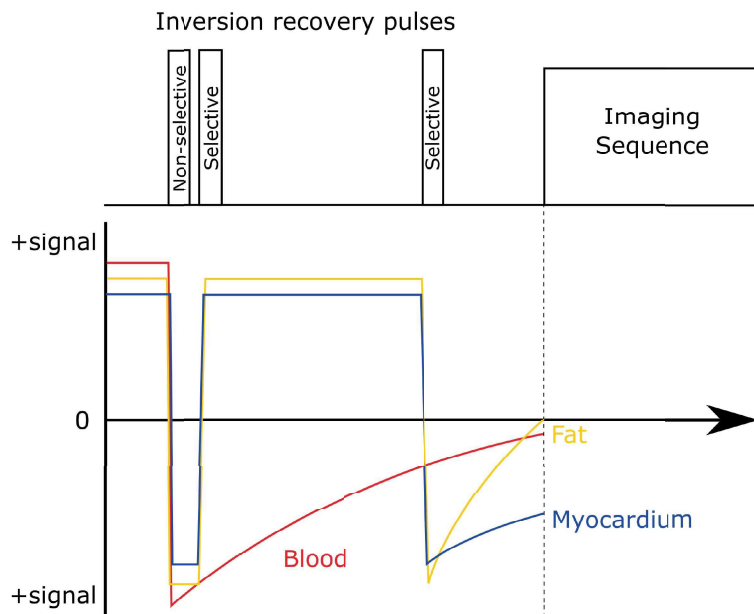


Figure 1.16: The T2-STIR pre-pulses consist of a non-selective inversion recovery pulse paired with a selective pulse and a second selective inversion recovery pulse. The non-selective pulse inverts magnetization in all tissues (here represented by blood, fat, and myocardium) after which magnetization of all tissues except blood is restored by the selective pulse. Application of these pulses is timed for magnetization of blood to recover close to 0 at the start of the imaging sequence, thereby canceling the signal. Fat suppression is performed similarly by timing inversion of tissues so that fat has recovered to 0 at the start of imaging. Tissues with longer T_1 , such as myocardium, will not reach 0 at this point and will therefore still contribute to signal.

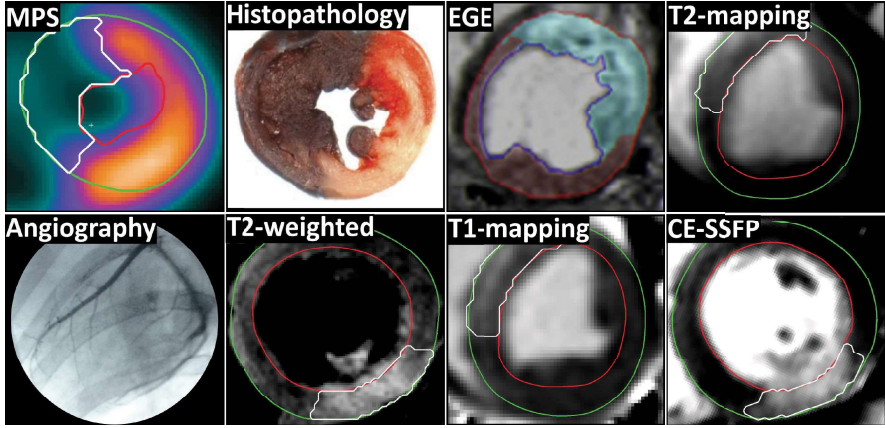


Figure 1.17: Examples of modalities used to measure MaR in different hearts. Angiography image shows contrast injection into the LAD and LCx and the other panels show midventricular short-axis images of the left ventricle. Myocardium at risk is colored white in the MPS, T2-mapping, T2-weighted, T1-mapping, and CE-SSFP images while it is teal in the early gadolinium enhancement (EGE) panel. In the histopathology panel, blue dye has been injected into the left ventricle during occlusion. Consequently the blue colored area in the image shows remote myocardium, red is salvaged myocardium, and white is infarcted myocardium. The histopathology image was adapted from Bohl *et al.* [136] and the EGE image was adapted from Hammer-Hansen *et al.* [137].

introducing gadolinium reduces T_1 as it facilitates dispersion of energy from spins. It also directly affects spins by changing their phase, thus decreasing T_2 [122, 123].

Gadolinium is usually chelated to a carrier molecule, such as diethylenetriaminepentaacetic acid (DTPA), which does not permeate cellular membranes and therefore stays in the extracellular space. In CMR imaging this is utilized to separate viable myocardium from infarcted myocardium where cellular membranes are no longer intact [135].

1.4 Methods of determining MaR

Myocardium at risk has been determined with methods using different principles (Figure 1.17). Recall that MaR is the myocardium that, following acute myocardial ischemia, was at risk of dying including both myocardium that did become infarcted and salvaged myocardium.

1.4.1 Myocardial perfusion SPECT

Single photon emission tomography (SPECT) is a method whereby the activity of radioactive isotope is quantified using detectors sensitive to gamma radiation [138]. For myocardial perfusion SPECT (MPS), an isotope such as ^{99m}Tc is bound to a suitable

carrier molecule and injected intravenously [139–141]. This isotope then distributes in proportion to perfusion and is taken up by myocytes with viable mitochondria. As a result, where there is an area of hypo-perfusion this is seen as an area with lower radioactive levels. Most commonly MPS is used to gauge whether there exists exercised-, or pharmacologically induced myocardial ischemia but if the opportunity exists to inject isotope during coronary occlusion just before reperfusion it could also be used to measure MaR by assessing the size of the area not supplied by blood [45, 142]. Needless to say this leaves a small window of opportunity to prepare the exam and requires the logistics to have radioisotope readily available.

1.4.2 Angiography

Coronary angiography has been employed to determine MaR. Where MPS indirectly measures the perfusion of the myocardium, angiographic measures take the anatomy of visible epicardial coronary vessels into account and weigh the findings by scoring them to estimate the amount of myocardium supplied by these arteries [143–145]. Angiographic scores have shown poor correlation with both MPS and T_2 -weighted CMR for measuring MaR and should be interpreted with caution [146, 147].

1.4.3 Histopathology and microspheres

Histopathological dyes such as Evans blue have can be used to color perfused myocardium by injection into the left ventricular cavity during coronary occlusion [148]. It binds to plasma albumin, distributes to perfused tissue and stains the tissue dark blue. Some issues with smearing of the Evans' blue dye have been reported and alternative dyes proposed [136]. Alternatively, fluorescent microspheres have been similarly used with the effect that MaR can be visualized under ultraviolet light [149]. Both the Evans' blue and microsphere techniques require the heart to be explanted and sliced for evaluation limiting their use to acute experiments and making them unsuitable for use in patients.

1.4.4 Cardiac MR

After the advent of so called late gadolinium enhancement (LGE) to determine infarct size by CMR it became increasingly appealing to develop an MR-sequence which could measure MaR and thereby allow determination of MSI through one modality. This section will cover some of the sequences developed for this purpose and will briefly touch upon possible mechanisms of action.

T_2 -weighted imaging

T_2 -weighted imaging was first thought to be a potential method of measuring infarct size without the use of contrast agent but increased T_2 was shown to also be seen in viable tissue [150]. Instead, T_2 -weighted imaging was shown to accurately depict MaR when

imaged 2 days after myocardial ischemia-reperfusion injury and later that it could be used for up to one week after the ischemic injury [27, 28]. These T_2 -sequences used so called "black-blood" (see T_2 -STIR) imaging which is theoretically appealing but seem to be outperformed by newer bright-blood sequences [151–153].

Early gadolinium enhancement

Early gadolinium enhancement (EGE) has come up as a potential method of quantifying MaR. It employs inversion recovery imaging similar to LGE but acquires images in the immediate first couple of minutes following contrast injection. EGE is validated with T_2 -weighted imaging and microspheres respectively however it is still unknown how sensitive it is to timing of imaging and there is a challenge in capturing whole-heart coverage in the limited time available [137, 154, 155].

T_1 - and T_2 -mapping

T_1 - and T_2 -mapping are techniques which not only utilize weighting depending on T_1 or T_2 but which quantify T_1 - or T_2 -values. The mapping techniques show promise and may be able to provide a more standardized way of evaluating myocardial edema [156, 157]. They are still relatively new and untested, however, and it remains to be seen how they perform in large trials.

Contrast enhanced SSFP

Contrast enhanced SSFP (CE-SSFP) is a relatively new technique utilizing the $\frac{T_2}{T_1}$ -weighting of the SSFP signal together with the effects of gadolinium-based contrast agent [158]. It has been validated against MPS in human patients and was compared to T_2 -STIR in a separate paper [29, 159]. The first paper of this thesis concerns the experimental validation of CE-SSFP wherein the effect of timing of imaging after administration of gadolinium is also investigated. The second paper of this thesis concerns the reliability of CE-SSFP in a clinical trial setting compared to T_2 -STIR.

Mechanism of action

Empirically it is evident that myocardium at risk can be visualized as a hyperintense area of myocardium [27–29, 151]. To understand the mechanism it seems prudent to investigate the differences between myocardium that has been ischemic and myocardium that hasn't. As mentioned before, following ischemia-reperfusion there is an increase in myocardial water content, myocardial edema, which expands the extracellular space [46, 100]. It has been showed that T_1 and T_2 both increase with increased water content in tissues [160–163]. For T_2 -weighted imaging this could explain an increase in signal of edematous tissue, and thus MaR, as transversal magnetization decays at a slower rate. The edema model of explanation does not, however, satisfactorily explain all findings [164]. Remember that MaR consists

of both infarcted and salvaged myocardium and that the increase in extracellular space is on the order of 2-3 times higher in infarcted vs salvaged myocardium [46]. Considering that for most of the techniques used to image MaR it is not possible to differentiate infarcted and salvaged myocardium by intensity, it seems that another explanation of the mechanisms is required. One such explanation concerns the magnetic properties in different states such as "bound" and "free" water. Bound water is used to refer to water that is gathered in hydration layers close to the surface of larger proteins/molecules or that is located within the structure of the proteins [165]. Protons in the vicinity of these molecules would be affected by for example hydrogen bonding which restricts their motion and thus causes more rapid dephasing of transversal magnetization, i.e. shorter T_2 [166]. Additionally the bound water and large proteins in themselves can be seen as "lattice" for the free water to deposit energy onto, resulting in shorter T_1 [166–168]. Some later studies have questioned whether water in hydration layer is restricted enough to contribute to faster relaxation but rather the effect could depend mainly on "intramolecular" water [169, 170]. Regardless, myocardial ischemia-reperfusion seems to decrease this effect and that way increase both T_1 , and T_2 , be it through changes in the structure/concentration of large proteins or some other mechanism [171].

Sequences acquired after administration of contrast agent, such as CE-SSFP, also seem to show little difference between infarcted myocardium and salvaged myocardium. Recall that the gadolinium-based contrast agents used distribute extracellularly, that extracellular space is greater in infarcted tissue compared to salvaged myocardium, and that gadolinium lowers both T_1 and T_2 [46, 122, 123]. It could be speculated that an increased fraction of free water in infarcted tissue would balance this change by increasing T_1 and T_2 causing the infarcted area to be of similar intensity as salvaged myocardium while still being of higher intensity than normal myocardium. To conclude this section it should be clarified that the mechanisms behind the contrast seen in the sequences used to visualize MaR are currently not thoroughly understood and work to elucidate these still remains to be done.

Chapter 2

Aims

This thesis validates a CMR method of measuring MaR and compares it to an existing method. It also applies the measurements of that method to better understand coronary artery distribution and which factors affect the development of myocardial infarction. The aims of the individual papers are stated below.

Paper I

To determine whether the CMR sequence CE-SSFP could be used for determining MaR *ex vivo* as well as *in vivo* and to determine whether the timing of imaging after contrast agent administration affects the quantification of MaR *in vivo*.

Paper II

To study how well the CMR sequences T2-STIR and CE-SSFP perform in quantifying MaR and determining culprit vessel across sites, MR camera vendors, treatments, and imaging timing using data from the CHILL-MI and MITOCARE trials.

Paper III

To quantify and visualize the extent of the perfusion territories for the 3 main coronary arteries, left anterior descending artery (LAD), left circumflex artery (LCx), and right coronary artery (RCA), using CE-SSFP and T2-STIR CMR sequences and to provide data on perfusion territories to be used for simulation and programming.

Paper IV

To investigate to what extent gender, smoking status, presence of diabetes or history of hypertension affects the rate at which infarct evolves by assessing the amount of infarction and myocardial salvage observed using CMR in a cohort of ST elevation myocardial infarction (STEMI) patients from three recent multi-center trials.

Chapter 3

Materials and methods

*The strongest argument proves nothing so long as the conclusions are not verified by experience.
Experimental science is the queen of sciences, and the goal of all speculation.*

Roger Bacon, *Opus Tertium*, 1267
Translation by Robert Belle Burke

3.1 Experimental model

For Paper I, an experimental porcine model was used. The study protocol was approved by the regional Ethics committee for animal experiments in Lund, Sweden. The protocol is described in greater detail in the methods section of Paper I [172].

3.1.1 Anesthesia and monitoring

Animals weighing 40-50 kg were sedated, intubated and mechanically ventilated while anesthesia was maintained on sevoflurane gas. Fluid balance was maintained using sodium chloride (0.9%), 5% glucose was given as a slow infusion, and fentanyl was used to prevent pain during interventions. During the experiment the animals were monitored including continuous arterial blood pressure, ECG, heart rate, temperature, pulse-oximetry, and serial blood gas analyses.

3.1.2 Interventions

Introducer sheaths were inserted in the femoral artery and vein as well as the carotid artery after which heparin was administered. An angiography catheter was inserted through the carotid introducer and a coronary angiogram was performed. Based on the appearance of the angiogram a balloon-tipped catheter was placed either before or after the second diagonal branch of the LAD to obtain a wide range of MaR without needlessly jeopardizing survival of the animal. The balloon was inflated, thus occluding the LAD, for 35 or 40

minutes before reperfusion. Prior to occlusion, an amiodarone infusion was administered to decrease potential arrhythmias due to ischemia-reperfusion. Ten minutes prior to reperfusion, isotope (^{99m}Tc tetrafosmine) was administered. Any malignant arrhythmias were treated by chest compressions and defibrillation.

After induction of ischemia-reperfusion the animal was transported to the MR department for imaging.

3.1.3 Imaging

CMR imaging

In-vivo CMR imaging included late gadolinium enhancement (LGE) to detect myocardial infarction and CE-SSFP to detect MaR. One midventricular left ventricular (LV) short-axis slice of SSFP was repeatedly acquired over 10 minutes following administration of gadolinium. After that a short-axis stack of SSFP covering the LV and 2-, 3-, and 4-chamber projections were acquired before another single short-axis slice at 20-30 minutes after gadolinium administration. One full coverage short-axis LV stack and long-axis images in the 2-, 3-, and 4-chamber projections of LGE images were acquired 15-20 minutes after gadolinium administration.

After *in-vivo* imaging an additional dose of gadolinium contrast agent was administered and allowed to circulate for 15 minutes. The animals were subsequently euthanized by intravenous administration of saturated potassium chloride solution and the hearts were excised and mounted in plastic jars for *ex-vivo* imaging.

The same SSFP sequence used *in vivo* was also used to acquire a full coverage left ventricular short-axis stack *ex vivo*. Additionally a short-axis stack of a high resolution T1-weighted sequence was acquired to be used for *ex-vivo* infarct quantification.

Myocardial perfusion SPECT

After *ex-vivo* MR imaging the hearts were imaged using myocardial perfusion SPECT (MPS). A dual head camera was used to record radioactivity of the ^{99m}Tc administered previously. As the ^{99m}Tc was administered during occlusion it would only distribute in the non-ischemic parts of the heart thus allowing quantification of MaR.

3.2 Patient data

The patient data in this thesis was collected in the context the three clinical trials CHILL-MI, MITOCARE, and SOCCER [21, 173, 174]. Paper II, III, and IV contain data from CHILL-MI and MITOCARE while only Paper IV contains data from the SOCCER trial.

3.2.1 CHILL-MI

The purpose of the CHILL-MI trial was to test whether cooling by an endovascular catheter reduced infarct size as a percentage of MaR. It did not show a reduction in the primary endpoint. However, when looking at the subgroup of patients with anterior myocardial ischemia who were in the cooling arm of the study there was a reduction in both infarct size and in the incidence of heart failure. A total of 101 patients underwent CMR in any of the 9 centers involved in the trial.

Inclusion criteria

- Patients of 18 to 75 years of age
- ST elevation >0.2 mV in 2 contiguous leads
- Inferior STEMI: total ST deviation of ≥ 0.8 mV
- Symptom duration <6 h

Exclusion criteria

- Cardiac arrest or Killip class II-IV
- Previous myocardial infarction
- Previous PCI or CABG
- Congestive heart failure
- End-stage kidney disease
- Hepatic failure
- Recent stroke or coagulopathy
- Pregnancy

3.2.2 MITOCARE

The MITOCARE trial was a cardioprotection trial testing an experimental drug called TRO40303, which previously have been shown to block mitochondrial permeability. The hope was therefore that it would have prevented reperfusion injury but TRO40303 did not show any effect on the primary endpoint of infarct size as percentage of MaR. Within the trial 111 patients underwent CMR from a total of 9 different centers.

Inclusion criteria

- Age >18 years old
- ST elevation in 2 contiguous leads:
 ≥ 0.2 mV in men in V2-V3
 ≥ 0.2 mV in women in V2-V3
 ≥ 0.1 mV in other leads
- Nitrate-resistant chest pain ≥ 30 min
- Symptom duration <6 h
- Clinical decision to treat with PCI
- Presenting TIMI flow 0-1 of culprit artery
- Occlusion of LAD, RCA, or LCx
- Signed informed consent
- Non-child-bearing-potential

Exclusion criteria

- Cardiac arrest or ventricular fibrillation
- Previous myocardial infarction/CABG
- Cardiogenic shock
- Pacemaker
- Stent thrombosis
- Angina ≤ 48 h before ischemia
- Fibrinolytic therapy ≤ 72 h prior to PCI
- Atrial fibrillation
- Claustrophobia at MR-scan
- Inflammatory/infectious/malignant disease
- Biliary obstruction/hepatic insufficiency
- Egg allergy

3.2.3 SOCCER

Oxygen therapy is routinely administered to STEMI patients in many centers but some data suggests it may be detrimental. The SOCCER trial compared patients receiving oxygen therapy in the setting of STEMI to those who did not, using infarct size as percentage of MaR as primary endpoint. A total of 103 patients from a single center underwent CMR within the scope of the trial.

Inclusion criteria

- STEMI
- Transport via ambulance
- Accepted for primary PCI at the study center
- Symptom duration <6h
- Blood oxygen saturation $\geq 94\%$
- Informed consent

Exclusion criteria

- Previous myocardial infarction
- Inability to make the decision to participate; dementia and the like
- Significant claustrophobia
- Magnetic material inside the body

3.3 Magnetic resonance imaging

3.3.1 Image acquisition

All CMR images were acquired on 1.5 T MR scanners from one of three major manufacturers; Philips (Philips Healthcare, Best, The Netherlands), Siemens (Siemens AG, Erlangen, Germany), or General electrics (GE Healthcare, Waukesha, WI, USA). The scans were performed within any of 17 centers throughout Europe, either by the center of the core laboratory Imacor AB (Lund, Sweden) or at a site which had received training by the core laboratory and undergone subsequent quality control. Imaging was performed on one occasion 1-8 days after inclusion in the respective clinical trial.

After placing subjects in a supine position, scout images were acquired and anatomical views of the heart were located. In order to minimize motion artifacts image acquisition was performed at end-expiratory breathhold and ECG-gating was used.

T2-STIR and CE-SSFP

A short-axis stack covering the entire left ventricle was acquired before contrast administration using the unmodified version of T2-STIR provided by each respective vendor (Philips, Siemens, or General Electrics).

Long-axis CE-SSFP images, and short-axis images corresponding to the T2-STIR images were acquired approximately 5 minutes after administration of gadolinium-based contrast agent. CE-SSFP images are cinematic images where temporal resolution typically was set to around 30 ms. Slices for both T2-STIR and CE-SSFP were set to 8 mm thickness and the typical in-plane resolution was 1,5 x 1,5 mm. For further details on imaging parameters see Paper II [175].

LGE

Late gadolinium enhancement short-axis images were acquired in the same position as the T2-STIR and CE-SSFP images after adjusting inversion times to minimize signal from viable myocardium [151]. In addition, long-axis images in the 2-chamber, 3-chamber, and 4-chamber projections were acquired. The LGE sequences used inversion-recover gradient recalled echoes with or without so called phase-sensitive reconstruction (PSIR). Similar to T2-STIR and CE-SSFP, slice thickness was set to 8 mm and in-plane resolution was set to 1,5 x 1,5 mm.

3.3.2 Image evaluation

Images used in the CHILL-MI and MITOCARE trials were analyzed in the context of the core-lab Imacor AB, of which two members are the supervisor and co-supervisor of this thesis. Images from studies not used in the trials as well as all data from the SOCCER trial was not analyzed as part of a core-lab assignment but all data was reviewed by at least one of the researchers participating in the CHILL-MI and MITOCARE core-lab analyzes. A second observer was used in all cases.

Data was analyzed using the software Segment [176]. Endocardial and epicardial borders were delineated in T2-STIR and LGE images as well as both in end-diastolic and end-systolic time-frames of the CE-SSFP images. Myocardium at risk was then delineated manually in T2-STIR and CE-SSFP images by including hyperintense myocardium. Hypointense myocardium within the hyperintense zone was considered to be microvascular obstruction or hemorrhage and was therefore included as MaR [98]. Observers were blinded to the CE-SSFP images and results when delineating T2-STIR and vice versa but had access to the LGE images to aid in confirming the infarcted area of interest.

Infarct was delineated by including hyperintense areas of myocardium in LGE images as well as hypointense areas within the hyperintense areas as for MaR-delineations (see above).

3.3.3 Polar plot visualization

It is a challenge to present 3-dimensional data such as from MR images in a 2-dimensional format such as a manuscript. Inevitably, all information will not be conferred to the reader so the best one can hope for is to select a mode of presentation which conveys the important points in an intuitive manner. Polar plots have been used in map-making to represent the world and this technique has been adapted to present the heart in a similar manner. In such a projection the apex of the heart will be in the center and as we move towards the base we also move outwards in the plot (Figure 3.1) [177]. For our purposes this can be used to visualize the extent of, for example, MaR or myocardial infarction in more than one slice at the time. However, the plot visualizes the myocardium in two dimensions and thus loses the ability to contain information about differences in the endocardial to epicardial extent

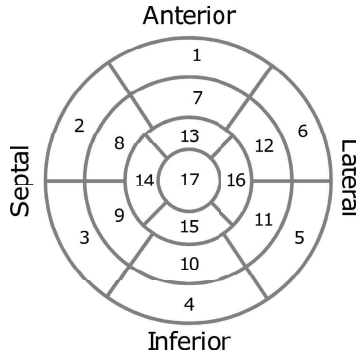


Figure 3.1: Polar plot of the left ventricle of the heart according to the American Heart Association 17-segment model. The middle segment (17) is the apex while the segments further out signify more basal segments.

of myocardium. Polar plots were used to visualize extent of MaR and infarct size in Paper III [178]. In an effort to compensate for the lack of information on endocardial to epicardial extent the polar plot was intensity coded on a gray scale. The intensity of the plot reflects the transmural extent of the parameter it's showing. For example, an infarct of 50% transmural extent would have an intensity of 50% compared to an infarct of 100% transmural extent. When adding information from several patients together and visualizing them simultaneously this means that the intensity of the polar plots reflect both the transmural extent of the parameter it's showing as well as the frequency at which any given part of myocardium contains the parameter. If 50% of patients had infarcted myocardium in a given part of the polar plot and of these the average transmural extent was 50% it would mean that the intensity of the polar plot, in that part, would be 25% of maximum intensity.

3.4 Coronary angiography

Coronary angiography was performed by in all patients within the scope of the original trials. The images were analyzed by experienced interventional cardiologists and reviewed by the author of this thesis.

Angiography images were analyzed with regards to culprit vessel, location of the coronary obstruction, degree of flow over the coronary obstruction before and after reperfusion according to the thrombolysis in myocardial infarction (TIMI) classification, and presence of collaterals according to Rentrop grading [179].

3.5 Statistical methods

3.5.1 Standard deviation and standard error

The standard deviation (SD) measures the spread of sample data and is therefore useful in describing that data. It is calculated by comparing the actual values measured to the mean value of those measurements according to Equation 3.1 where y_i are the individual values of the sample, \bar{y} is the sample mean and N is the sample size. Note that even though sample size is part of the equation, SD is not necessarily affected by it since it is included only to correct for the number of comparisons between y_i and \bar{y} .

$$SD = \sqrt{\sum_{i=1}^N \frac{(y_i - \bar{y})^2}{N}} \quad (3.1)$$

Standard error, instead, is a measure of the precision of the data and therefore can be used to make predictions about the entire population that the sample is representative of. When used to describe the precision of determining a mean value it is referred to as standard error of the mean (SEM) which can be calculated according to Equation 3.2. In contrast to SD, SEM will decrease with increasing sample size as the degree to which the sample is representative of the population increases.

$$SEM = \frac{SD}{\sqrt{N}} \quad (3.2)$$

3.5.2 Sample size

When designing a study it is important to determine what number of participants is appropriate. In hypothesis driven research a null hypothesis is defined, allowing for calculations of statistical power by taking into account how large the sample needs to be to show a difference of predefined size. The CHILL-MI trial, for example, defined a 25% reduction in MSI as a positive outcome, making the null hypothesis: There is no difference greater than 25% between the study groups. Assuming a similar spread in MSI as in previous studies with similar populations, the number of patients calculated to reach statistical power would be a total of 72 [173].

Paper I of this thesis is not hypothesis driven in the sense that clinical trials are. Clinical trials seek to ensure a causal relationship between the intervention and the effect measured while Paper I, a validation study, seeks to determine the accuracy and precision of the method in question. Thus the sample sized required becomes harder to define. Still, there are some aspects that can be taken into consideration. (1) How good already existing methods are, a new method would need to be at least as accurate and precise to be useful. (2) What degree of accuracy and precision is enough for the intended purpose, such as determining MSI in cardioprotection trials. (3) How much adding more data increases statistical

certainty. In an experimental study adding more data could be an ethical concern if it does not meaningfully increase the value of the output.

Existing methods

Comparable studies using T2-weighted imaging and the previously published CE-SSFP validation in patients typically show a bias of 0-2% with an SD of around 5% compared to the reference method [27–29]. It could be argued that the reference methods used could be a limiting factor. However, as the interobserver variability of CE-SSFP for detecting MaR was $1.6 \pm 3.7\%$ it is unlikely that the SD of the difference will be lower than a few percent [29].

Cardioprotection trials

The cardioprotection trials that are relevant for using CE-SSFP as a method to detect MaR typically use MSI as endpoint. The spread of MSI in patient populations varies depending on where in the world the trial is undertaken but for our purposes lets consider MSI for CHILL-MI, MITOCARE, and SOCCER which, when pooled, is a mean of $53\% \pm$ an SD of 20%. This means that a 10% error in calculating MaR gives an 8% error in MSI, a 5% error in MaR gives a 5% error in MSI, and 1% MaR gives a 1% error in MSI. These trials all have around 100 patients included and it may be reasonable to accept a measurement error of a few percent. At 5% or 10% error, however, it would add considerably to the spread in data and thus the number of patients needed to power the trial [180].

Effect of increasing sample size

Keeping the previous sections in mind, a rough goal in designing the validation of CE-SSFP would be for it to detect a bias of more than a few percent. This has to be weighed against the ethical implications of how many animals the experiment warrants. Therefore it is prudent to understand the impact of increasing sample size.

The spread of the mean value, as noted previously, is the SEM. Consequently, two measures with small SEM:s require smaller samples to discern a true difference than do measures with large SEM. As SEM is dependent on SD and N (Equation 3.2) it is illustrative to plot SEM as a percentage of SD versus N, as we are interested in the effect of sample size (Equation 3.2). The plot shows that with a sample size of 4 SEM is half of SD, with a sample size of 8 it is roughly 35% of SD, and with a sample size of 12 it is roughly 29% of SD. The SD of the bias for CMR-methods to determine MaR and reference method has previously been around 5% (see previous section). Thus, according to Equation 3.2, testing the accuracy of the technique down to a few percent would require at least approximately 6-8 subjects. Six to ten subjects would also be an amount which is fairly resistant to single outliers skewing the result.

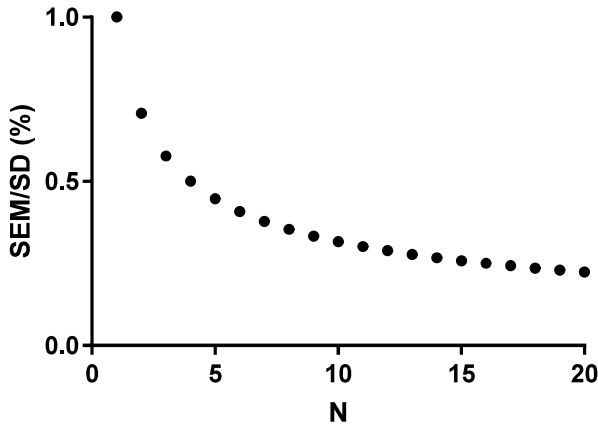


Figure 3.2: This figure is intended to show the effect of sample size on standard error of the mean (SEM), and thereby statistical power, by correcting for standard deviation (SD). y-axis: Standard error of the mean (SEM) divided by standard deviation (SD), x-axis: Sample size (N)

3.5.3 Statistical testing

Comparing means

The statistical method for comparing means between two groups was chosen depending on whether the data was paired/unpaired and whether it could be assumed that the data was distributed according to Gaussian distribution (i.e. whether it was parametric or non-parametric). Paired data which was deemed parametric was tested using a paired t-test, non-paired parametric data using an independent t-test, and non-paired non-parametric data using the Wilcoxon rang test [181, 182]. In one instance, concerning comparisons of diagnostic quality in Paper II, it was not clear from viewing the data whether it could be considered parametric. Therefore the D'Agostino-Pearson test for normality was run, testing the symmetry and kurtosis of the data to guide in the decision [183].

When comparing means of several groups at the same time an ANOVA-test was used for Paper II, excluding missing data [184]. Since N was substantially smaller in Paper I and, due to sub-grouping, in Paper III linear mixed models were created for repeated measurements including incomplete datasets.

Comparisons of ratios between two groups, such as the ratio of correctly assigned culprit artery in Paper II, were performed using Fishers' exact test [185].

Correlation

The Pearson correlation coefficient is appropriate in data either of Gaussian distribution or of large enough sample size [186, 187]. It was used to calculate correlation in Paper I-III. For Paper IV a two pronged approach was used to test multiple variables. First a univariable analysis was performed where all results significant to $p < 0.10$ were entered into a multivariable analysis.

Agreement

When comparing two methods, using mean difference can be deceptively misleading as there can be large variances in random error. Such data should therefore be visualized and judged in the context it is to be used. In that regard, Bland Altman analysis is a simple way to visualize the differences over the entire spectrum of values [188]. The Bland Altman method plots the difference in the values attained from each respective method against the mean of those two methods. If one method is considered reference method it may instead be appropriate to plot the difference of the methods against the reference method.

Chapter 4

Results and discussion

There is no more difficult art to acquire than the art of observation, and for some men it is quite as difficult to record an observation in brief and plain language.

William Osler, *On the Educational Value of the Medical Society*, 1903

4.1 Introduction

This chapter serve to give an overview of the results and a brief discussion to put them in context. For more detailed results and discussion please refer to each respective paper.

4.2 CE-SSFP for measuring MaR

4.2.1 Validation of CE-SSFP

There was excellent agreement and low bias when comparing *ex-vivo* CE-SSFP to *ex-vivo* MPS, *ex-vivo* CE-SSFP to *in-vivo* CE-SSFP, and when comparing *in-vivo* CE-SSFP to *ex-vivo* MPS (Figure 4.1).

4.2.2 Timing after contrast administration

There was no difference in size of MaR when comparing acquisitions of CE-SSFP taken sequentially between 2-30 minutes after contrast administration (Figure 4.2).

4.2.3 Performance and reliability

When comparing analysis of MaR using CE-SSFP to T2-STIR, more data of diagnostic quality was found using CE-SSFP (Figure 4.3). There was neither a difference in size of MaR achieved between sequences in images of diagnostic quality, nor was there any difference between treatment groups and/or controls (Figure 4.4). The ratio of diagnostic

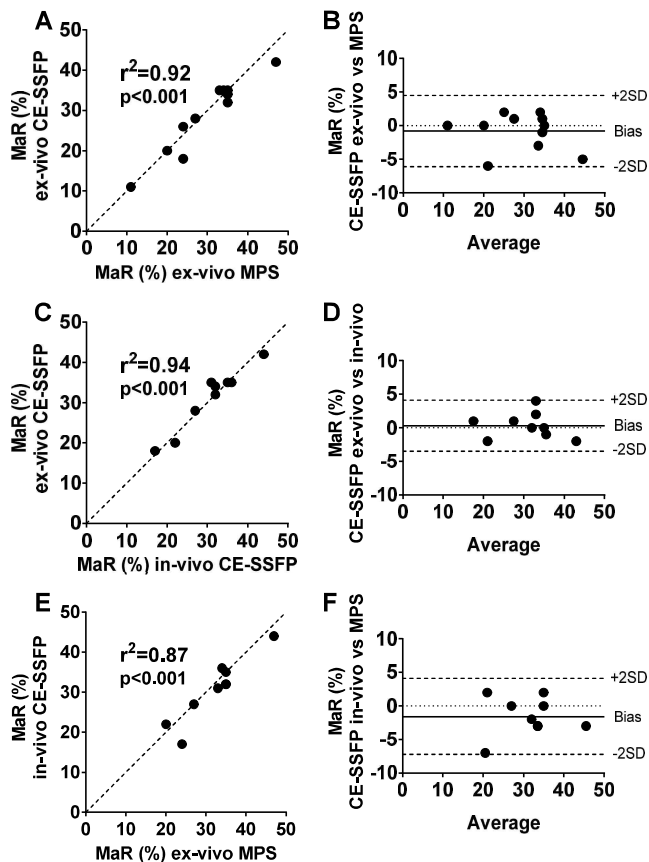


Figure 4.1: Myocardium at risk (MaR) by MRI and MPS show overall good correlation and agreement. Panel a shows a good correlation between MaR by *ex-vivo* CE-SSFP and MaR by myocardial perfusion SPECT (MPS). The corresponding Bland-Altman plot in panel b shows a low bias. Panel c shows a good correlation between MaR by *ex-vivo* CE-SSFP and MaR by *in-vivo* CE-SSFP, with a low bias (panel d). Panel e shows a good correlation between MaR by *in-vivo* CE-SSFP and MaR by MPS. The corresponding Bland-Altman plot in panel f shows a low bias. In all cases, MaR is expressed as percent of left ventricular mass. The dotted lines in a, c and e represent the line of identity

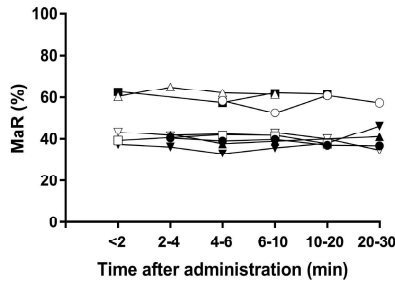


Figure 4.2: Myocardium at risk (MaR) by CE-SSFP over time after contrast agent administration in single midventricular slices. There was no change in MaR up to 30 min after contrast agent administration ($p=0.95$)

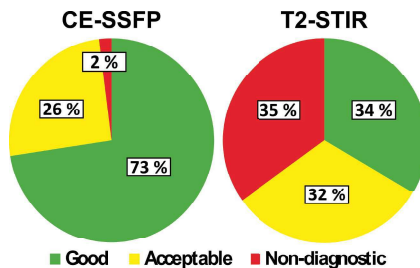


Figure 4.3: Image quality by T2-STIR and CE-SSFP. Pie charts show per cent of datasets where MaR was considered not of diagnostic quality, acceptable, or good in a total of 200 T2-STIR and 204 CE-SSFP datasets.

datasets differed markedly between different centers and vendors for T2-STIR but not for CE-SSFP (Figure 4.5).

4.2.4 Discussion

Measuring MaR using CE-SSFP is an accurate, precise and reliable method across different vendors and centers. It has previously been validated in humans using MPS as reference standard and has been compared head-to-head with T2w imaging. However, Paper I of this thesis is the first to validate the use of CE-SSFP experimentally [29, 159]. Experimental validation is necessary to ensure the appropriateness in using the technique for future experimental models. Maybe more importantly, it provides stronger evidence that the technique is accurate compared to validation in patients alone. The experimental model is controlled and standardized in a way which is not feasible in patients. It is also possible to study the heart histologically to, for example, visualize infarct size independently of any MR-based methods.

While using contrast in conjunction with SSFP imaging to determine MaR is relatively

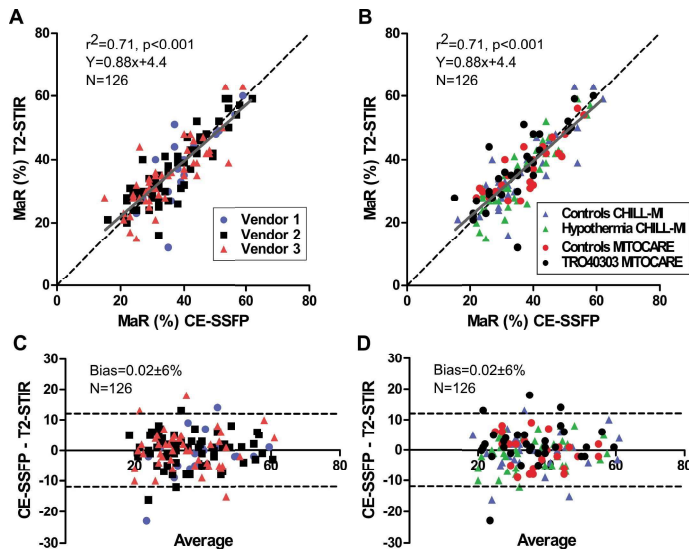


Figure 4.4: Myocardium at risk by T2-STIR and CE-SSFP. (A) MaR by T2-STIR vs. CE-SSFP divided by vendors, $r^2 \approx 0.71$. (B) MaR by T2-STIR vs. CE-SSFP divided by treatment groups. Dashed lines are identity and solid lines regression. (C) The Bland–Altman plot of CE-SSFP and T2-STIR divided by vendors, and (D) the Bland–Altman plot of CE-SSFP and T2-STIR divided by treatment groups, mean difference $0.02\pm6\%$, dashed lines indicate $\pm 2SD$. Measurements are expressed as % of LV mass. MaR, myocardium at risk.

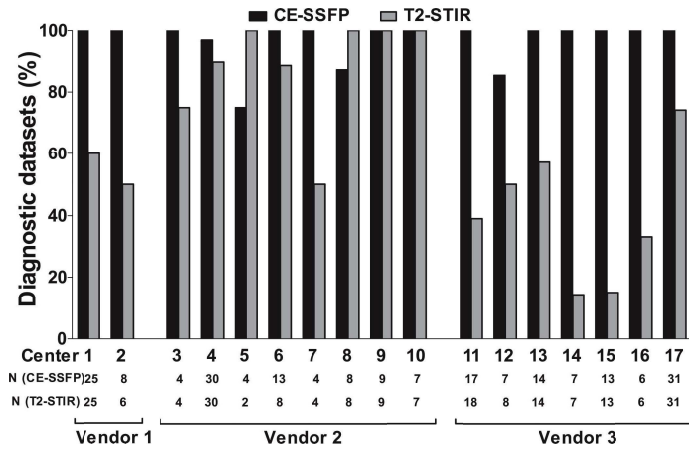


Figure 4.5: Datasets of diagnostic quality divided by site. All 17 sites that participated in the CHILL-MI and MITOCARE trials are represented. Numbers are expressed as per cent of total datasets. Note that CE-SSFP had a higher rate of images of diagnostic quality compared with T2-STIR in 13 of the sites.

new, SSFP imaging has been used for many decades in different contexts [29]. Since it is a useful sequence that has been used for a long time it has been thoroughly developed and tested for a broad range of vendors and applications. In contrast, T2-STIR has more limited and specialized applications and since imaging MaR has not been a priority in clinical routine it could be speculated to not have been as fully developed and tested on all systems. Additionally it requires the timing of 3 different sets of pulses to match the properties of blood and fat for maximum quality while the steady-state signal of CE-SSFP is reached irrespective of timing (though it is of course not completely insensitive to timing). As the name implies, CE-SSFP uses gadolinium-based contrast to accentuate the differences between MaR and remote myocardium. As this increases the physical difference between MaR and remote it may not be far fetched to imagine that it would be easier to detect more consistently than the non-contrast enhanced techniques.

In the light of thorough validation and high degree of reliability CE-SSFP is an appealing choice for quantifying MaR in studies where CMR is available. Other methods such as T1- or T2-mapping have been proposed as possible alternatives [156, 157]. These are promising in that they may offer more objective and reproducible ways to determine MaR but a lot of work remains before they are validated and standardized to a degree which make them reliable enough for clinical trials.

Validation and reliability aside, the mechanism behind tissue contrast in CE-SSFP still remains largely unknown and is the subject of speculation. Understanding the mechanism will be important when applying CE-SSFP in different populations. It is, for example, conceivable that a potential cardioprotective treatment may affect the measurement of MaR in itself [189, 190]. The more we understand about what underlies generation tissue contrast, the more it will be possible to predict challenges such as these and design trials accordingly.

4.3 Extent of coronary perfusion

Paper II used the extent of MaR by CE-SSFP and T2-STIR to map the coronary perfusion territories. The results are presented in Figure 4.6. These were then visually compared to previous work using MPS (Figure 4.7).

Discussion

The available data on coronary perfusion areas in humans have previously largely been attained either from studies of coronary anatomy or have been studied using MPS. While it is possible to collect data on coronary anatomy in a large number of patients through for example coronary angiography or CT, it is not possible to depict smaller vessels in the myocardium using these methods. Therefore any conclusions regarding coronary perfusion will be rough estimations. As for MPS, the logistical challenges involved, such as handling of isotopes and need to inject during coronary occlusion, result in studies with few patients and technical limitations result in a low effective spatial resolution [191, 192]. Paper III of

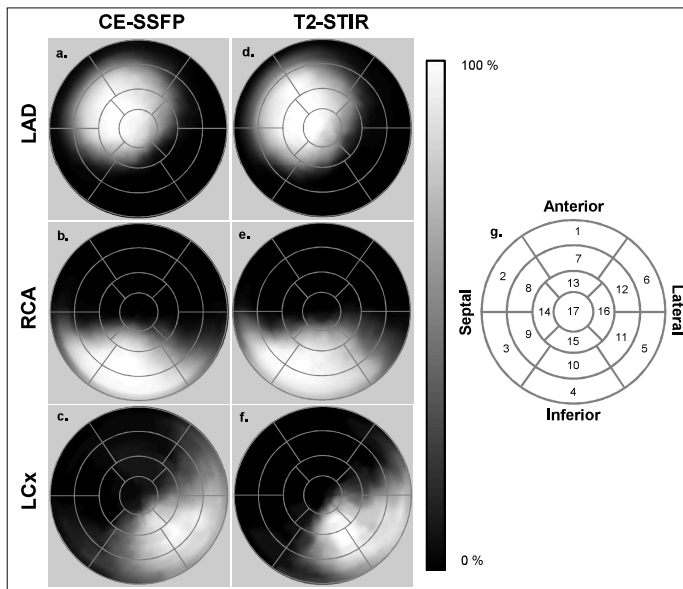


Figure 4.6: Polar plots of myocardium at risk (MaR). On the left are average contrastenhanced steady state free precession (CE-SSFP) polar plots of (a) the left anterior descending artery (LAD), using 78 patients (b) the right coronary artery (RCA), using 99 patients, and (c) the left circumflex artery (LCx), using 25 patients. The polar plots on the right use T2-weighted short tau inversion recovery (T2-STIR) to show (d) the LAD, using 61 patients (e) the RCA, using 69 patients, and (f) the LCx, using 17 patients. The intensity of the plots reflect the fraction of patients with MaR in that area as shown on the bar that ranges from 0% to 100%. For reference purposes, the 17-segment model is shown in g.

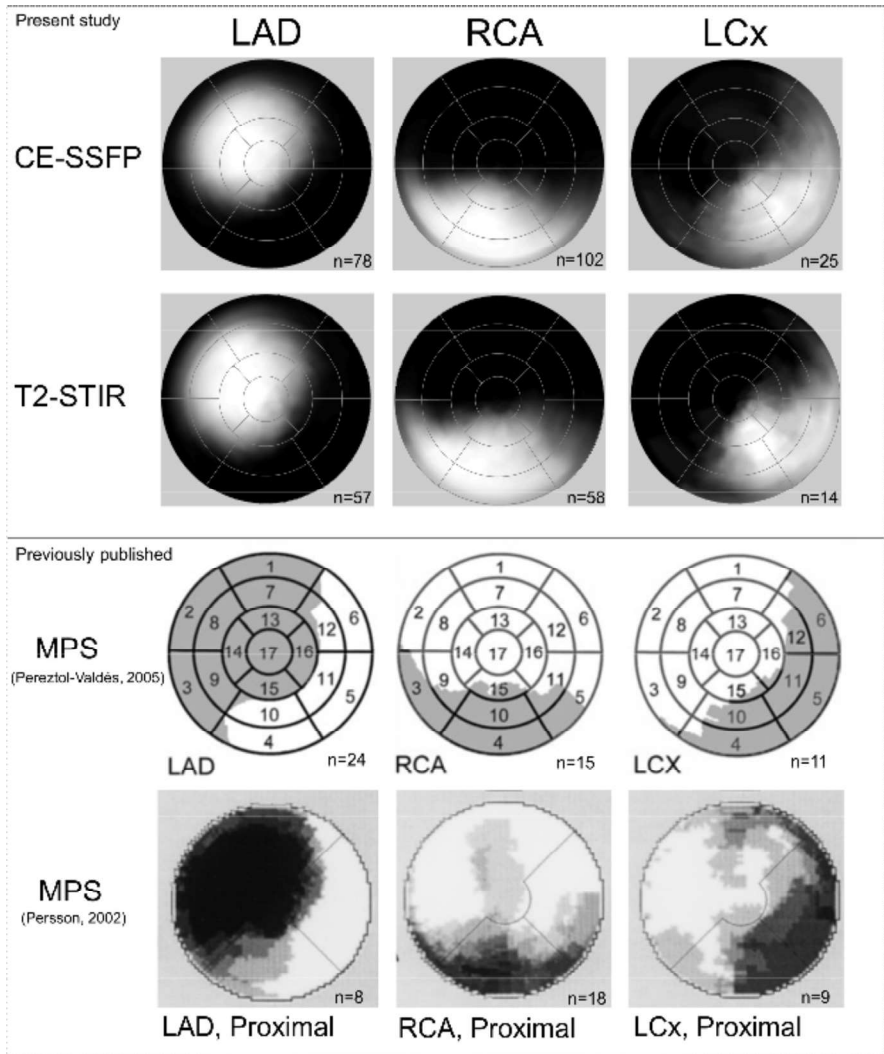


Figure 4.7: Polar plots, comparison between cardiovascular magnetic resonance (CMR) and myocardial perfusion single-photon emission computed tomography (MPS). The first and second rows show contrast-enhanced steady state free precession (CE-SSFP) and T2-weighted short tau inversion recovery (T2-STIR) images from the present study. The third row shows maximal extent of perfusion territories using MPS (Pereztol-Valdés et al [191]). The fourth row shows perfusion territories also using MPS (Persson et al [192]). The left column shows left anterior descending artery (LAD), the middle column right coronary artery (RCA), and the right column left circumflex coronary artery (LCx). The intensity of the plot is proportional to the fraction of patients with myocardium at risk in that area.

Chapter 5

Conclusions

Words can be meaningless. If they are used in such a way that no sharp conclusion can be drawn.

Richard Feynman, *The meaning of it all: Thoughts of a citizen-scientist*, 1963

- Contrast-enhanced SSFP cine CMR imaging can be used to measure MaR, both *in vivo* and *ex vivo*, in a porcine model with good accuracy and precision over the first 30 min after contrast injection. This offers the option to use the less complex *ex-vivo* imaging when determining myocardial salvage in experimental studies. (Paper I)
- In data from three multi-center trials and in images of diagnostic quality, T2-STIR and CE-SSFP provided similar estimates of MaR, were constant over the first week, and were not affected by treatment. (Paper II)
- CE-SSFP had a higher degree of diagnostic quality images compared with T2 imaging for sequences from two out of the three vendors based on data from three multi-center trials. Therefore, CE-SSFP is currently more suitable for implementation in multicentre, multi-vendor clinical trials. (Paper II)
- The coronary perfusion territories for the 3 main coronary arteries LAD, RCA, and LCx were visualized using CE-SSFP and T2-STIR. The agreement with MPS, which acts by a different mechanism, makes it likely that these 3 methods depict MaR accurately. (Paper III)
- Female gender, but not diabetes, hypertension or smoking, was associated with smaller infarct size and higher myocardial salvage when adjusting for confounders, suggesting a pathophysiological difference in infarct evolution between men and women. (Paper IV)

...I don't think it was for reading. It was for having written...

Terry Pratchett

References

- [1] Chow D. C., Wenning L. A., Miller W. M., and Papoutsakis E. T. Modeling pO₂ distributions in the bone marrow hematopoietic compartment. I. Krogh's model. *Biophysical Journal*, 81(2):675–684, 2001.
- [2] Harvey W. *Exercitatio anatomica de motu cordis et sanguinis in animalibus*. 1628.
- [3] Keele K. D. Leonardo da Vinci's views on arteriosclerosis. *Medical history*, 17(3): 304–8, 1973.
- [4] Osler W. *Lectures on angina pectoris and allied states*. Appleton and Company, New York, 1897.
- [5] Fletcher A. P., Alkjaersig N., Smyrniotis F. E., and Sherry S. The treatment of patients suffering from early myocardial infarction with massive and prolonged streptokinase therapy. *Transactions of the Association of American Physicians*, 71:287–96, 1958.
- [6] Grüntzig A. R., Senning Ø., and Siegenthaler W. E. Nonoperative dilatation of coronary-artery stenosis. *New England Journal of Medicine*, 301(2):61–68, 1979.
- [7] Rosamond W. D., Chambless L. E., Folsom A. R., Cooper L. S., Conwill D. E., Clegg L., Wang C. H., and Heiss G. Trends in the incidence of myocardial infarction and in mortality due to coronary heart disease, 1987 to 1994. *The New England journal of medicine*, 339(13):861–7, 1998.
- [8] McGovern P. G., Jacobs D. R., Shahar E., Arnett D. K., Folsom A. R., Blackburn H., and Luepker R. V. Trends in acute coronary heart disease mortality, morbidity, and medical care from 1985 through 1997: the Minnesota heart survey. *Circulation*, 104(1):19–24, 2001.
- [9] GBD 2013 Mortality and Causes of Death Collaborators. Global, regional, and national age-sex specific all-cause and cause-specific mortality for 240 causes of death, 1990–2013: a systematic analysis for the Global Burden of Disease Study 2013. *Lancet (London, England)*, 385(9963):117–71, 2015.

- [10] Heyndrickx G. R., Millard R. W., McRitchie R. J., Maroko P. R., and Vatner S. F. Regional myocardial functional and electrophysiological alterations after brief coronary artery occlusion in conscious dogs. *Journal of Clinical Investigation*, 56(4): 978–985, 1975.
- [11] Bolli R., Jeroudi M. O., Patel B. S., Aruoma O. I., Halliwell B., Lai E. K., and McCay P. B. Marked reduction of free radical generation and contractile dysfunction by antioxidant therapy begun at the time of reperfusion. Evidence that myocardial “stunning” is a manifestation of reperfusion injury. *Circulation research*, 65(3):607–22, 1989.
- [12] Sörensson P., Saleh N., Bouvier F., Böhm F., Settergren M., Caidahl K., Tornvall P., Arheden H., Rydén L., and Pernow J. Effect of postconditioning on infarct size in patients with ST elevation myocardial infarction. *Heart (British Cardiac Society)*, 96 (21):1710–5, 2010.
- [13] Cung T.-T., Morel O., Cayla G., Rioufol G., Garcia-Dorado D., Angoulvant D., Bonnefoy-Cudraz E., Guérin P., Elbaz M., Delarche N., Coste P., Vanzetto G., Metge M., Aupetit J.-F., Jouve B., Motreff P., Tron C., Labeque J.-N., Steg P. G., Cottin Y., Range G., Clerc J., Claeys M. J., Coussement P., Prunier F., Moulin F., Roth O., Belle L., Dubois P., Barragan P., Gilard M., Piot C., Colin P., De Poli F., Morice M.-C., Ider O., Dubois-Randé J.-L., Untersee T., Le Breton H., Béard T., Blanchard D., Grollier G., Malquarti V., Staat P., Sudre A., Elmer E., Hansson M. J., Bergerot C., Boussaha I., Jossan C., Derumeaux G., Mewton N., and Ovize M. Cyclosporine before PCI in patients with acute myocardial infarction. *New England Journal of Medicine*, 373(11):1021–1031, 2015.
- [14] Stone G. W., Martin J. L., de Boer M.-J., Margheri M., Bramucci E., Blankenship J. C., Metzger D. C., Gibbons R. J., Lindsay B. S., Weiner B. H., Lansky A. J., Krucoff M. W., Fahy M., Boscardin W. J., and AMIHOT-II Trial Investigators. Effect of supersaturated oxygen delivery on infarct size after percutaneous coronary intervention in acute myocardial infarction. *Circulation. Cardiovascular interventions*, 2 (5):366–75, 2009.
- [15] Kitakaze M., Asakura M., Kim J., Shintani Y., Asanuma H., Hamasaki T., Seguchi O., Myoishi M., Minamino T., Ohara T., Nagai Y., Nanto S., Watanabe K., Fukuzawa S., Hirayama A., Nakamura N., Kimura K., Fujii K., Ishihara M., Saito Y., Tomoike H., Kitamura S., and J-WIND investigators. Human atrial natriuretic peptide and nicorandil as adjuncts to reperfusion treatment for acute myocardial infarction (J-WIND): two randomised trials. *Lancet (London, England)*, 370(9597): 1483–93, 2007.
- [16] Mahaffey K. W., Puma J. A., Barbagelata N. A., DiCarli M. F., Leesar M. A.,

- Browne K. F., Eisenberg P. R., Bolli R., Casas A. C., Molina-Viamonte V., Orlandi C., Blevins R., Gibbons R. J., Califf R. M., and Granger C. B. Adenosine as an adjunct to thrombolytic therapy for acute myocardial infarction: results of a multicenter, randomized, placebo-controlled trial: the Acute Myocardial Infarction Study of Adenosine (AMISTAD) trial. *Journal of the American College of Cardiology*, 34(6):1711–20, 1999.
- [17] Ross A. M., Gibbons R. J., Stone G. W., Kloner R. A., Alexander R. W., and AMISTAD-II Investigators. A randomized, double-blinded, placebo-controlled multicenter trial of adenosine as an adjunct to reperfusion in the treatment of acute myocardial infarction (AMISTAD-II). *Journal of the American College of Cardiology*, 45(11):1775–80, 2005.
- [18] O'Neill W. W., Martin J. L., Dixon S. R., Bartorelli A. L., Trabattoni D., Oemrawsingh P. V., Atsma D. E., Chang M., Marquardt W., Oh J. K., Krucoff M. W., Gibbons R. J., Spears J. R., and AMIHOT Investigators. Acute Myocardial Infarction with Hyperoxemic Therapy (AMIHOT): a prospective, randomized trial of intracoronary hyperoxemic reperfusion after percutaneous coronary intervention. *Journal of the American College of Cardiology*, 50(5):397–405, 2007.
- [19] GISSI-3: effects of lisinopril and transdermal glyceryl trinitrate singly and together on 6-week mortality and ventricular function after acute myocardial infarction. Gruppo Italiano per lo Studio della Sopravvivenza nell'infarto Miocardico. *Lancet (London, England)*, 343(8906):1115–22, 1994.
- [20] ISIS-4: a randomised factorial trial assessing early oral captopril, oral mononitrate, and intravenous magnesium sulphate in 58,050 patients with suspected acute myocardial infarction. ISIS-4 (Fourth International Study of Infarct Survival) Collaborative. *Lancet (London, England)*, 345(8951):669–85, 1995.
- [21] Atar D., Arheden H., Berdeaux A., Bonnet J.-L., Carlsson M., Clemmensen P., Cuvier V., Danchin N., Dubois-Rande J.-L., Engblom H., Erlinge D., Firat H., Halvorsen S., Hansen H. S., Hauke W., Heiberg E., Koul S., Larsen A.-I., Le Corvoisier P., Nordrehaug J. E., Paganelli F., Pruss R. M., Rousseau H., Schaller S., Sonou G., Tuseth V., Veys J., Vicaut E., and Jensen S. E. Effect of intravenous TRO40303 as an adjunct to primary percutaneous coronary intervention for acute ST-elevation myocardial infarction: MITOCARE study results. *European Heart Journal*, 36(2):112–119, 2015.
- [22] Odeblad E. and Lindstrom G. Some Preliminary Observations on the Proton Magnetic Resonance in Biologic Samples. *Acta Radiologica*, 43(6):469–476, 1955.
- [23] Hahn E. L. Spin Echoes. *Physical Review*, 80(4):580–594, 1950.

- [24] Lauterbur P. C. Image formation by induced local interactions: examples employing nuclear magnetic resonance. *Nature*, 242(5394):190–191, 1973.
- [25] Kim R. J., Hillenbrand H. B., and Judd R. M. Evaluation of myocardial viability by MRI. *Herz*, 25(4):417–30, 2000.
- [26] Arheden H., Saeed M., Higgins C. B., Gao D. W., Ursell P. C., Bremerich J., Wyttenbach R., Dae M. W., and Wendland M. F. Reperfused rat myocardium subjected to various durations of ischemia: estimation of the distribution volume of contrast material with echo-planar MR imaging. *Radiology*, 215(2):520–8, 2000.
- [27] Aletras A. H., Tilak G. S., Natanzon A., Hsu L.-Y., Gonzalez F. M., Hoyt R. F. J., and Arai A. E. Retrospective determination of the area at risk for reperfused acute myocardial infarction with T2-weighted cardiac magnetic resonance imaging: histopathological and displacement encoding with stimulated echoes (DENSE) functional validations. *Circulation*, 113(15):1865–1870, 2006.
- [28] Carlsson M., Ubachs J. F. A., Hedström E., Heiberg E., Jovinge S., and Arheden H. Myocardium at risk after acute infarction in humans on cardiac magnetic resonance: quantitative assessment during follow-up and validation with single-photon emission computed tomography. *JACC. Cardiovascular imaging*, 2(5):569–576, 2009.
- [29] Sörensson P., Heiberg E., Saleh N., Bouvier F., Caidahl K., Tornvall P., Rydén L., Pernow J., and Arheden H. Assessment of myocardium at risk with contrast enhanced steady-state free precession cine cardiovascular magnetic resonance compared to single-photon emission computed tomography. *Journal of Cardiovascular Magnetic Resonance*, 12(1):25, 2010.
- [30] Thygesen K., Alpert J. S., Jaffe A. S., Simoons M. L., Chaitman B. R., and White H. D. Third universal definition of myocardial infarction. *Circulation*, 126(16):2020–2035, 2012.
- [31] Davies M. J. Anatomic features in victims of sudden coronary death. Coronary artery pathology. *Circulation*, 85(1 Suppl):19–24, 1992.
- [32] DeWood M. A., Spores J., Notske R., Mouser L. T., Burroughs R., Golden M. S., and Lang H. T. Prevalence of total coronary occlusion during the early hours of transmural myocardial infarction. *New England Journal of Medicine*, 303(16):897–902, 1980.
- [33] van der Wal A. C., Becker A. E., van der Loos C. M., and Das P. K. Site of intimal rupture or erosion of thrombosed coronary atherosclerotic plaques is characterized by an inflammatory process irrespective of the dominant plaque morphology. *Circulation*, 89(1):36–44, 1994.

- [34] Farb A., Burke A. P., Tang A. L., Liang T. Y., Mannan P., Smialek J., and Virmani R. Coronary plaque erosion without rupture into a lipid core. A frequent cause of coronary thrombosis in sudden coronary death. *Circulation*, 93(7):1354–63, 1996.
- [35] Khan N. A., Daskalopoulou S. S., Karp I., Eisenberg M. J., Pelletier R., Tsadok M. A., Dasgupta K., Norris C. M., Pilote L., and GENESIS PRAXY Team. Sex differences in prodromal symptoms in acute coronary syndrome in patients aged 55 years or younger. *Heart (British Cardiac Society)*, 103(11):863–869, 2017.
- [36] Stone G. W., Machara A., Lansky A. J., de Bruyne B., Cristea E., Mintz G. S., Mehran R., McPherson J., Farhat N., Marso S. P., Parise H., Templin B., White R., Zhang Z., and Serruys P. W. A prospective natural-history study of coronary atherosclerosis. *The New England journal of medicine*, 364(3):226–235, 2011.
- [37] Angelini P., Villason S., Chan Jr. A. V., and Diez J. G. *Normal and anomalous coronary arteries in humans. In: Coronary artery anomalies: a comprehensive approach.* Lippincott Williams & Wilkins, Philadelphia, 1999.
- [38] Perlmutter L. M., Jay M. E., and Levin D. C. Variations in the blood supply of the left ventricular apex. *Investigative radiology*, 18(2):138–40.
- [39] Baroldi G. and Scomazzoni G. *Coronary circulation in the normal and the pathologic heart.* Office of the Surgeon General, Dept. of the Army, 2 edition, 1967.
- [40] Reimer K. A., Lowe J. E., Rasmussen M. M., and Jennings R. B. The wavefront phenomenon of ischemic cell death. 1. Myocardial infarct size vs duration of coronary occlusion in dogs. *Circulation*, 56(5):786–794, 1977.
- [41] Reimer K. A. and Jennings R. B. The "wavefront phenomenon" of myocardial ischemic cell death. II. Transmural progression of necrosis within the framework of ischemic bed size (myocardium at risk) and collateral flow. *Laboratory Investigation; a Journal of Technical Methods and Pathology*, 40(6):633–644, 1979.
- [42] Becker L. C., Fortuin N. J., and Pitt B. Effect of ischemia and antianginal drugs on the distribution of radioactive microspheres in the canine left ventricle. *Circulation research*, 28(2):263–9, 1971.
- [43] Dunn R. B. and Griggs D. M. Transmural gradients in ventricular tissue metabolites produced by stopping coronary blood flow in the dog. *Circulation research*, 37(4): 438–45, 1975.
- [44] Leshnower B. G., Sakamoto H., Hamamoto H., Zeeshan A., Gorman J. H., and Gorman R. C. Progression of myocardial injury during coronary occlusion in the collateral-deficient heart: a non-wavefront phenomenon. *AJP: Heart and Circulatory Physiology*, 293(3):H1799–H1804, 2007.

- [45] Hedström E., Engblom H., Frogner E., Aström-Olsson K., Ohlin H., Jovinge S., and Arheden H. Infarct evolution in man studied in patients with first-time coronary occlusion in comparison to different species - implications for assessment of myocardial salvage. *Journal of cardiovascular magnetic resonance : official journal of the Society for Cardiovascular Magnetic Resonance*, 11:38, 2009.
- [46] Arheden H., Saeed M., Higgins C. B., Gao D. W., Ursell P. C., Bremerich J., Wyttenbach R., Dae M. W., and Wendland M. F. Reperfused rat myocardium subjected to various durations of ischemia: estimation of the distribution volume of contrast material with echo-planar MR imaging. *Radiology*, 215(2):520–528, 2000.
- [47] Reimer K. A., Vander Heide R. S., and Richard V. J. Reperfusion in acute myocardial infarction: effect of timing and modulating factors in experimental models. *The American journal of cardiology*, 72(19):13G–21G, 1993.
- [48] Fujiwara H., Matsuda M., Fujiwara Y., Ishida M., Kawamura A., Takemura G., Kida M., Uegaito T., Tanaka M., and Horike K. Infarct size and the protection of ischemic myocardium in pig, dog and human. *Japanese circulation journal*, 53(9): 1092–7, 1989.
- [49] Hale S. L. and Kloner R. A. Effect of early coronary artery reperfusion on infarct development in a model of low collateral flow. *Cardiovascular research*, 21(9):668–73, 1987.
- [50] Kloner R. A., Ellis S. G., Lange R., and Braunwald E. Studies of experimental coronary artery reperfusion. Effects on infarct size, myocardial function, biochemistry, ultrastructure and microvascular damage. *Circulation*, 68(2 Pt 2):8–15, 1983.
- [51] Näslund U., Häggmark S., Johansson G., Pennert K., Reiz S., and Marklund S. L. Effects of reperfusion and superoxide dismutase on myocardial infarct size in a closed chest pig model. *Cardiovascular research*, 26(2):170–8, 1992.
- [52] Aquaro G. D., Pingitore A., Strata E., Di Bella G., Palmieri C., Rovai D., Petronio A. S., L'Abbate A., and Lombardi M. Relation of pain-to-balloon time and myocardial infarct size in patients transferred for primary percutaneous coronary intervention. *The American journal of cardiology*, 100(1):28–34, 2007.
- [53] Maxwell M. P., Hearse D. J., and Yellon D. M. Species variation in the coronary collateral circulation during regional myocardial ischaemia: a critical determinant of the rate of evolution and extent of myocardial infarction. *Cardiovascular research*, 21(10):737–46, 1987.
- [54] Widimský P., Groch L., Zelízko M., Aschermann M., Bednár F., and Suryapranata H. Multicentre randomized trial comparing transport to primary angioplasty vs

- immediate thrombolysis vs combined strategy for patients with acute myocardial infarction presenting to a community hospital without a catheterization laboratory. The PRAGUE study. *European heart journal*, 21(10):823–31, 2000.
- [55] Magid D. J., Calonge B. N., Rumsfeld J. S., Canto J. G., Frederick P. D., Every N. R., Barron H. V., and National Registry of Myocardial Infarction 2 and 3 Investigators. Relation between hospital primary angioplasty volume and mortality for patients with acute MI treated with primary angioplasty vs thrombolytic therapy. *JAMA*, 284(24):3131–8, 2000.
- [56] Grines C. L., Westerhausen D. R., Grines L. L., Hanlon J. T., Logemann T. L., Niemela M., Weaver W. D., Graham M., Boura J., O'Neill W. W., Balestrini C., and Air PAMI Study Group. A randomized trial of transfer for primary angioplasty versus on-site thrombolysis in patients with high-risk myocardial infarction: the Air Primary Angioplasty in Myocardial Infarction study. *Journal of the American College of Cardiology*, 39(11):1713–9, 2002.
- [57] Ibanez B., James S., Agewall S., Antunes M. J., Bucciarelli-Ducci C., Bueno H., Caforio A. L. P., Crea F., Goudevenos J. A., Halvorsen S., Hindricks G., Kastrati A., Lenzen M. J., Prescott E., Roffi M., Valgimigli M., Varenhorst C., Vranckx P., and Widimský P. 2017 ESC Guidelines for the management of acute myocardial infarction in patients presenting with ST-segment elevation. *European Heart Journal*, 00:1–66, 2017.
- [58] Roffi M., Patrono C., Collet J.-P., Mueller C., Valgimigli M., Andreotti F., Bax J. J., Borger M. A., Brotons C., Chew D. P., Gencer B., Hasenfuss G., Kjeldsen S., Landmesser U., Landmesser U., Mchilli J., Mukherjee D., Storey R. F., and Windecker S. 2015 ESC Guidelines for the management of acute coronary syndromes in patients presenting without persistent ST-segment elevation. *European Heart Journal*, 37(3): 267–315, 2016.
- [59] Embden G., Deuticke H. J., and Kraft G. Über die intermediären vorgänge bei der glykolyse in der muskulatur. *Klinische Wochenschrift*, 12(6):213–215, 1933.
- [60] Annau E., Banga I., Göszy B., Huszák S., Laki K., Straub B., and Szent-Györgyi A. Über die bedeutung der fumarsäure für die tierische gewebssatmung. *Hoppe-Seyler's Ztschr. f. physiolog. Chem.*, 1935.
- [61] Krebs H. A. and Johnson W. A. Metabolism of ketonic acids in animal tissues. *The Biochemical journal*, 31(4):645–60, 1937.
- [62] Lehninger A. L. Letters to the Editors : Fatty acid oxidation and the Krebs tricarboxylic acid cycle. *J. Biol. Chem.*, 161:413–414, 1945.

- [63] Lehninger A. L. The oxidation of higher fatty acids in heart muscle suspensions. *The Journal of biological chemistry*, 165(1):131–145, 1946.
- [64] Jennings R. B. and Ganote C. E. Mitochondrial structure and function in acute myocardial ischemic injury. *Circulation research*, 38(5 Suppl 1):80–91, 1976.
- [65] Jennings R. B. and Ganote C. E. Structural changes in myocardium during acute ischemia. *Circulation research*, 35 Suppl 3:156–72, 1974.
- [66] Garlid K. D. and Paucek P. Mitochondrial potassium transport: the K(+) cycle. *Biochimica et biophysica acta*, 1606(1-3):23–41, 2003.
- [67] Gao W., Pu Y., Luo K. Q., and Chang D. C. Temporal relationship between cytochrome c release and mitochondrial swelling during UV-induced apoptosis in living HeLa cells. *Journal of cell science*, 114(Pt 15):2855–62, 2001.
- [68] Mannella C. A., Pfeiffer D. R., Bradshaw P. C., Moraru I. I., Slepchenko B., Loew L. M., Hsieh C. E., Buttler K., and Marko M. Topology of the mitochondrial inner membrane: dynamics and bioenergetic implications. *IUBMB life*, 52(3-5):93–100.
- [69] Haworth R. A. and Hunter D. R. The Ca²⁺-induced membrane transition in mitochondria. II. Nature of the Ca²⁺ trigger site. *Archives of biochemistry and biophysics*, 195(2):460–7, 1979.
- [70] Gogvadze V., Robertson J. D., Enoksson M., Zhivotovsky B., and Orrenius S. Mitochondrial cytochrome c release may occur by volume-dependent mechanisms not involving permeability transition. *Biochemical Journal*, 378(1):213–217, 2004.
- [71] Costa A. D. T., Quinlan C. L., Andrukhiv A., West I. C., Jabůrek M., and Garlid K. D. The direct physiological effects of mitoK(ATP) opening on heart mitochondria. *American journal of physiology. Heart and circulatory physiology*, 290(1):406–15, 2006.
- [72] Garlid K. D., Dos Santos P., Xie Z.-J., Costa A. D. T., and Paucek P. Mitochondrial potassium transport: the role of the mitochondrial ATP-sensitive K(+) channel in cardiac function and cardioprotection. *Biochimica et biophysica acta*, 1606(1-3):1–21, 2003.
- [73] Vághy P. L. Role of mitochondrial oxidative phosphorylation in the maintenance of intracellular pH. *Journal of molecular and cellular cardiology*, 11(10):933–40, 1979.
- [74] Robergs R. A., Ghiasvand F., and Parker D. Biochemistry of exercise-induced metabolic acidosis. *American journal of physiology. Regulatory, integrative and comparative physiology*, 287(3):502–16, 2004.

- [75] Steenbergen C., Hill M. L., and Jennings R. B. Volume regulation and plasma membrane injury in aerobic, anaerobic, and ischemic myocardium in vitro. Effects of osmotic cell swelling on plasma membrane integrity. *Circulation research*, 57(6): 864–875, 1985.
- [76] Inscerte J., Garcia-Dorado D., Ruiz-Meana M., Solares J., and Soler J. The role of Na^+/H^+ exchange occurring during hypoxia in the genesis of reoxygenation-induced myocardial oedema. *Journal of molecular and cellular cardiology*, 29(4):1167–1175, 1997.
- [77] Anderson S. E., Murphy E., Steenbergen C., London R. E., and Cala P. M. Na^+/H^+ exchange in myocardium: effects of hypoxia and acidification on Na^+ and Ca^{2+} . *The American journal of physiology*, 259(6 Pt 1):940–8, 1990.
- [78] Klein H. H., Pich S., Bohle R. M., Wollenweber J., and Nebendahl K. Myocardial protection by Na^+/H^+ exchange inhibition in ischemic, reperfused porcine hearts. *Circulation*, 92(4):912–7, 1995.
- [79] Kloner R. A., Ganote C. E., Whalen D. A., and Jennings R. B. Effect of a transient period of ischemia on myocardial cells. II. Fine structure during the first few minutes of reflow. *The American journal of pathology*, 74(3):399–422, 1974.
- [80] Kelley K. O. and Gould K. L. Coronary reactive hyperaemia after brief occlusion and after deoxygenated perfusion. *Cardiovascular research*, 15(11):615–22, 1981.
- [81] Olivecrona G. K., Gotberg M., Harnek J., Wang L., Jacobson K. A., and Erlinge D. Coronary artery reperfusion: The ADP receptor P2Y_1 mediates early reactive hyperemia in vivo in pigs. *Purinergic Signalling*, 1(1):59–65, 2004.
- [82] Green H. D. and Wégria R. Effects of asphyxia, anoxia and myocardial ischemia on the coronary blood flow. *American Journal of Physiology – Legacy Content*, 135(2): 271 LP – 280, 1941.
- [83] Gryglewski R. J., Chlopicki S., Niezabitowski P., Jakubowski A., and Lomnicka M. Ischaemic cardiac hyperaemia: role of nitric oxide and other mediators. *Physiological research*, 45(4):255–60, 1996.
- [84] Zatta A. J. and Headrick J. P. Mediators of coronary reactive hyperaemia in isolated mouse heart. *British journal of pharmacology*, 144(4):576–87, 2005.
- [85] Kingsbury M. P., Robinson H., Flores N. A., and Sheridan D. J. Investigation of mechanisms that mediate reactive hyperaemia in guinea-pig hearts: role of K^+/ATP channels, adenosine, nitric oxide and prostaglandins. *British journal of pharmacology*, 132(6):1209–16, 2001.

- [86] Saito D., Steinhart C. R., Nixon D. G., and Olsson R. A. Intracoronary adenosine deaminase reduces canine myocardial reactive hyperemia. *Circulation research*, 49(6):1262–7, 1981.
- [87] Higginson L. A., White F., Heggteit H. A., Sanders T. M., Bloor C. M., and Covell J. W. Determinants of myocardial hemorrhage after coronary reperfusion in the anesthetized dog. *Circulation*, 65(1):62–69, 1982.
- [88] Kurbel S., Kurbel B., Belovari T., Marić S., Steiner R., and Božić D. Model of interstitial pressure as a result of cyclical changes in the capillary wall fluid transport. *Medical hypotheses*, 57(2):161–6, 2001.
- [89] Whalen D. A., Hamilton D. G., Ganote C. E., and Jennings R. B. Effect of a transient period of ischemia on myocardial cells. I. Effects on cell volume regulation. *The American journal of pathology*, 74(3):381–97, 1974.
- [90] Kasseckert S. A., Schäfer C., Kluger A., Gligorievski D., Tillmann J., Schlüter K.-D., Noll T., Sauer H., Piper H. M., and Abdallah Y. Stimulation of cGMP signalling protects coronary endothelium against reperfusion-induced intercellular gap formation. *Cardiovascular research*, 83(2):381–7, 2009.
- [91] Warth A., Eckle T., Köhler D., Faigle M., Zug S., Klingel K., Eltzhig H. K., and Wolburg H. Upregulation of the water channel aquaporin-4 as a potential cause of postischemic cell swelling in a murine model of myocardial infarction. *Cardiology*, 107(4):402–10, 2007.
- [92] Severs N. J., Dupont E., Thomas N., Kaba R., Rothery S., Jain R., Sharpey K., and Fry C. H. Alterations in cardiac connexin expression in cardiomyopathies. In *Cardiovascular Gap Junctions*, pages 228–242. KARGER, Basel, 2006.
- [93] Rodríguez-Sinovas A., Sánchez J. A., Fernandez-Sanz C., Ruiz-Meana M., and Garcia-Dorado D. Connexin and pannexin as modulators of myocardial injury. *Biochimica et biophysica acta*, 1818(8):1962–70, 2012.
- [94] Crompton M., Costi A., and Hayat L. Evidence for the presence of a reversible Ca^{2+} -dependent pore activated by oxidative stress in heart mitochondria. *The Biochemical journal*, 245(3):915–8, 1987.
- [95] Kloner R. A., Giacomelli F., Alker K. J., Hale S. L., Matthews R., and Bellows S. Influx of neutrophils into the walls of large epicardial coronary arteries in response to ischemia/reperfusion. *Circulation*, 84(4):1758–1772, 1991.
- [96] Vermeiren G. L., Claeys M. J., Van Bockstaele D., Grobбен B., Slegers H., Bossaert L., and Jorens P. G. Reperfusion injury after focal myocardial ischaemia: polymorphonuclear leukocyte activation and its clinical implications. *Resuscitation*, 45(1):35–61, 2000.

- [97] Buja L. M., Hagler H. K., and Willerson J. T. Altered calcium homeostasis in the pathogenesis of myocardial ischemic and hypoxic injury. *Cell calcium*, 9(5-6):205–17, 1988.
- [98] Kloner R. A., Ganote C. E., and Jennings R. B. The “no-reflow” phenomenon after temporary coronary occlusion in the dog. *Journal of Clinical Investigation*, 54(6): 1496–1508, 1974.
- [99] Jennings R. B., Schaper J., Hill M. L., Steenbergen C., and Reimer K. A. Effect of reperfusion late in the phase of reversible ischemic injury. Changes in cell volume, electrolytes, metabolites, and ultrastructure. *Circulation Research*, 56(2):262–278, 1985.
- [100] Arheden H., Saced M., Higgins C. B., Gao D. W., Bremerich J., Wyttenbach R., Dae M. W., and Wendland M. F. Measurement of the distribution volume of gadopentetate dimeglumine at echo-planar MR imaging to quantify myocardial infarction: comparison with 99mTc-DTPA autoradiography in rats. *Radiology*, 211(3):698–708, 1999.
- [101] Jablonowski R., Engblom H., Kanski M., Nordlund D., Koul S., van der Pals J., Englund E., Heiberg E., Erlinge D., Carlsson M., and Arheden H. Contrast-enhanced CMR overestimates early myocardial infarct size: mechanistic insights using ECV measurements on day 1 and day 7. *JACC. Cardiovascular imaging*, 8(12):1379–89, 2015.
- [102] Fischer U. M., Cox C. S., Stewart R. H., Laine G. A., and Allen S. J. Impact of acute myocardial edema on left ventricular function. *Journal of investigative surgery : the official journal of the Academy of Surgical Research*, 19(1):31–8.
- [103] Desai K. V., Laine G. A., Stewart R. H., Cox C. S., Quick C. M., Allen S. J., and Fischer U. M. Mechanics of the left ventricular myocardial interstitium: effects of acute and chronic myocardial edema. *AJP: Heart and Circulatory Physiology*, 294(6): H2428–H2434, 2008.
- [104] Follette D. M., Fey K., Buckberg G. D., Helly J. J., Steed D. L., Foglia R. P., and Maloney J. V. Reducing postischemic damage by temporary modification of reperfusate calcium, potassium, pH, and osmolarity. *The Journal of thoracic and cardiovascular surgery*, 82(2):221–38, 1981.
- [105] Foglia R. P., Steed D. L., Follette D. M., DeLand E., and Buckberg G. D. Iatrogenic myocardial edema with potassium cardioplegia. *The Journal of thoracic and cardiovascular surgery*, 78(2):217–22, 1979.

- [106] Kloner R. A., Reimer K. A., Willerson J. T., and Jennings R. B. Reduction of experimental myocardial infarct size with hyperosmolar mannitol. *Proceedings of the Society for Experimental Biology and Medicine. Society for Experimental Biology and Medicine (New York, N.Y.)*, 151(4):677–83, 1976.
- [107] Kerr J. F., Wyllie A. H., and Currie A. R. Apoptosis: a basic biological phenomenon with wide-ranging implications in tissue kinetics. *British journal of cancer*, 26(4): 239–57, 1972.
- [108] Recklinghausen F. v. *Untersuchungen über Rachitis und Osteomalacie*. Verlag Gustav Fischer, Jena, 1910.
- [109] Klionsky D. J. Autophagy revisited: a conversation with Christian de Duve. *Autophagy*, 4(6):740–3, 2008.
- [110] Balvan J., Krizova A., Gumulec J., Raudenska M., Sladek Z., Sedlackova M., Babula P., Sztalmachova M., Kizek R., Chmelik R., and Masarik M. Multimodal holographic microscopy: distinction between apoptosis and oncosis. *PLOS ONE*, 10(3): e0121674, 2015.
- [111] Lockshin R. A. and Williams C. M. Programmed cell death—II. Endocrine potentiation of the breakdown of the intersegmental muscles of silkmooths. *Journal of Insect Physiology*, 10(4):643–649, 1964.
- [112] Whelan R. S., Konstantinidis K., Wei A.-C., Chen Y., Reyna D. E., Jha S., Yang Y., Calvert J. W., Lindsten T., Thompson C. B., Crow M. T., Gavathiotis E., Dorn G. W., O'Rourke B., and Kitsis R. N. Bax regulates primary necrosis through mitochondrial dynamics. *Proceedings of the National Academy of Sciences*, 109(17): 6566–6571, 2012.
- [113] Kristen A. V., Ackermann K., Buss S., Lehmann L., Schnabel P. A., Haunstetter A., Katus H. A., and Hardt S. E. Inhibition of apoptosis by the intrinsic but not the extrinsic apoptotic pathway in myocardial ischemia-reperfusion. *Cardiovascular pathology: the official journal of the Society for Cardiovascular Pathology*, 22(4):280–6.
- [114] Trump B. E., Berezesky I. K., Chang S. H., and Phelps P. C. The pathways of cell death: oncosis, apoptosis, and necrosis. *Toxicologic Pathology*, 25(1):82–88, 1997.
- [115] Weerasinghe P. and Buja L. M. Oncosis: an important non-apoptotic mode of cell death. *Experimental and molecular pathology*, 93(3):302–8, 2012.
- [116] Rock K. L. and Kono H. The inflammatory response to cell death. *Annual review of pathology*, 3:99–126, 2008.

- [117] Yan L., Sadoshima J., Vatner D. E., and Vatner S. F. Autophagy in ischemic preconditioning and hibernating myocardium. *Autophagy*, 5(5):709–12, 2009.
- [118] Fraser R. G. J. The effective cross section of the oriented hydrogen atom. *Proceedings of the Royal Society A: Mathematical, Physical and Engineering Sciences*, 114(767): 212–221, 1927.
- [119] Bloch F. Nuclear Induction. *Physical Review*, 70(7-8):460–474, 1946.
- [120] Larmor J. A dynamical theory of the electric and luminiferous medium. Part III. Relations with material media. *Philosophical Transactions of the Royal Society A: Mathematical, Physical and Engineering Sciences*, 190:205–493, 1897.
- [121] Anderson L. Cardiovascular T2-star (T2*) magnetic resonance for the early diagnosis of myocardial iron overload. *European Heart Journal*, 22(23):2171–2179, 2001.
- [122] Graif M., Bydder G. M., Steiner R. E., Niendorf P., Thomas D. G., and Young I. R. Contrast-enhanced MR imaging of malignant brain tumors. *AJNR. American journal of neuroradiology*, 6(6):855–62.
- [123] Carr D. H., Brown J., Bydder G. M., Weinmann H. J., Speck U., Thomas D. J., and Young I. R. Intravenous chelated gadolinium as a contrast agent in NMR imaging of cerebral tumours. *Lancet (London, England)*, 1(8375):484–6, 1984.
- [124] Garroway A. N., Grannell P. K., and Mansfield P. Image formation in NMR by a selective irradiative process. *Journal of Physics C: Solid State Physics*, 7(24):L457–L462, 1974.
- [125] Kumar A., Welti D., and Ernst R. NMR Fourier zeugmatography. *Journal of Magnetic Resonance*, 18:69–83, 1975.
- [126] Axel L. Revised glossary of MR terms. *Radiology*, 162(3):874–874, 1987.
- [127] Carr H. Y. Steady-state free precession in nuclear magnetic resonance. *Physical Review*, 112(5):1693–1701, 1958.
- [128] Carr J. C., Simonetti O., Bundy J., Li D., Pereles S., and Finn J. P. Cine MR angiography of the heart with segmented true fast imaging with steady-state precession. *Radiology*, 219(3):828–34, 2001.
- [129] Scheffler K. and Hennig J. Is TrueFISP a gradient-echo or a spin-echo sequence? *Magnetic resonance in medicine*, 49(2):395–7, 2003.
- [130] Oppelt A., Graumann R., Barfuss H., Fischer H., Hartl W., and Schajor W. FISP: a new fast MRI sequence. *Electromedica (Engl Ed)*, 54:15–18, 1986.

- [131] Zur Y., Stokar S., and Bendel P. An analysis of fast imaging sequences with steady-state transverse magnetization refocusing. *Magnetic resonance in medicine*, 6(2):175–93, 1988.
- [132] Simonetti O. P., Finn J. P., White R. D., Laub G., and Henry D. A. "Black blood" T2-weighted inversion-recovery MR imaging of the heart. *Radiology*, 199(1):49–57, 1996.
- [133] Hahn E. L. An accurate nuclear magnetic resonance method for measuring spin-lattice relaxation times. *Physical Review*, 76(1):145–146, 1949.
- [134] Bydder G. M., Steiner R. E., Young I. R., Hall A. S., Thomas D. J., Marshall J., Pallis C. A., and Legg N. J. Clinical NMR imaging of the brain: 140 cases. *AJR. American journal of roentgenology*, 139(2):215–36, 1982.
- [135] Kim R. J., Fieno D. S., Parrish T. B., Harris K., Chen E. L., Simonetti O., Bundy J., Finn J. P., Klocke F. J., and Judd R. M. Relationship of MRI delayed contrast enhancement to irreversible injury, infarct age, and contractile function. *Circulation*, 100(19):1992–2002, 1999.
- [136] Bohl S., Medway D. J., Schulz-Menger J., Schneider J. E., Neubauer S., and Lygate C. A. Refined approach for quantification of in vivo ischemia-reperfusion injury in the mouse heart. *American journal of physiology. Heart and circulatory physiology*, 297(6):2054–8, 2009.
- [137] Hammer-Hansen S., Leung S. W., Hsu L.-Y., Wilson J. R., Taylor J., Greve A. M., Thune J. J., Køber L., Kellman P., and Arai A. E. Early gadolinium enhancement for determination of area at risk. *JACC: Cardiovascular Imaging*, 10(2):130–139, 2017.
- [138] Anger H. O. Scintillation camera with multichannel collimators. *Journal of nuclear medicine : official publication, Society of Nuclear Medicine*, 5:515–31, 1964.
- [139] Deutsch E., Bushong W., Glavan K. A., Elder R. C., Sodd V. J., Scholz K. L., Fortman D. L., and Lukes S. J. Heart imaging with cationic complexes of technetium. *Science (New York, N.Y.)*, 214(4516):85–6, 1981.
- [140] Okada R. D., Williams S. J., Glover D. K., and Dragatokis D. Cardiac imaging and myocardial kinetics of technetium-tertiary butyl-isonitrile during dipyridamole-induced hyperemia. *American heart journal*, 116(4):979–88, 1988.
- [141] Gerson M. C., Deutsch E. A., Nishiyama H., Libson K. F., Adolph R. J., Grossman L. W., Sodd V. J., Fortman D. L., Vanderheyden J. L., and Williams C. C. Myocardial perfusion imaging with ^{99m}Tc -DMPE in man. *European journal of nuclear medicine*, 8(9):371–4, 1983.

- [142] Vitola J. V., Shaw L. J., Allam A. H., Orellana P., Peix A., Ellmann A., Allman K. C., Lee B. N., Siritara C., Keng F. Y. J., Sambuceti G., Kiess M. C., Giubbini R., Bouyoucef S. E., He Z.-X., Thomas G. S., Mut F., and Dondi M. Assessing the need for nuclear cardiology and other advanced cardiac imaging modalities in the developing world. *Journal of Nuclear Cardiology*, 16(6):956–961, 2009.
- [143] Califf R. M., Phillips H. R., Hindman M. C., Mark D. B., Lee K. L., Behar V. S., Johnson R. A., Pryor D. B., Rosati R. A., and Wagner G. S. Prognostic value of a coronary artery jeopardy score. *Journal of the American College of Cardiology*, 5(5): 1055–63, 1985.
- [144] Alderman E. and Stadius M. The angiographic definitions of the bypass angioplasty revascularization investigation. *Coronary Artery Disease*, 12(3):1189–1207, 1992.
- [145] Graham M. M., Faris P. D., Ghali W. A., Galbraith P., Norris C. M., Badry J. T., Mitchell L., Curtis M. J., and Knudtson M. L. Validation of three myocardial jeopardy scores in a population-based cardiac catheterization cohort. *American Heart Journal*, 142(2):254–262, 2001.
- [146] Huber K. C., Bresnahan J. F., Bresnahan D. R., Pellikka P. A., Behrenbeck T., and Gibbons R. J. Measurement of myocardium at risk by technetium-99m sestamibi: Correlation with coronary angiography. *Journal of the American College of Cardiology*, 19(1):67–73, 1992.
- [147] Wright J., Adriaenssens T., Dymarkowski S., Desmet W., and Bogaert J. Quantification of myocardial area at risk with T2-weighted CMR. *JACC: Cardiovascular Imaging*, 2(7):825–831, 2009.
- [148] Freedman F. B. and Johnson J. A. Equilibrium and kinetic properties of the Evans blue-albumin system. *The American journal of physiology*, 216(3):675–81, 1969.
- [149] Hale S. L., Vivaldi M. T., and Kloner R. A. Fluorescent microspheres: a new tool for visualization of ischemic myocardium in rats. *The American journal of physiology*, 251(4 Pt 2):863–8, 1986.
- [150] Miller S., Helber U., Kramer U., Hahn U., Carr J., Stauder N. I., Hoffmeister H. M., and Claussen C. D. Subacute myocardial infarction: assessment by STIR T2-weighted MR imaging in comparison to regional function. *Magma (New York, N.Y.)*, 13(1):8–14, 2001.
- [151] Aletras A. H., Kellman P., Derbyshire J. A., and Arai A. E. ACUT2E TSE-SSFP: A hybrid method for T2-weighted imaging of edema in the heart. *Magnetic Resonance in Medicine*, 59(2):229–235, 2008.

- [152] Payne A. R., Casey M., McClure J., McGeoch R., Murphy A., Woodward R., Saul A., Bi X., Zuehlsdorff S., Oldroyd K. G., Tzemos N., and Berry C. Bright-blood T2-weighted MRI has higher diagnostic accuracy than dark-blood short tau inversion recovery MRI for detection of acute myocardial infarction and for assessment of the ischemic area at risk and myocardial salvage. *Circulation: Cardiovascular Imaging*, 4(3):210–219, 2011.
- [153] Berry C., Kellman P., Mancini C., Chen M. Y., Bandettini W. P., Lowrey T., Hsu L.-Y., Aletras A. H., and Arai A. E. Magnetic resonance imaging delineates the ischemic area at risk and myocardial salvage in patients with acute myocardial infarction. *Circulation. Cardiovascular imaging*, 3(5):527–35, 2010.
- [154] Matsumoto H., Matsuda T., Miyamoto K., Shimada T., Mikuri M., and Hiraoka Y. Peri-infarct zone on early contrast-enhanced CMR imaging in patients with acute myocardial infarction. *JACC. Cardiovascular imaging*, 4(6):610–8, 2011.
- [155] Matsumoto H., Matsuda T., Miyamoto K., Shimada T., Ushimaru S., Mikuri M., and Yamazaki T. Temporal change of enhancement after gadolinium injection on contrast-enhanced CMR in reperfused acute myocardial infarction. *Journal of cardiology*, 65(1):76–81, 2015.
- [156] Verhaert D., Thavendiranathan P., Giri S., Mihai G., Rajagopalan S., Simonetti O. P., and Raman S. V. Direct T2 quantification of myocardial edema in acute ischemic injury. *JACC: Cardiovascular Imaging*, 4(3):269–278, 2011.
- [157] Ferreira V. M., Piechnik S. K., Dall’Armellina E., Karamitsos T. D., Francis J. M., Choudhury R. P., Friedrich M. G., Robson M. D., and Neubauer S. Non-contrast T1-mapping detects acute myocardial edema with high diagnostic accuracy: a comparison to T2-weighted cardiovascular magnetic resonance. *Journal of cardiovascular magnetic resonance : official journal of the Society for Cardiovascular Magnetic Resonance*, 14:42, 2012.
- [158] Kumar A., Beohar N., Arumana J. M., Larose E., Li D., Friedrich M. G., and Dharmakumar R. CMR imaging of edema in myocardial infarction using cine balanced steady-state free precession. *JACC: Cardiovascular Imaging*, 4(12):1265–1273, 2011.
- [159] Ubachs J. F. A., Sorensson P., Engblom H., Carlsson M., Jovinge S., Pernow J., and Arheden H. Myocardium at risk by magnetic resonance imaging: head-to-head comparison of T2-weighted imaging and contrast-enhanced steady-state free precession. *European Heart Journal - Cardiovascular Imaging*, 13(12):1008–1015, 2012.

- [160] Higgins C. B., Herfkens R., Lipton M. J., Sievers R., Sheldon P., Kaufman L., and Crooks L. E. Nuclear magnetic resonance imaging of acute myocardial infarction in dogs: alterations in magnetic relaxation times. *The American journal of cardiology*, 52(1):184–188, 1983.
- [161] Inch W. R., McCredie J. A., Knispel R. R., Thompson R. T., and Pintar M. M. Water content and proton spin relaxation time for neoplastic and non-neoplastic tissues from mice and humans. *Journal of the National Cancer Institute*, 52(2):353–6, 1974.
- [162] Naruse S., Horikawa Y., Tanaka C., Hirakawa K., Nishikawa H., and Yoshizaki K. Proton nuclear magnetic resonance studies on brain edema. *Journal of neurosurgery*, 56(6):747–52, 1982.
- [163] Inch W. R., McCredie J. A., Geiger C., and Boctor Y. Spin-lattice relaxation times for mixtures of water and gelatin or cotton, compared with normal and malignant tissue. *Journal of the National Cancer Institute*, 53(3):689–90, 1974.
- [164] Canby R. C., Reeves R. C., Evanochko W. T., Elgavish G. A., and Pohost G. M. Proton nuclear magnetic resonance relaxation times in severe myocardial ischemia. *Journal of the American College of Cardiology*, 10(2):412–20, 1987.
- [165] Escanye J. M., Canet D., and Robert J. Frequency dependence of water proton longitudinal nuclear magnetic relaxation times in mouse tissues at 20 degrees C. *Biochimica et biophysica acta*, 721(3):305–11, 1982.
- [166] Grad J., Mendelson D., Hyder F., and Bryant R. G. Direct measurements of longitudinal relaxation and magnetization transfer in heterogeneous systems. *Journal of Magnetic Resonance (1969)*, 86(2):416–419, 1990.
- [167] Wolff S. D. and Balaban R. S. Magnetization transfer contrast (MTC) and tissue water proton relaxation in vivo. *Magnetic resonance in medicine*, 10(1):135–44, 1989.
- [168] Kaneoke Y., Furuse M., Inao S., Saso K., Yoshida K., Motegi Y., Mizuno M., and Izawa A. Spin-lattice relaxation times of bound water—Its determination and implications for tissue discrimination. *Magnetic Resonance Imaging*, 5(6):415–420, 1987.
- [169] Wüthrich K., Otting G., and Liepinsh E. Protein hydration in aqueous solution. *Faraday discussions*, (93):35–45, 1992.
- [170] Denisov V. P. and Halle B. Protein hydration dynamics in aqueous solution: a comparison of bovine pancreatic trypsin inhibitor and ubiquitin by oxygen-17 spin relaxation dispersion. *Journal of molecular biology*, 245(5):682–97, 1995.

- [171] Weber O. M., Speier P., Scheffler K., and Bieri O. Assessment of magnetization transfer effects in myocardial tissue using balanced steady-state free precession (bSSFP) cine MRI. *Magnetic resonance in medicine*, 62(3):699–705, 2009.
- [172] Nordlund D., Kanski M., Jablonowski R., Koul S., Erlinge D., Carlsson M., Engblom H., Aletras A. H., and Arheden H. Experimental validation of contrast-enhanced SSFP cine CMR for quantification of myocardium at risk in acute myocardial infarction. *Journal of Cardiovascular Magnetic Resonance*, 19(1):12, 2017.
- [173] Erlinge D., Götberg M., Lang I., Holzer M., Noc M., Clemmensen P., Jensen U., Metzler B., James S., Bötter H. E., Omerovic E., Engblom H., Carlsson M., Arheden H., Östlund O., Wallentin L., Harnek J., and Olivecrona G. K. Rapid endovascular catheter core cooling combined with cold saline as an adjunct to percutaneous coronary intervention for the treatment of acute myocardial infarction. *Journal of the American College of Cardiology*, 63(18):1857–1865, 2014.
- [174] Khoshnood A., Carlsson M., Akbarzadeh M., Bhiladvala P., Roijer A., Nordlund D., Höglund P., Zughaft D., Todorova L., Mokhtari A., Arheden H., Erlinge D., and Ekelund U. Effect of oxygen therapy on myocardial salvage in ST elevation myocardial infarction: the randomized SOCCER trial. *European journal of emergency medicine : official journal of the European Society for Emergency Medicine*, 2016.
- [175] Nordlund D., Klug G., Heiberg E., Koul S., Larsen T. H., Hoffmann P., Metzler B., Erlinge D., Atar D., Aletras A. H., Carlsson M., Engblom H., and Arheden H. Multi-vendor, multicentre comparison of contrast-enhanced SSFP and T2-STIR CMR for determining myocardium at risk in ST-elevation myocardial infarction. *European Heart Journal Cardiovascular Imaging*, 17(7):744–753, 2016.
- [176] Heiberg E., Sjögren J., Ugander M., Carlsson M., Engblom H., and Arheden H. Design and validation of Segment—freely available software for cardiovascular image analysis. *BMC medical imaging*, 10:1, 2010.
- [177] Cerqueira M. D. Standardized myocardial segmentation and nomenclature for tomographic imaging of the heart: a statement for healthcare professionals from the cardiac imaging committee of the council on clinical cardiology of the American Heart Association. *Circulation*, 105(4):539–542, 2002.
- [178] Nordlund D., Heiberg E., Carlsson M., Frønd E. T., Hoffmann P., Koul S., Atar D., Aletras A. H., Erlinge D., Engblom H., and Arheden H. Extent of myocardium at risk for left anterior descending artery, right coronary artery, and left circumflex artery occlusion depicted by contrast-enhanced steady state free precession and T2-weighted short tau inversion recovery magnetic resonance imaging. *Circulation: Cardiovascular Imaging*, 9(7):e004376, 2016.

- [179] Peter Rentrop K., Cohen M., Blanke H., and Phillips R. A. Changes in collateral channel filling immediately after controlled coronary artery occlusion by an angioplasty balloon in human subjects. *Journal of the American College of Cardiology*, 5 (3):587–592, 1985.
- [180] Engblom H., Heiberg E., Jensen S., Nordrehaug J., Dubois-Randé J.-L., Halvorsen S., Koul S., Erlinge D., Atar D., Carlsson M., and Arheden H. Design of clinical cardioprotection trials using CMR: impact of myocardial salvage index and a narrow inclusion window on sample size. *Journal of Cardiovascular Magnetic Resonance*, 17 (Suppl 1):P90, 2015.
- [181] Student. The probable error of a mean. *Biometrika*, 6(1):1, 1908.
- [182] Wilcoxon F. Individual comparisons by ranking methods. *Biometrics Bulletin*, 1(6): 80, 1945.
- [183] D’Agostino R. “Tests for Normal Distribution” in *Goodness-Of-Fit Techniques*. Macel Dekker, 1986.
- [184] Fisher R. On the “probable error” of a coefficient of correlation deduced from a small sample. *Metron*, 1:3–32, 1921.
- [185] Fisher R. *The design of experiments*. Oliver and Boyd, Edinburgh, 1935.
- [186] Galton F. Co-relations and their measurement, chiefly from anthropometric data. *Proceedings of the Royal Society London*, 45:135–145, 1888.
- [187] Pearson K. Notes on regression and inheritance in the case of two parents. *Proceedings of the Royal Society of London*, 58:240–242, 1885.
- [188] Bland J. M. and Altman D. G. Statistical methods for assessing agreement between two methods of clinical measurement. *Lancet (London, England)*, 1(8476):307–10, 1986.
- [189] Thuny F., Lairez O., Roubille F., Mewton N., Rioufol G., Sportouch C., Sanchez I., Bergerot C., Thibault H., Cung T. T., Finet G., Argaud L., Revel D., Derumeaux G., Bonnefoy-Cudraz E., Elbaz M., Piot C., Ovize M., and Croisille P. Post-conditioning reduces infarct size and edema in patients with ST-segment elevation myocardial infarction. *Journal of the American College of Cardiology*, 59(24):2175–2181, 2012.
- [190] White S. K., Frohlich G. M., Sado D. M., Maestrini V., Fontana M., Treibel T. A., Tehrani S., Flett A. S., Meier P., Ariti C., Davies J. R., Moon J. C., Yellon D. M., and Hausenloy D. J. Remote ischemic conditioning reduces myocardial infarct size and edema in patients with ST-segment elevation myocardial infarction. *JACC: Cardiovascular Interventions*, 2014.

- [191] Pereztol-Valdés O., Candell-Riera J., Santana-Boado C., Angel J., Aguadé-Bruix S., Castell-Conesa J., Garcia E. V., and Soler-Soler J. Correspondence between left ventricular 17 myocardial segments and coronary arteries. *European heart journal*, 26(24):2637–2643, 2005.
- [192] Persson E., Palmer J., Pettersson J., Warren S. G., Borges-Neto S., Wagner G. S., and Pahlm O. Quantification of myocardial hypoperfusion with 99m Tc-sestamibi in patients undergoing prolonged coronary artery balloon occlusion. *Nuclear medicine communications*, 23(3):219–228, 2002.
- [193] Tufvesson J., Carlsson M., Aletras A. H., Engblom H., Deux J.-F., Koul S., Sörenson P., Pernow J., Atar D., Erlinge D., Arheden H., and Heiberg E. Automatic segmentation of myocardium at risk from contrast enhanced SSFP CMR: validation against expert readers and SPECT. *BMC medical imaging*, 16(1):19, 2016.
- [194] Engblom H., Tufvesson J., Jablonowski R., Carlsson M., Aletras A. H., Hoffmann P., Jacquier A., Kober F., Metzler B., Erlinge D., Atar D., Arheden H., and Heiberg E. A new automatic algorithm for quantification of myocardial infarction imaged by late gadolinium enhancement cardiovascular magnetic resonance: experimental validation and comparison to expert delineations in multi-center, multi-vendor patient data. *Journal of Cardiovascular Magnetic Resonance*, 18(1):27, 2016.
- [195] Arai A. E., Leung S., and Kellman P. Controversies in cardiovascular MR imaging: reasons why imaging myocardial T2 has clinical and pathophysiologic value in acute myocardial infarction. *Radiology*, 265(1):23–32, 2012.
- [196] Croisille P., Kim H. W., and Kim R. J. Controversies in cardiovascular MR imaging: T2-weighted imaging should not be used to delineate the area at risk in ischemic myocardial injury. *Radiology*, 265(1):12–22, 2012.
- [197] Friedrich M. G., Kim H. W., and Kim R. J. T2-weighted imaging to assess post-infarct myocardium at risk. *JACC: Cardiovascular Imaging*, 4(9):1014–1021, 2011.
- [198] De Luca G., Suryapranata H., Dambrink J.-H., Ottervanger J. P., van ’t Hof A. W. J., Zijlstra F., Hoorntje J. C. A., Gosselink A. T. M., and de Boer M.-J. Sex-related differences in outcome after ST-segment elevation myocardial infarction treated by primary angioplasty: data from the Zwolle Myocardial Infarction study. *American heart journal*, 148(5):852–6, 2004.
- [199] Mega J. L., Morrow D. A., Ostör E., Dorobantu M., Qin J., Antman E. M., and Braunwald E. Outcomes and optimal antithrombotic therapy in women undergoing fibrinolysis for ST-elevation myocardial infarction. *Circulation*, 115(22):2822–8, 2007.

REFERENCES

- [200] Writing Group Members, Mozaffarian D., Benjamin E. J., Go A. S., Arnett D. K., Blaha M. J., Cushman M., Das S. R., de Ferranti S., Després J.-P., Fullerton H. J., Howard V. J., Huffman M. D., Isasi C. R., Jiménez M. C., Judd S. E., Kissela B. M., Lichtman J. H., Lisabeth L. D., Liu S., Mackey R. H., Magid D. J., McGuire D. K., Mohler E. R., Moy C. S., Muntner P., Mussolino M. E., Nasir K., Neumar R. W., Nichol G., Palaniappan L., Pandey D. K., Reeves M. J., Rodriguez C. J., Rosamond W., Sorlie P. D., Stein J., Towfighi A., Turan T. N., Virani S. S., Woo D., Yeh R. W., Turner M. B., American Heart Association Statistics Committee, and Stroke Statistics Subcommittee. Heart disease and stroke statistics-2016 update: a report from the American Heart Association. *Circulation*, 133(4):38–360, 2016.
- [201] Rosengren A. Sex differences in survival after myocardial infarction in Sweden. Data from the Swedish National Acute Myocardial Infarction register. *European Heart Journal*, 22(4):314–322, 2001.
- [202] Lawesson S. S., Alfredsson J., Fredrikson M., and Swahn E. A gender perspective on short- and long term mortality in ST-elevation myocardial infarction—a report from the SWEDEHEART register. *International journal of cardiology*, 168(2):1041–7, 2013.
- [203] Canali E., Masci P., Bogaert J., Bucciarelli Ducci C., Francone M., McAlindon E., Carbone I., Lombardi M., Desmet W., Janssens S., and Agati L. Impact of gender differences on myocardial salvage and post-ischaemic left ventricular remodelling after primary coronary angioplasty: new insights from cardiovascular magnetic resonance. *European Heart Journal - Cardiovascular Imaging*, 13(11):948–953, 2012.
- [204] Eitel I., Desch S., Fuernau G., Hildebrand L., Gutberlet M., Schuler G., and Thiele H. Prognostic significance and determinants of myocardial salvage assessed by cardiovascular magnetic resonance in acute reperfused myocardial infarction. *Journal of the American College of Cardiology*, 55(22):2470–2479, 2010.
- [205] Langhans B., Ibrahim T., Hausleiter J., Sonne C., Martinoff S., Schömig A., and Hadamitzky M. Gender differences in contrast-enhanced magnetic resonance imaging after acute myocardial infarction. *The international journal of cardiovascular imaging*, 29(3):643–50, 2013.

Part II

Research papers

Author contributions

Paper I

As first author I participated in study design, experimental data collection, evaluation of the MR and MPS data, statistical analysis, writing the manuscript, and submitting and revising the manuscript.

Paper II

As first author I participated in analysis of MR and angiography data, designing and participating in quality analysis of MR images, performing statistical analysis, writing the manuscript, and submitting and revising the manuscript.

Paper III

As first author I participated in analysis of MR and angiography data, performing statistical analysis, participating in the design of polar plots, writing the manuscript, and submitting and revising the manuscript.

Paper IV

As first author I participated in analysis of MR and angiography data, performing statistical analysis supported by a statistician, writing the manuscript, and submitting the manuscript.

Paper I




RESEARCH

Open Access



Experimental validation of contrast-enhanced SSFP cine CMR for quantification of myocardium at risk in acute myocardial infarction

David Nordlund¹ , Mikael Kanski¹, Robert Jablonowski¹, Sasha Koul², David Erlinge², Marcus Carlsson¹, Henrik Engblom¹, Anthony H. Aletras^{1,3} and Håkan Arheden^{1*}

Abstract

Background: Accurate assessment of myocardium at risk (MaR) after acute myocardial infarction (AMI) is necessary when assessing myocardial salvage. Contrast-enhanced steady-state free precession (CE-SSFP) is a recently developed cardiovascular magnetic resonance (CMR) method for assessment of MaR up to 1 week after AMI. Our aim was to validate CE-SSFP for determination of MaR in an experimental porcine model using myocardial perfusion single-photon emission computed tomography (MPS) as a reference standard and to test the stability of MaR-quantification over time after injecting gadolinium-based contrast.

Methods: Eleven pigs were subjected to either 35 or 40 min occlusion of the left anterior descending artery followed by six hours of reperfusion. A technetium-based perfusion tracer was administered intravenously ten minutes before reperfusion. In-vivo and ex-vivo CE-SSFP CMR was performed followed by ex-vivo MPS imaging. MaR was expressed as % of left ventricular mass (LVM).

Results: There was good agreement between MaR by ex-vivo CMR and MaR by MPS (bias: $1 \pm 3\%$ LVM, $r^2 = 0.92$, $p < 0.001$), between ex-vivo and in-vivo CMR (bias $0 \pm 2\%$ LVM, $r^2 = 0.94$, $p < 0.001$) and between in-vivo CMR and MPS (bias $-2 \pm 3\%$ LVM, $r^2 = 0.87$, $p < 0.001$). No change in MaR was seen over the first 30 min after contrast injection ($p = 0.95$).

Conclusions: Contrast-enhanced SSFP cine CMR can be used to measure MaR, both in vivo and ex vivo, in a porcine model with good accuracy and precision over the first 30 min after contrast injection. This offers the option to use the less complex ex-vivo imaging when determining myocardial salvage in experimental studies.

Keywords: Myocardium at risk, CE-SSFP, AAR, Area at risk

Background

Treatment options for acute myocardial infarction (AMI) have steadily increased over the recent decades. Experimental models have been instrumental to this since they offer a controlled environment where treatment effects can be developed and assessed prior to patient trials. An important endpoint for such models is myocardial salvage and myocardial salvage index (MSI) [1], used to quantify treatment efficacy. Myocardial

salvage is defined as myocardium at risk (MaR) minus infarct size and MSI is defined as myocardial salvage divided by MaR.

Cardiovascular magnetic resonance (CMR) is considered the reference standard for determining infarct size in vivo using late gadolinium enhancement (LGE) imaging typically performed 15–20 min after contrast administration [2, 3]. Furthermore, CMR has been shown to enable assessment of MaR using T2-weighted (T2w) imaging which has been validated both in an experimental AMI model [4] and in patients up to 1 week after AMI [5]. However, T2w imaging performs inconsistently depending on vendor [6] and on the particular

* Correspondence: hakan.arheden@med.lu.se

¹Department of Clinical Physiology, Clinical Sciences, Lund University and Lund University Hospital, Lund, Sweden

Full list of author information is available at the end of the article



© The Author(s). 2017 **Open Access** This article is distributed under the terms of the Creative Commons Attribution 4.0 International License (<http://creativecommons.org/licenses/by/4.0/>), which permits unrestricted use, distribution, and reproduction in any medium, provided you give appropriate credit to the original author(s) and the source, provide a link to the Creative Commons license, and indicate if changes were made. The Creative Commons Public Domain Dedication waiver (<http://creativecommons.org/publicdomain/zero/1.0/>) applies to the data made available in this article, unless otherwise stated.

implementation of the T2w pulse sequence. Also, T2w imaging has been shown to be prone to artefacts [7, 8]. Another CMR method for MaR quantification is contrast-enhanced steady state free precession (CE-SSFP), which is based on standard SSFP cine images acquired after contrast injection [9]. Since SSFP cine imaging performs consistently for all vendors and since images are included in the majority of standard CMR protocols for assessment of cardiac function, CE-SSFP can be implemented across centers and does not add to the total scanning time [6]. CE-SSFP has been validated in patients with myocardial perfusion single-photon emission computed tomography (MPS) [9], compared head-to-head with T2w imaging [10] and used in two multinational cardio-protection trials, CHILL-MI and MITOCARE [11, 12]. However, to date CE-SSFP has not been validated experimentally.

The specific aims for this study were: A. To determine whether CE-SSFP could be used for determining MaR in an ex-vivo setting, which would be advantageous for designing cardioprotective studies where performing complex in-vivo CMR is not possible. B. To test if the findings in patients with respect to quantification of MaR with CE-SSFP would also hold in an in-vivo animal model and C. To determine whether the timing of imaging after contrast agent administration affects the quantification of MaR in vivo.

Methods

Experimental model

The study was approved by the local Ethics Committee for animal experiments. Pigs (weighing 40–50 kg) were pre-medicated with ketamine 15 mg/kg (Ketaminol, Intervet, Danderyd, Sweden) and midazolam 0.5 mg/kg intramuscularly (Dormicum, Roche AB, Stockholm, Sweden) after overnight fasting with free access to water. Anesthesia was induced with propofol 20 mg/ml (Propofol Sandoz A S, Copenhagen, Denmark) and the animals were intubated using cuffed endotracheal tubes. Anesthesia was maintained with inhalation of sevoflurane gas (Sevorane, Baxter Medical AB, Kista, Sweden) using a disposable administration system (AnaConDa, Sedana Medical AB, Uppsala, Sweden) and titrating to desired effect. Mechanical ventilation was established using a 900C ventilator (Siemens AB, Upplands Väsby, Sweden) in volume controlled mode regulated to a $p\text{CO}_2$ of 5.0–6.0 kPa. Monitoring included arterial blood pressure, heart rate, ECG, pulse-oximetry and temperature. Arterial blood gases were drawn and analyzed directly after establishing arterial access, before occlusion, after reperfusion, and to follow up any unexpected deviation of the blood gas results or change in the clinical condition of the animal. Venous and arterial femoral access, jugular access and carotid access were

established using 6–8Fr introducer sheaths. After establishing all accesses, 20,000 IU of heparin (LEO Pharma AB, Malmö Sweden) was administered intravenously and 5% glucose (Baxter Medical AB, Kista, Sweden) was slowly infused. During the experiments amiodarone (Sanofi AB, Stockholm, Sweden), fentanyl (50 mikrog/ml, B. Braun Medical AB, Danderyd, Sweden) and sodium chloride (0.9% Baxter Medical AB, Kista, Sweden) was titrated to desired effect.

Experimental protocol

Pigs were subjected to either 35 or 40-min of left anterior descending (LAD)-occlusion using a balloon-tipped catheter, followed by six hours of reperfusion. The balloon occluder was placed either after the first or the second diagonal branch of the LAD to obtain a wide range of MaR. An angiogram was acquired after inflation of the balloon and before deflation in order to confirm occlusion of the coronary vessel and correct balloon placement. Isotope (1000 MBq ^{99m}Tc tetrofosmine) for MPS imaging was administered ten minutes prior to reperfusion. After deflation of the balloon a subsequent angiogram was performed to verify restoration of blood flow. After reperfusion, animals were transported to the MR department.

CMR

In vivo

Imaging was performed on a 1.5 T MR scanner (Philips Achieva, Best, Netherlands) using a 32-channel cardiac coil. During in-vivo imaging 0.2 mmol/kg gadolinium (Gd) based contrast agent (Gd-DOTA) (Dotarem, Guerbet, Roissy, France) was administered intravenously 15 min before LGE-CMR. Using a retrospectively gated SSFP single slice sequence, a midventricular short-axis slice of the left ventricle (LV) was repeatedly acquired during the first ten minutes after contrast injection. Then, a short-axis stack covering the entire LV was acquired, using the same sequence parameters as for the single slice (typical parameters: TE 1.40 ms, TR 2.8 ms, flip angle 60°, 25 phases, slice thickness 8 mm, no slice gap, acquisition matrix 230 x 230, reconstructed matrix 240 x 240, FOV 320 x 320 mm, pixel bandwidth 860 Hz/pixel). LGE images were acquired 15–20 min after contrast injection using an inversion recovery gradient echo sequence (typical parameters: TE 3.0, TR 6.1 ms, TI 320 ms, slice thickness 8 mm, no slice gap, acquisition matrix 200 x 158, reconstructed matrix 510 x 510, FOV 320 x 320 mm, pixel bandwidth 260 Hz/pixel).

After CE-SSFP and LGE imaging an additional single slice of SSFP in the same position as above was acquired 20–30 min after contrast injection. Both CE-SSFP and

LGE slices were obtained during end-expiratory breath hold. Long axis 2-, 3 and 4-chamber views using both CE-SSFP and LGE were also acquired. Fifteen minutes before euthanization an additional 0.2 mmol/kg Gd-DOTA was administered. Pigs were euthanized with a rapid infusion of saturated potassium chloride solution and the hearts were explanted and suspended in plastic containers with deuterated water-filled balloons in the ventricles for ex-vivo imaging.

Ex vivo

ex-vivo CMR was performed on the same scanner as above, using a simulated ECG with heart rate 60 beats per minute for triggering. A full coverage LV short-axis stack was acquired using the same settings as for the in-vivo sequence above (typical parameters: TE 1.40 ms, TR 2.8 ms, flip angle 60°, 25 phases, slice thickness 8 mm, no slice gap, acquisition matrix 60 × 50, reconstructed matrix 80 × 80, FOV 100 × 100 mm, pixel bandwidth 1400 Hz/pixel). A high resolution T1-weighted short axis stack was acquired for detailed infarct visualization (TE 3.4 ms, TR 20 ms, 0.5 mm isotropic voxels, no slice gap, acquisition matrix 200 × 200, reconstructed matrix 220 × 220, FOV 100 × 100 mm, pixel bandwidth 440 Hz/pixel).

MPS

ex-vivo MPS was performed approximately 8–10 h after intravenous injection of a 1000 MBq dose of ^{99m}Tc-tetrofosmin using a dual head camera (Philips SKYlight, Best, the Netherlands) and a vertex high resolution collimator (ADAC Vertex, Milpitas, CA, USA) at 32 projections (40 s per projection) with a 64 × 64 matrix yielding a digital resolution of 4.24 mm isotropic voxels. Iterative reconstruction using maximum likelihood expectation maximization (MLEM) was performed with a low resolution Butterworth filter with a cut-off frequency set to 0.6 of Nyquist and order 5.0. No attenuation or scatter correction was applied. Finally, a short-axis image stack was reconstructed using commercially available software (AutoSPECT Plus, Pegasys software version 5.01, Philips, Best, The Netherlands).

Image analysis

All images were analyzed using the software Segment, version 1.9 R3314 (<http://segment.heiberg.se>) [13]. MaR from the in-vivo CE-SSFP images was assessed according to a previously described method [9]. In short, LVM was defined by manual delineation of the epicardial and endocardial borders in end-diastolic and end-systolic timeframes. Hyperintense myocardium was then manually delineated and defined as MaR. The same method was used to delineate MaR in ex-vivo CE-SSFP images. The analysis of CE-SSFP images was performed both by a blinded primary observer and an independent, blinded

secondary observer. When delineating CE-SSFP images over time after injection of gadolinium all images were sorted randomly both between timepoints and between experiments and observers were blinded to the randomization.

Infarcted myocardium was delineated from the in-vivo short-axis LGE images according to a previously defined method [14]. In short, the endocardial and epicardial borders were manually traced with exclusion of the papillary muscles. The LGE myocardium was defined using a computer algorithm that takes into consideration partial volume effects within the infarcted region [14]. Manual adjustments were made when image artefacts caused misinterpretation by the computer algorithm. Hypointense signal within the area of LGE, microvascular obstruction [15], was included and considered as infarction.

The high resolution T1-weighted ex-vivo images were also delineated according to a previously described and validated method [16]. In short, the endocardial and epicardial borders were traced manually including the papillary muscles. Infarct was defined as >8 standard deviations from a manually defined remote region. Manual adjustments were made if the computer algorithm was clearly wrong due to image artefacts or inclusion of intramyocardial fat as infarct.

MaR and infarct size was expressed as percentage of LVM. Myocardial salvage index (MSI) was calculated as (MaR-infarct size)/MaR = MSI.

Evaluation of MPS images was performed by using anatomical information from the high resolution T1-weighted ex-vivo images and perfusion information from MPS according to a previously described method [17]. In short, both T1-weighted and MPS images were re-sampled to similar resolutions and were spatially matched using purpose-designed software. Delineations of endocardium and epicardium from the T1-weighted images were then used for defining the myocardium in the MPS images. MaR was then automatically defined by calculating and applying a threshold and performing manual adjustments as previously described [17].

Statistics

Analyses were performed using GraphPad Prism (version 6.00, GraphPad Software, San Diego, USA) or IBM SPSS Statistics (version 23, IBM Corporation, New York, USA). Results for continuous variables are expressed as mean ± standard deviation. Bias according to Bland-Altman was used to compare MaR by MPS, in-vivo CE-SSFP and ex-vivo CE-SSFP. Bias according to Bland-Altman was also used to compare MaR by MPS, in-vivo CE-SSFP and ex-vivo CE-SSFP to infarct size by LGE imaging [18], and for inter-observer analysis. A paired *t*-test was used to test ex-vivo CE-SSFP vs MPS and in-

vivo CE-SSFP vs ex-vivo CE-SSFP. Pearson correlation coefficient was used for assessment of correlation between ex-vivo CE-SSFP, MPS, in-vivo CE-SSFP, infarct, and for inter-observer analysis. When comparing MaR over time for the single-slice images, the MaR was normalized to MaR of the first acquired slice. Subsequently a repeated measures linear mixed model using time as a nominal variable and a fixed effect was used to test for differences in MaR between different time points after contrast injection. $P < 0.05$ indicated statistical significance.

Results

Study population

Twelve pigs were included in the study. In one pig no infarct or MaR could be identified neither with in-vivo or ex-vivo CMR nor with MPS. In two pigs the in-vivo images were considered of non-diagnostic quality due to severe arrhythmias and high heart rate (>120 bpm). MPS images were of diagnostic quality in all pigs.

MaR

Images of MaR by ex-vivo CE-SSFP and MPS from one pig of typical quality is shown in Fig. 1. A good correlation with a low bias was found between MaR by ex-vivo CE-SSFP ($29 \pm 9\%$) and MPS ($30 \pm 9\%$) ($n = 11$, bias: $1 \pm 3\%$, $r^2 = 0.92$, $p < 0.001$, Fig. 2). There was also a good correlation with a low bias between MaR by in-vivo CE-SSFP ($31 \pm 8\%$) and ex-vivo CE-SSFP ($n = 9$, bias: $0 \pm 2\%$, $r^2 = 0.94$, $p < 0.001$, Fig. 2). MaR by in-vivo CE-SSFP vs MPS showed a low bias ($-2 \pm 3\%$) and a good correlation ($n = 9$, $r^2 = 0.87$, $p < 0.001$, Fig. 2). Inter-observer analysis for the ex-vivo CE-SSFP showed a low bias ($n = 11$, bias: $-1.5 \pm 3.7\%$, $r^2 = 0.98$). For the in-vivo CE-SSFP bias was also low ($n = 9$, bias: $-0.4 \pm 4.3\%$, $r^2 = 0.77$).

Infarct

Examples of infarct- and MaR-images in vivo and ex vivo of typical quality are seen in Fig. 3. Infarct size was $13 \pm 10\%$ by high-resolution T1-weighted ex-vivo imaging. Infarct size on average was smaller than MaR by MPS, CE-SSFP ex vivo and CE-SSFP in vivo in all pigs (mean difference $17 \pm 10\%$, $15 \pm 8\%$ and $16 \pm 9\%$ respectively).

Myocardial salvage Index

Myocardial salvage index was $52 \pm 28\%$ by ex-vivo CE-SSFP and high resolution T1-weighted ex-vivo imaging.

MaR over time

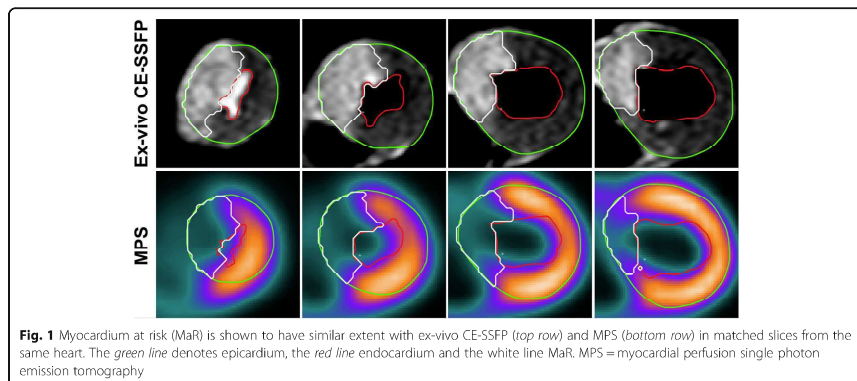
Images of MaR over time in one animal are seen in Fig. 4. On average, the MaR at baseline did not change over 30 min after contrast injection ($p = 0.95$). Bias for different times after contrast injection compared to baseline is shown in Fig. 5. Inter-observer analysis for MaR over time showed a low bias ($0.9 \pm 5.7\%$, $r^2 = 0.77$).

Discussion

This study validates CE-SSFP in an experimental setting and shows that this technique can be used to measure MaR with high accuracy and precision in vivo and ex vivo. It also shows that CE-SSFP for measurement of MaR is stable at least up to 30 min after contrast injection.

Potential mechanisms for detecting MaR with CE-SSFP

The increased signal found in the entire MaR is likely explained by a shift in the T2/T1 ratio that determines signal contrast for the balanced SSFP sequence [19]. Without the contrast agent the tissue edema results in a higher ratio as T2 seems to be



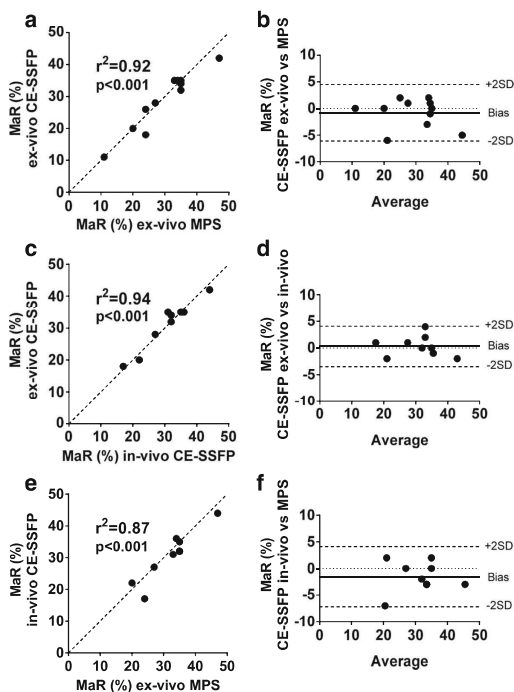


Fig. 2 Myocardium at risk (MaR) by MRI and MPS show overall good correlation and agreement. Panel **a** shows a good correlation between MaR by ex-vivo CE-SSFP and MaR by myocardial perfusion SPECT (MPS). The corresponding Bland-Altman plot in panel **b** shows a low bias. Panel **c** shows a good correlation between MaR by ex-vivo CE-SSFP and MaR by in-vivo CE-SSFP, with a low bias (panel **d**). Panel **e** shows a good correlation between MaR by in-vivo CE-SSFP and MaR by MPS. The corresponding Bland-Altman plot in panel **f** shows a low bias. In all cases, MaR is expressed as percent of left ventricular mass. The dotted lines in a, c and e represent the line of identity

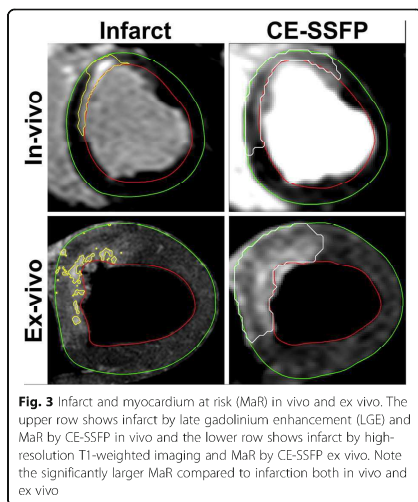
proportionally more increased than T1 [20]. At certain concentrations of contrast agent myocardial T1 may decrease proportionally more than T2, thus further increasing the T2/T1 ratio. It has been shown that the MaR has an increased distribution volume of contrast agent compared to remote myocardium [21–23], which could allow for the contrast agent to affect the T2/T1 ratio to a greater degree in MaR yielding an observable difference in signal intensity. Further studies will be needed to elucidate the mechanisms behind the tissue contrast between MaR and remote myocardium in CE-SSFP.

The single-slice data over time shows that CE-SSFP MaR imaging can be performed from less than 2 min up to 30 min after contrast agent injection with no

detectable changes in the extent of the MaR. This suggests a rapidly established equilibrium of contrast agent between the extracellular compartments (in blood, remote myocardium, MaR, infarct) in which the contrast agent is distributed (excepting areas of microvascular obstruction wherein contrast wash in is delayed or wholly obstructed). Previous studies have shown an increase in T1-relaxation times that is proportional between the extracellular compartments over 30 min after contrast injection which corroborates this finding [21, 22, 24, 25].

Previous studies using CE-SSFP for MaR

Sörensson et al. validated CE-SSFP using MPS as reference standard in patients with ST-elevation myocardial



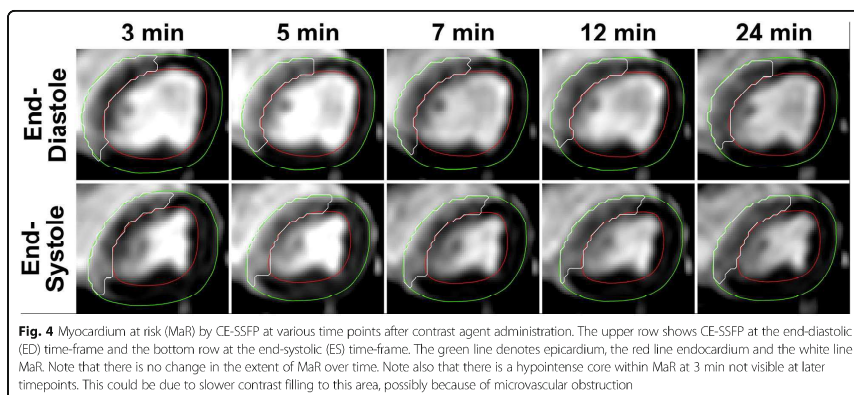
infarction [9]. They found a bias of $0.5 \pm 5.1\%$ with a correlation of $r^2 = 0.78$. In addition, Ubachs et al. showed good agreement between T2-STIR and CE-SSFP for assessment of MaR in a single-center, single-vendor setting [10]. More recently, CE-SSFP has been shown to be more robust than T2-STIR in a multi-center, multi-vendor setting [6]. Furthermore, in accordance with the findings in the present study that

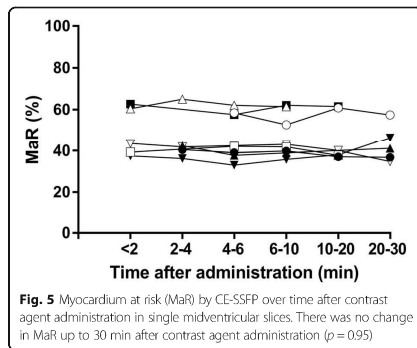
MaR is constant over time early after contrast injection, Ubachs et al. showed a constant relationship between MaR by pre-contrast T2-STIR and CE-SSFP acquired 2–12 min after contrast injection [10].

Thus, CE-SSFP offers a robust method for determination of MaR which has made it the method of choice for several clinical cardioprotection trials [11, 12, 26].

Experimental and clinical implications

MaR has been determined experimentally for several decades but has required separate modalities such as histopathology dyes, microspheres, and radioisotope imaging, making image co-registration a challenge [4, 21, 22, 27, 28]. Using CE-SSFP to determine MaR abolishes the need for separate modalities as both infarct size and MaR can be assessed in one single CMR session. Thus, co-registration of infarct and MaR can be performed accurately on a slice-by-slice basis. Furthermore, CE-SSFP cine imaging enables assessment of both MaR and myocardial function which enables calculation of myocardial salvage and myocardial salvage index and reducing the number of subjects with preserved power [29]. Since myocardial function is an essential part of most in-vivo protocols, the use of CE-SSFP shortens the CMR examination as it abolishes the need for separate scanning for assessment of MaR and myocardial function. In addition. The ability to use ex-vivo or in-vivo CE-SSFP interchangeably confers the option to perform only ex-vivo scanning and forego the more complex in-vivo scanning when determining myocardial salvage in experimental studies.





Limitations

The findings in the present study should be interpreted in the light of the following limitations. First, when comparing MaR-size over time, single midventricular slices, and not full LV coverage, were acquired. Thus, the total MaR was not assessed repeatedly, rather the percentage of MaR in a single slice. Second, the data over time after contrast-injection could not be acquired at all timepoints for all animals. This was due to both technical (e.g. triggering problems) and medical reasons (e.g. hemodynamic instability requiring intervention), interrupting imaging acquisition in some animals. Third, manual delineation was used to assess MaR. Manual delineation has, however, been validated against MPS [9]. In future studies, techniques such as T1- or T2-mapping sequences could potentially allow automatic or semi-automatic evaluation of MaR [20, 30], however, more standardization and validation is needed before these techniques can be used in clinical trials.

Conclusion

Contrast-enhanced SSFP cine CMR imaging can be used to measure MaR, both in vivo and ex vivo, in a porcine model with good accuracy and precision over the first 30 min after contrast injection. This offers the option to use the less complex ex-vivo imaging when determining myocardial salvage in experimental studies.

Abbreviations

AMI: Acute myocardial infarction; CE-SSFP: Contrast-enhanced steady state free precession; CMR: Cardiovascular magnetic resonance; LGE: Late gadolinium enhancement; LV: Left ventricle; LVM: Left ventricular mass; MaR: Myocardium at risk; MPS: Myocardial perfusion single photon emission tomography; T2w: T2-weighted; TE: Echo time; TI: Inversion time; TR: Repetition time

Acknowledgements

The authors would like to thank Joni Fleming Taylor, National Heart Lung and Blood Institute, National Institutes of Health, Bethesda, Maryland, for her significant contributions to improve the experimental model for this study.

Funding

Funding for this study was received from The Swedish Heart and Lung Foundation, The Medical Faculty at Lund University, Sweden and the Region of Scania, Sweden.

Availability of data and materials

The datasets acquired and analyzed during the current study are available from the corresponding author on reasonable request.

Authors' contributions

HA conceived the study. DN, MC, HE, and HA participated in the design of the study and the experiments. DN, SK and DE performed the invasive instrumentation. DN, MK, RJ and HE participated in data acquisition. DN, MC and HE performed image analysis. DN prepared the manuscript. All authors participated in editing the manuscript for intellectual content. All authors read and approved the final manuscript.

Competing interests

HA is a shareholder of Imacor AB, Lund. HE and MC have received consultancy fees from Imacor AB.

Consent for publication

Not applicable.

Ethics approval

The study was approved by the local Ethics Committee on animal experiments in Lund, Sweden (reference number M94-14).

Author details

¹Department of Clinical Physiology, Clinical Sciences, Lund University and Lund University Hospital, Lund, Sweden. ²Department of Cardiology, Clinical Sciences, Lund University and Lund University Hospital, Lund, Sweden. ³Laboratory of Computing and Medical Informatics, School of Medicine, Aristotle University of Thessaloniki, Thessaloniki, Greece.

Received: 14 September 2016 Accepted: 12 January 2017

Published online: 30 January 2017

References

- Reimer KA, Jennings RB. The "wavefront phenomenon" of myocardial ischemic cell death. II. Transmural progression of necrosis within the framework of ischemic bed size (myocardium at risk) and collateral flow. *Lab Invest*. 1979;40:633–44.
- Kim RJ, Wu E, Rafael A, Chen E-L, Parker MA, Simonetti O, Klocke FJ, Bonow RO, Judd RM. The Use of Contrast-Enhanced Magnetic Resonance Imaging to Identify Reversible Myocardial Dysfunction. *N Engl J Med*. 2000;343:1445–53.
- Simonetti OP, Kim RJ, Fieno DS, Hillenbrand HB, Wu E, Bundy JM, Finn JP, Judd RM. An improved MRI imaging technique for the visualization of myocardial infarction. *Radiology*. 2001;218:215–23.
- Aletras AH, Tilak GS, Natanzon A, Hsu L-Y, Gonzalez FM, Hoyt RFJ, Arai AE. Retrospective determination of the area at risk for reperfusion acute myocardial infarction with T2-weighted cardiac magnetic resonance imaging: histopathological and displacement encoding with stimulated echoes (DENSE) functional validations. *Circulation*. 2006;113:1865–70.
- Carlsson M, Ubachs JFA, Hedström E, Helberg E, Jovinge S, Arheden H. Myocardium at Risk After Acute Infarction in Humans on Cardiac Magnetic Resonance. *JACC Cardiovasc Imaging*. 2009;2:569–76.
- Nordlund D, Klug G, Helberg E, Koul S, Larsen TH, Hoffmann P, Metzler B, Erlinge D, Atar D, Aletras AH, Carlsson M, Engblom H, Arheden H. Multivendor, multicentre comparison of contrast-enhanced SSFP and T2-STIR CMR for determining myocardium at risk in ST-elevation myocardial infarction. *Eur Hear J – Cardiovasc Imaging*. 2016;17:44–53.
- Keegan J, Gatehouse PD, Prasad SK, Firmin DN. Improved turbo spin-echo imaging of the heart with motion-tracking. *J Magn Reson Imaging*. 2006;24:563–70.
- Kellman P, Aletras AH, Mancini C, McVeigh ER, Arai AE. T2-prepared SSFP improves diagnostic confidence in edema imaging in acute myocardial infarction compared to turbo spin echo. *Magn Reson Med*. 2007;57:891–7.
- Sörensen P, Helberg E, Saleh N, Bouvier F, Caidahl K, Tornvall P, Rydén L, Pernow J, Arheden H. Assessment of myocardium at risk with contrast enhanced steady-state free precession cine cardiovascular magnetic

- resonance compared to single-photon emission computed tomography. *J Cardiovasc Magn Reson*. 2010;12:25.
10. Ubachs JFA, Sorensen P, Engblom H, Carlsson M, Jovinge S, Perrow J, Arheden H. Myocardium at risk by magnetic resonance imaging: head-to-head comparison of T2-weighted imaging and contrast-enhanced steady-state free precession. *Eur Heart J - Cardiovasc Imaging*. 2012;13:1008–15.
 11. Erlinge D, Götberg M, Lang I, Holzer M, Noc M, Clemmensen P, Jensen U, Metzler B, James S, Bötker HE, Omerovic E, Engblom H, Carlsson M, Arheden H, Östlund O, Wallentin L, Harnek J, Olivecrona GK. Rapid Endovascular Catheter Core Cooling Combined With Cold Saline as an Adjunct to Percutaneous Coronary Intervention for the Treatment of Acute Myocardial Infarction. *J Am Coll Cardiol*. 2014;63:1857–65.
 12. Atar D, Arheden H, Berdeaux A, Bonnet J-L, Carlsson M, Clemmensen P, Cuvier V, Danchin N, Dubois-Randé J-L, Engblom H, Erlinge D, Firat H, Halvorsen S, Hansen HS, Hauke W, Heiberg E, Koul S, Larsen A-L, Le Convoisier P, Nordrehaug JE, Paganelli F, Pruss RM, Rousseau H, Schaller S, Sonou G, Tusev V, Veys J, Vicaut E, Jensen SE. Effect of intravenous TRO40303 as an adjunct to primary percutaneous coronary intervention for acute ST-elevation myocardial infarction: MITOCARE study results. *Eur Heart J*. 2014;36:1–8.
 13. Heiberg E, Sjögren J, Ugander M, Carlsson M, Engblom H, Arheden H. Design and validation of Segment-freely available software for cardiovascular image analysis. *BMC Med Imaging*. 2010;10:1.
 14. Engblom H, Tufvesson J, Jablonowski R, Carlsson M, Aletras AH, Hoffmann P, Jacquier A, Kober F, Metzler B, Erlinge D, Atar D, Arheden H, Heiberg E. A new automatic algorithm for quantification of myocardial infarction imaged by late gadolinium enhancement cardiovascular magnetic resonance: experimental validation and comparison to expert delineations in multi-center, multi-vendor patient data. *J Cardiovasc Magn Reson*. 2016;18:27.
 15. Kloner RA, Ganote CE, Jennings RB. The "No-Reflow" Phenomenon after Temporary Coronary Occlusion in the Dog. *J Clin Invest*. 1974;54:1496–508.
 16. Heiberg E, Ugander M, Engblom H, Götberg M, Olivecrona GK, Erlinge D, Arheden H. Automated quantification of myocardial infarction from MR images by accounting for partial volume effects: animal, phantom, and human study. *Radiology*. 2008;246:581–8.
 17. Ugander M, Sonesson H, Engblom H, van der Pals J, Erlinge D, Heiberg E, Arheden H. Quantification of myocardium at risk in myocardial perfusion SPECT by co-registration and fusion with delayed contrast-enhanced magnetic resonance imaging—an experimental ex vivo study. *Clin Physiol Funct Imaging*. 2012;32:33–8.
 18. Altman DG, Bland JM. Measurement in Medicine: The Analysis of Method Comparison Studies. *Stat*. 1983;32:307.
 19. Bieri Q, Scheffler K. Fundamentals of balanced steady state free precession MRI. *J Magn Res Imaging*. 2013;38(1):2–11.
 20. Ugander M, Bagi PS, Oki AJ, Chen B, Hsu L-Y, Aletras AH, Shah S, Greiser A, Kellman P, Arai AE. Myocardial Edema as Detected by Pre-Contrast T1 and T2 CMR Delineates Area at Risk Associated With Acute Myocardial Infarction. *JACC Cardiovasc Imaging*. 2012;5:596–603.
 21. Arheden H, Saeed M, Higgins CB, Gao DW, Bremerich J, Wytenbach R, Dae MW, Wenland MF. Measurement of the distribution volume of gadopentetate dimeglumine at echo-planar MR imaging to quantify myocardial infarction: comparison with ^{99m}Tc-DTPA autoradiography in rats. *Radiology*. 1999;211:698–708.
 22. Arheden H, Saeed M, Higgins CB, Gao DW, Ursell PC, Bremerich J, Wytenbach R, Dae MW, Wenland MF. Reperfused rat myocardium subjected to various durations of ischemia: estimation of the distribution volume of contrast material with echo-planar MR imaging. *Radiology*. 2000;215:520–8.
 23. Jablonowski R, Engblom H, Kandji M, Nordlund D, Koul S, van der Pals J, Englund E, Heiberg E, Erlinge D, Carlsson M, Arheden H. Contrast-Enhanced CMR Overestimates Early Myocardial Infarct Size: Mechanistic Insights Using ECV Measurements on Day 1 and Day 7. *JACC Cardiovasc Imaging*. 2015;8:1379–89.
 24. Wenland MF, Saeed M, Lauerman K, Derugin N, Mintonovitch J, Cavagna FM, Higgins CB. Alterations in T1 of normal and reperfused infarcted myocardium after Gd-BOPTA versus Gd-DTPA on inversion recovery EPI. *Magn Reson Med*. 1997;37:448–56.
 25. Ugander M, Oki AJ, Hsu LY, Kellman P, Greiser A, Aletras AH, Sibley CT, Chen MY, Patricia Bandettini W, Arai AE. Extracellular volume imaging by magnetic resonance imaging provides insights into overt and sub-clinical myocardial pathology. *Eur Heart J*. 2012;33:1268–78.
 26. Khoshnood A, Carlsson M, Akbarzadeh M, Bhalladvala P, Roijer A, Bodotsof S, Höglund P, Zughaft D, Todorova L, Erlinge DEU. The Effects of Oxygen Therapy on Myocardial Salvage in ST Elevation Myocardial Infarction Treated with Acute Percutaneous Coronary Intervention: The Supplemental Oxygen in Catheterized Coronary Emergency Reperfusion (SOCCER) Study. *Cardiology*. 2015;132:16–21.
 27. De Coster PM, Wijns W, Cauwe F, Robert A, Beckers C, Mellin JA. Area-at-risk determination by technetium-99 m-hexakis-2-methoxyisobutyl isonitrite in experimental reperfused myocardial infarction. *Circulation*. 1990;82:2152–62.
 28. Garcia-Dorado D, Théroux P, Duran JM, Solares J, Alonso J, Sanz E, Munoz R, Elizaga J, Botas J, Fernandez-Aviles F. Selective inhibition of the contractile apparatus. A new approach to modification of infarct size, infarct composition, and infarct geometry during coronary artery occlusion and reperfusion. *Circulation*. 1992;85:1160–74.
 29. Engblom H, Heiberg E, Erlinge D, Jensen SE, Nordrehaug JE, Dubois-Randé J-L, Halvorsen S, Hoffmann P, Koul S, Carlsson M, Atar D, Arheden H. Pals J. Myocardial Salvage Index, Infarct Size, or Biochemical Markers as Endpoint. *J Am Heart Assoc*. 2016;5:e002708.
 30. Bulluck H, White SK, Rosmini S, Bhuvu A, Treibel TA, Fontana M, Abdel-Gadir A, Herrey A, Manisty C, Wan SMY, Groves A, Menezes L, Moon JC, Hausenloy DJ. T1 mapping and T2 mapping at 3 T for quantifying the area-at-risk in reperfused STEMI patients. *J Cardiovasc Magn Reson*. 2015;17:73.

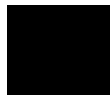
Submit your next manuscript to BioMed Central and we will help you at every step:

- We accept pre-submission inquiries
- Our selector tool helps you to find the most relevant journal
- We provide round the clock customer support
- Convenient online submission
- Thorough peer review
- Inclusion in PubMed and all major indexing services
- Maximum visibility for your research

Submit your manuscript at
www.biomedcentral.com/submit



Paper II



Multi-vendor, multicentre comparison of contrast-enhanced SSFP and T2-STIR CMR for determining myocardium at risk in ST-elevation myocardial infarction

David Nordlund¹, Gert Klug², Einar Heiberg^{1,3}, Sasha Koul⁴, Terje H. Larsen^{5,6}, Pavel Hoffmann⁷, Bernhard Metzler², David Erlinge⁴, Dan Atar⁸, Anthony H. Aletras^{1,9}, Marcus Carlsson¹, Henrik Engblom¹, and Håkan Arheden^{1*}

¹Department of Clinical Physiology, Clinical Sciences, Lund University, Lund, Sweden; ²University Clinic of Internal Medicine III, Cardiology and Angiology, Medical University of Innsbruck, Innsbruck, Austria; ³Department of Biomedical Engineering, Faculty of Engineering, Lund University, Sweden; ⁴Department of Cardiology, Clinical Sciences, Lund University, Lund, Sweden; ⁵Department of Heart Disease, Haukeland University Hospital, Bergen; ⁶Department of Biomedicine, University of Bergen, Bergen, Norway; ⁷Section for Interventional Cardiology, Department of Cardiology, Oslo University Hospital, Ullevål, Oslo, Norway; ⁸Department of Cardiology B, Oslo University Hospital Ullevål, University of Oslo, Oslo, Norway; and ⁹Laboratory of Medical Informatics, School of Medicine, Aristotle University of Thessaloniki, Thessaloniki, Greece

online publish-ahead-of-print 21 March 2016

Aims

Myocardial salvage, determined by cardiac magnetic resonance imaging (CMR), is used as end point in cardioprotection trials. To calculate myocardial salvage, infarct size is related to myocardium at risk (MaR), which can be assessed by T2-short tau inversion recovery (T2-STIR) and contrast-enhanced steady-state free precession magnetic resonance imaging (CE-SSFP). We aimed to determine how T2-STIR and CE-SSFP perform in determining MaR when applied in multicentre, multi-vendor settings.

Methods and results

A total of 215 patients from 17 centres were included after percutaneous coronary intervention (PCI) for ST-elevation myocardial infarction. CMR was performed within 1–8 days. These patients participated in the MITOCARE or CHILL-MI cardioprotection trials. Additionally, 8 patients from a previous study, imaged 1 day post-CMR, were included. Late gadolinium enhancement, T2-STIR, and CE-SSFP images were acquired on 1.5T MR scanners (Philips, Siemens, or GE). In 65% of the patients, T2-STIR was of diagnostic quality compared with 97% for CE-SSFP. In diagnostic quality images, there was no difference in MaR by T2-STIR and CE-SSFP (bias: $0.02 \pm 6\%$, $P = 0.96$, $r^2 = 0.71$, $P < 0.001$), or between treatment and control arms. No change in size or quality of MaR nor ability to identify culprit artery was seen over the first week after the acute event ($P = 0.44$).

Conclusion

In diagnostic quality images, T2-STIR and CE-SSFP provide similar estimates of MaR, were constant over the first week, and were not affected by treatment. CE-SSFP had a higher degree of diagnostic quality images compared with T2 imaging for sequences from two out of three vendors. Therefore, CE-SSFP is currently more suitable for implementation in multicentre, multi-vendor clinical trials.

Keywords

ischaemia • magnetic resonance imaging • myocardium at risk • AAR • area at risk

Introduction

ST-elevation myocardial infarction is a major cause of death worldwide. The myocardium supplied by an occluded coronary vessel

becomes ischaemic and is known as myocardium at risk (MaR). Over time, MaR will gradually develop into infarction until reperfusion occurs.^{1–4} The main objective with acute cardioprotective therapy is to inhibit infarct evolution by timely reperfusion and to

* Corresponding author. Tel: +46 46 173328; Fax: +46 46 151769. E-mail: hakan.arheden@med.lu.se

© The Author 2016. Published by Oxford University Press on behalf of the European Society of Cardiology.

This is an Open Access article distributed under the terms of the Creative Commons Attribution Non-Commercial License (<http://creativecommons.org/licenses/by-nc/4.0/>), which permits non-commercial re-use, distribution, and reproduction in any medium, provided the original work is properly cited. For commercial re-use, please contact journals.permissions@oup.com

minimize further injury associated with reperfusion therapy, thus minimizing final infarct size (IS).³ To evaluate the efficacy of such treatments, IS in relation to MaR is used to calculate myocardial salvage index (MSI) defined as 1-IS/MaR.^{6,7}

Late gadolinium enhancement (LGE) cardiac magnetic resonance (CMR) is currently considered the clinical reference method for quantification of IS.^{8,9} Assessment of MaR, however, is challenging. Recently, CMR has shown potential for quantification of MaR up to 7 days after the acute event using either T2-weighted magnetic resonance (MR) imaging^{6,10–14} or contrast-enhanced steady-state free precession magnetic resonance imaging (CE-SSFP).¹⁵ Both sequences have been validated against myocardial perfusion SPECT^{10,15} and compared against each other in a single-centre setting.¹⁶ However, it is not known how these techniques perform in a multicentre, multi-vendor setting or whether cardioprotection treatments affect MaR. Recently, two international, multicentre, multi-vendor cardioprotection trials, CHILL-MI¹⁷ and MITOCARE,¹⁸ used MSI assessed by CMR as primary (CHILL-MI) or secondary (MITOCARE) end point. Both T2-STIR and CE-SSFP images were acquired during a CMR examination performed 2–6 days after the acute event in these trials.

The aim of the present study was to determine how well T2-STIR and CE-SSFP perform in quantifying MaR and determining culprit vessel across vendors, sites, treatments, and imaging timing using data from the CHILL-MI and MITOCARE trials.

Methods

Study population and design

Patients from the CHILL-MI and MITOCARE trials ($n = 215$) underwent CMR imaging at one occasion within 1–8 days after primary PCI for first-time STEMI.¹⁷ Inclusion and exclusion criteria for the clinical trials have been previously published.^{17,19} In short, all patients had clinical signs of acute myocardial infarction defined as symptoms and electrocardiogram (ECG) consistent with ST-elevation infarction or new left bundle branch block (LBBB) and were ≥ 18 years old with symptom duration < 6 h. Patients with previous myocardial infarction or PCI were excluded. Both the CHILL-MI and MITOCARE trials were approved by the institutional review boards/ethics committees. All patients provided written informed consent.

Since the amount of patients with MR Day 1 was limited in the CHILL-MI and MITOCARE materials, 8 patients with T2-STIR CMR performed on the first day after STEMI from a previous material¹⁰ were included and pooled with the CHILL-MI and MITOCARE data exclusively for the analysis concerning changes in MaR over the first week after infarction. Inclusion criteria for this material have been previously published.¹⁰ In short, patients with no history of MI, presenting with acute STEMI and TIMI 0 flow, were included.

Coronary angiography

Coronary angiography was used to determine culprit vessel. Angiography data from the CHILL-MI trial were analysed by a core laboratory, while angiographic data from the MITOCARE trial were analysed at the respective site.^{17–19}

CMR image acquisition

All CMR examinations were performed on 1.5T scanners from Philips (Philips Healthcare, Best, The Netherlands), Siemens (Siemens AG, Erlangen, Germany), or General Electric (GE Healthcare, Waukesha, WI, USA). Throughout this article, the vendors have been placed in

random order as Vendor 1, 2, and 3. Subjects were placed in a supine position, and images were acquired at end-expiratory breath hold with ECG gating. Initial scout images were acquired to locate the anatomical views of the heart. A black-blood triple inversion recovery T2-weighted sequence (T2-STIR) was used to acquire short-axis imaging covering the entire left ventricle from base to apex before intravenous administration of a gadolinium-based extracellular contrast agent (0.2 mmol/kg). The T2-STIR sequences used were the ones provided by the respective vendor for the particular hardware/scanner model, and no further optimization was performed. Approximately 5 min after the contrast injection, a multi-slice, multi-phase, contrast-enhanced steady-state free precession (CE-SSFP) sequence was applied to acquire short-axis images corresponding to the T2-STIR images.^{15,16} Slice thickness was 8 mm with no slice gap. In-plane resolution was typically 1.5×1.5 mm.

For details regarding imaging and analysis by LGE imaging, see Appendix 1.

For detailed imaging parameters and quality control protocol, see Appendix 2.

CMR analysis

Images were analysed using Segment, version 1.9R3314 (<http://segment.heiberg.se>).²⁰ MaR was assessed from the T2-STIR and CE-SSFP short-axis images as previously described.^{10,15} In short, for T2-STIR images, left ventricular (LV) myocardium was defined by manual delineation of epicardial and endocardial borders. The same was performed for CE-SSFP images in end-diastole and end-systole as previously described.¹⁶ Hyperintense myocardium in T2-STIR and CE-SSFP images was manually delineated for assessment of MaR. If present, hypointense myocardium within the hyperintense area was included as MaR (microvascular obstruction or haemorrhagic infarct). For CE-SSFP, the end-diastolic and end-systolic values of LV mass and MaR were averaged. The delineation of each data set, T2-STIR or CE-SSFP, was performed by one of the three experienced observers (H.E., M.C., and H.A. with 13, 14, and 20 years of experience). Every case was read by a second observer to ensure high-quality measurements. The observer was blinded to the other method for MaR assessment (T2-STIR or CE-SSFP) when performing image analysis. Different opinions were resolved in consensus with a third observer when necessary. Observers had access to LGE images when delineating T2-STIR and CE-SSFP. MaR was expressed as per cent of the LV mass.

MaR by CE-SSFP and infarct delineations were performed by a core laboratory (Imacor AB) as a part of the original MITOCARE and CHILL-MI data analysis, and T2-STIR was analysed by the same observers blinded to the CE-SSFP data ~ 1.5 years later.

Image qualitative analysis

Qualitative analysis was performed separately for T2-STIR and CE-SSFP, by HE blinded to all other data. Images were rated as follows: (i) not diagnostic quality, (ii) acceptable, or (iii) good for defining MaR. Not diagnostic quality were those where MaR could not be evaluated due to artefacts, low signal, high noise levels, or where no clear demarcation between MaR and remote could be identified. Acceptable were those where MaR could be identified, even though some of the issues above were present. Good were those without any of the issues above. The same scale was employed to rate ability to define endo- and epicardium. Acceptable and good images were considered to be of diagnostic quality. The observer also identified the culprit artery as the left anterior descending artery (LAD), right coronary artery (RCA), or left circumflex artery (LCx), without information from LGE images. In cases of left dominance where the MaR involved both the lateral and inferior wall, the observer had to

designate the most probable culprit vessel (LCx or RCA). This was compared with the culprit artery by coronary angiography.

Statistical analysis

Results for continuous variables are expressed as mean \pm standard deviation. Bias according to Bland–Altman was used to compare MaR for T2-STIR and CE-SSFP in patients with complete T2-STIR and CE-SSFP data of diagnostic quality ($n = 127$). The D'Agostino and Pearson test was used to test for normality (Appendix 3). Paired *t*-test was used to test the difference between T2-STIR and CE-SSFP. When comparing MaR in controls and treated groups, an independent *t*-test was used. The Pearson correlations coefficient was used for assessment of correlation between T2-STIR and CE-SSFP. For comparing image quality, the Wilcoxon test was used. Fisher's exact test was used to compare ratio of diagnostic tests and correctly assigned culprit arteries between T2-STIR and CE-SSFP. Assessment of differences in size and quality of MaR over time and heart rates for different image quality groups was tested using a one-way ANOVA test. $P < 0.05$ indicated statistical significance. Analyses were performed using Graphpad Prism (version 5.02, GraphPad Software, San Diego, CA, USA).

Results

Study population

Of the 215 patients included in the study, 200 (93%) had complete T2-STIR datasets, 204 (95%) had complete CE-SSFP datasets, and 191 (89%) had complete LGE datasets. Fifty patients (50%) from the CHILL-MI trial received adjuvant hypothermia treatment, and 60 patients (52%) from the MITOCARE trial received adjuvant treatment with TRO40303. For patient and CMR characteristics, see Appendix 4.

Image quality

Sixty-five per cent of T2-STIR vs. 97% of CE-SSFP datasets were considered of diagnostic quality ($P < 0.001$, Figure 1). Ratio of datasets of diagnostic quality for T2-STIR was 73% for LAD, 65% for LCx, and 59% for RCA, whereas for CE-SSFP it was 97% for LAD, 100% for LCx, and 98% for RCA. Anterior (LAD) ischaemia trended towards higher level of T2-STIR images of diagnostic quality compared with lateral and inferior (LCx + RCA) culprit vessels, $P = 0.068$, while there was no difference between vessels for CE-SSFP, $P = 1.0$. Image quality of MaR for T2-STIR was 1.8 ± 1.1 and for CE-SSFP 2.7 ± 0.5 ($P < 0.001$). Heart rate did not differ with image quality for T2-STIR (image quality 1: 68 ± 16 , 2: 69 ± 10 , 3: 68 ± 10 , $P = 0.87$) or CE-SSFP (image quality 1: 71 ± 12 , 2: 67 ± 14 , 3: 68 ± 11 , $P = 0.81$). Image quality (score 1–3) for endo- and epicardial delineation was 2.3 ± 0.7 for T2-STIR and 2.8 ± 0.4 for CE-SSFP ($P < 0.001$).

T2-STIR vs. CE-SSFP for MaR

Figure 2 shows correlation between T2-STIR and CE-SSFP images by vendor and treatment groups. For images of diagnostic quality, bias between MaR by T2-STIR and CE-SSFP was $0.02 \pm 6\%$ ($P = 0.96$, $n = 126$), while size of MaR was $36 \pm 11\%$ by T2-STIR and $36 \pm 10\%$ by CE-SSFP. There was a strong correlation between MaR by T2-STIR and CE-SSFP in images of diagnostic quality ($r^2 = 0.71$, $P < 0.001$, $n = 126$). MaR by culprit artery did not differ between T2-STIR and CE-SSFP in images of diagnostic quality

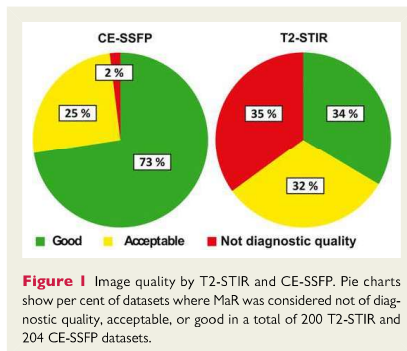


Figure 1 Image quality by T2-STIR and CE-SSFP. Pie charts show per cent of datasets where MaR was considered not of diagnostic quality, acceptable, or good in a total of 200 T2-STIR and 204 CE-SSFP datasets.

(LAD: 44 ± 9 vs. $43 \pm 10\%$, $P = 0.45$, $n = 55$; LCx: 26 ± 7 vs. $28 \pm 8\%$, $P = 0.57$, $n = 14$; RCA: 31 ± 7 vs. $32 \pm 6\%$, $P = 0.68$, $n = 57$). Figure 3 shows examples of T2-STIR, CE-SSFP, and LGE images from two patients.

Treated vs. controls

There was no difference in MaR between controls and patients treated with hypothermia in the CHILL-MI trial (bias by T2-STIR: $1.66 \pm 2.84\%$, $P = 0.56$; bias by CE-SSFP $0.23 \pm 2.25\%$, $P = 0.91$). Neither was there any difference in MaR between controls and patients receiving TRO40303 treatment (bias by T2-STIR: $-0.69 \pm 2.64\%$, $P = 0.80$; bias by CE-SSFP: $0.14 \pm 1.94\%$, $P = 0.94$). For details, see Appendix 4.

Culprit vessel

CMR located correct culprit vessel in 89% of patients by T2-STIR and 97% of patients by CE-SSFP ($P = 0.0015$, Table 1). Sensitivity for LCx was lower than LAD/RCA for both T2-STIR and CE-SSFP. Using T2-STIR, the observer was unable to assign culprit vessel in 11% of patients with RCA occlusion, 17% of patients with LCx occlusions, and 4% of patients with LAD occlusion. All patients were assigned a culprit vessel using CE-SSFP. A low sensitivity for assigning LCx as culprit artery was due to incorrect classification as RCA in five patients for CE-SSFP, while for T2-STIR it was incorrect classification as LAD for one patient, RCA for two patients, and inability to assign culprit vessel in four patients.

Differences between vendors and sites

Vendors 1 and 3 had lower rates of T2-STIR datasets of diagnostic quality compared with CE-SSFP (T2-STIR: 58 and 48%, CE-SSFP: 100 and 99%, respectively, $P < 0.001$), whereas no difference was found for Vendor 2 (T2-STIR: 90% and CE-SSFP: 96%, $P = 0.19$, Figure 4). Figure 5 shows examples of T2-STIR and CE-SSFP images from each vendor. In 13 sites, rate of CE-SSFP of diagnostic quality was higher compared with T2-STIR (Figure 6), and the remaining four sites were using MR cameras from Vendor 2. Rate of datasets of diagnostic quality for sites using Vendor 1 was: $55 \pm 5\%$ by T2-STIR and $100 \pm 0\%$ by CE-SSFP, for vendor 2: $88 \pm 17\%$ by

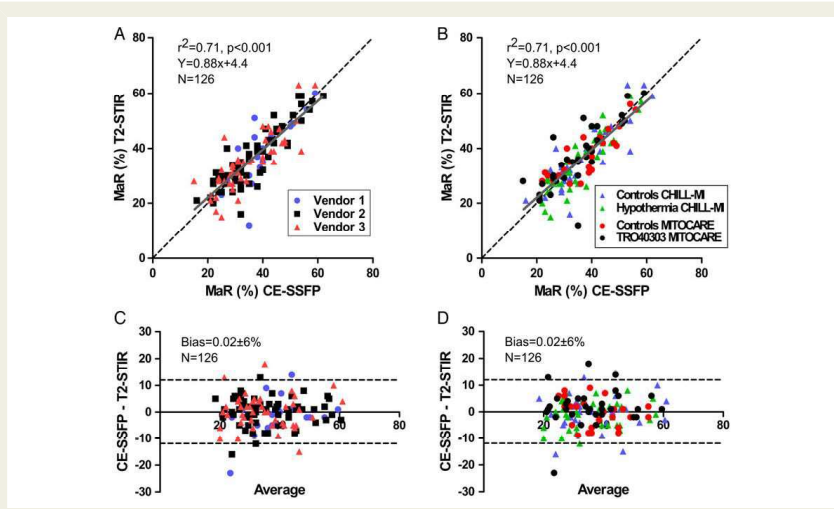


Figure 2 MaR by T2-STIR and CE-SSFP. (A) MaR by T2-STIR vs. CE-SSFP divided by vendors, $r^2 = 0.71$. (B) MaR by T2-STIR vs. CE-SSFP divided by treatment groups. Dashed lines are identity and solid lines regression. (C) The Bland–Altman plot of CE-SSFP and T2-STIR divided by vendors, and (D) the Bland–Altman plot of CE-SSFP and T2-STIR divided by treatment groups, mean difference $0.02 \pm 6\%$, dashed lines indicate $\pm 2SD$. Measurements are expressed as % of LV mass. MaR, myocardium at risk.

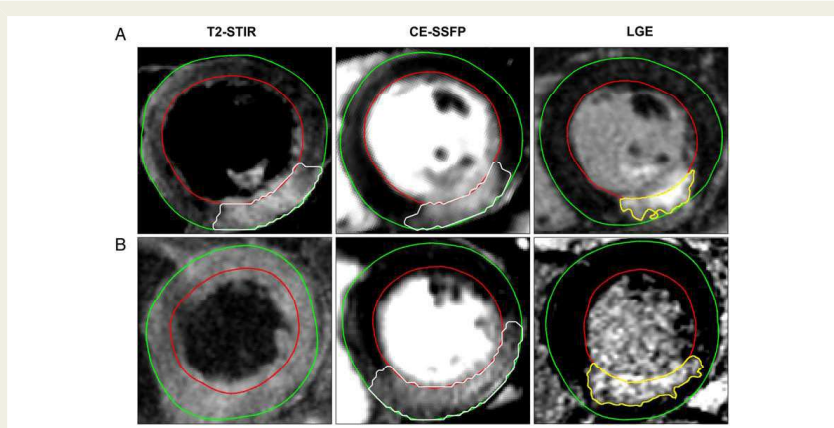


Figure 3 MaR by T2-STIR and CE-SSFP and infarct by LGE in corresponding mid-ventricular short-axis slices from two patients. Upper row (A) shows corresponding T2-STIR and CE-SSFP images of good quality. Bottom row (B) shows T2-STIR not of diagnostic quality with corresponding CE-SSFP image. For technical details on image acquisition see Appendix 5. LGE, late gadolinium enhancement.

Table 1 Culprit arteries by T2-STIR and CE-SSFP in relation to angiography, presented as sensitivity and specificity

	Sensitivity (%)	Specificity (%)	n (angiography)
T2-STIR			
LAD	96	98	78
LCx	70	100	23
RCA	88	98	99
CE-SSFP			
LAD	100	100	79
LCx	80	99	25
RCA	99	95	100

Culprit artery was correctly identified in 89% of patients using T2-STIR and 97% of patients using CE-SSFP ($P = 0.0015$).
T2-STIR, T2-weighted short tau inversion recovery; CE-SSFP, contrast-enhanced SSFP; LAD, left anterior descending artery; LCx, left circumflex artery; RCA, right coronary artery; n, number of patients for each culprit vessel decided by angiography.

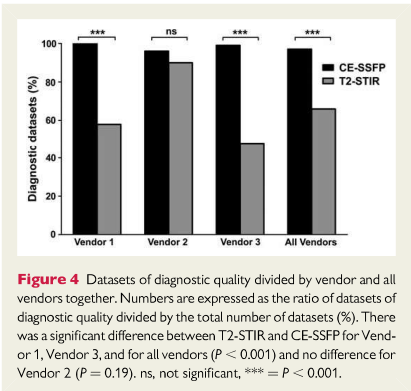


Figure 4 Datasets of diagnostic quality divided by vendor and all vendors together. Numbers are expressed as the ratio of datasets of diagnostic quality divided by the total number of datasets (%). There was a significant difference between T2-STIR and CE-SSFP for Vendor 1, Vendor 3, and for all vendors ($P < 0.001$) and no difference for Vendor 2 ($P = 0.19$). ns, not significant, *** = $P < 0.001$.

T2-STIR and $95 \pm 9\%$ by CE-SSFP, and for Vendor 3: $40 \pm 20\%$ by T2-STIR and $98 \pm 5\%$ by CE-SSFP. Two sites (5 and 8, both using Vendor 2) had a higher rate of T2-STIR of diagnostic quality compared with CE-SSFP. For these sites, only one CE-SSFP dataset was not of diagnostic quality (Figure 6).

Changes in MaR over time

No change in size or quality of MaR or ability to identify culprit artery was seen over the first week after ischaemia reperfusion ($P = 0.44$, Figure 7).

Discussion

The findings in the present study, with data from two multicentre, multi-vendor studies on cardioprotection, showed that CE-SSFP

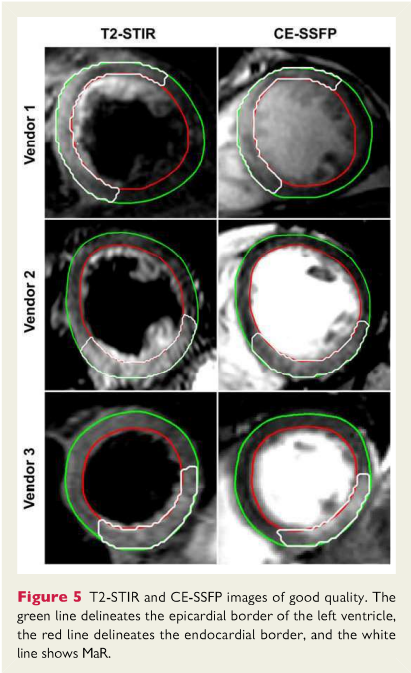


Figure 5 T2-STIR and CE-SSFP images of good quality. The green line delineates the epicardial border of the left ventricle, the red line delineates the endocardial border, and the white line shows MaR.

enabled determination of MaR across vendors and sites, whereas T2-STIR imaging was not of diagnostic quality in approximately one-third of patients. In images of diagnostic quality, however, CE-SSFP and T2-STIR showed a good agreement for assessment of MaR.

A non-contrast-enhanced balanced SSFP yields a T_2/T_1 -weighted contrast that creates an extraordinarily high steady-state signal. After myocardial ischaemia, both T_1 and T_2 are increased due to oedema with T_2 being affected to a higher degree, thus increasing the T_2/T_1 ratio. Gadolinium-based contrast agent distributes in proportion to extracellular space, which is greater in salvaged than in normal myocardium and even greater in infarcted myocardium.^{21,22} As T_1 time is affected more than T_2 time at lower concentrations of gadolinium, the T_2/T_1 ratio increases further in salvaged myocardium, but the effect may be attenuated at higher gadolinium concentrations, such as in infarcted myocardium, when the effect on T_2 time is more marked.²³ This might explain the homogenous appearance of MaR in CE-SSFP images; however, further investigation is needed to elucidate these mechanisms.

The differences in diagnostic quality may have several explanations. Since CE-SSFP is a multi-phase cine sequence, MaR can be visualized and quantified in several timeframes; thus, the distinction between MaR and remote myocardium may be easier to appreciate.

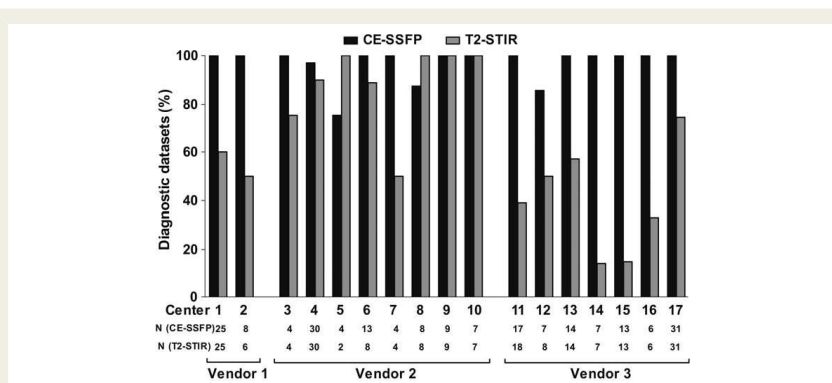


Figure 6 Datasets of diagnostic quality divided by site. All 17 sites that participated in the CHILL-MI and MITOCARE trials are represented. Numbers are expressed as per cent of total datasets. Note that CE-SSFP had a higher rate of images of diagnostic quality compared with T2-STIR in 13 of the sites.

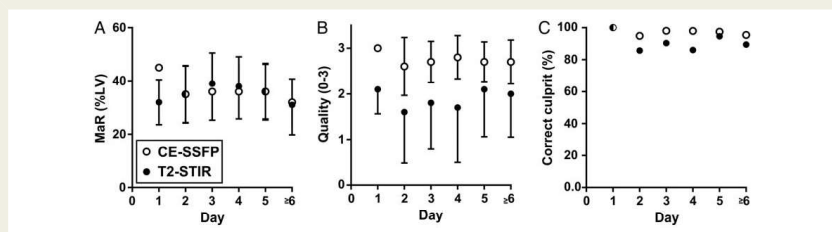


Figure 7 MaR by T2-STIR and CE-SSFP over the first week. (A) MaR as per cent of LV mass over time, (B) image of diagnostic quality over time, and (C) ratio of correctly assigned culprit vessel compared with angiography over time. Note that there is no significant change in MaR during the first week in any of the above aspects. Open and closed circles show mean values of MaR by CE-SSFP and T2-STIR, respectively. Error bars show ± 1 SD. MaR, myocardium at risk; LV, left ventricular mass.

Differences in experience with CMR between the different sites could also affect image quality and implementation of the different sequences. However, since CE-SSFP images were considered of diagnostic quality in almost all the patients (97%), this technique seems to be independent of the level of experience. SSFP cine imaging is included in most CMR protocols, and the implementation of this sequence is highly standardized, which can be appreciated when considering the similarities in imaging parameters (Appendix 2) compared with T2-STIR where imaging parameters were markedly different. CE-SSFP is also known to be robust to changes in TR and thus image resolution.²⁴ The implementation of T2-STIR may, however, differ with regard to, e.g., surface coil sensitivity correction, resulting in differences in image quality. It has previously been shown that dark-blood T2-STIR imaging is subject to artefacts due to through-plane motion, particularly in the lateral and inferior LV

wall.^{12,25} This might explain the trend towards a difference in diagnostic quality of MaR by T2-STIR seen in different vessels, with more images of diagnostic quality in the anterior lesions (LAD: 74%) compared with the lateral and inferior lesions (LCx: 65% and RCA: 59%). It could also explain the inability to assign culprit artery to patients with LCx occlusion using T2-STIR. The incorrect assignment of LCx occlusions as RCA by using CE-SSFP is, however, to be expected based on the significant overlap of their distribution territories.^{26,27} Some of these limitations with black-blood T2-STIR imaging might be overcome by using white-blood T2-weighted sequences such as T2-prepared SSFP¹² or ACUT₂E-TSE-SSFP,¹⁷ which has been shown to provide improved image quality and diagnostic accuracy compared with black-blood T2-weighted imaging.^{28,29} Furthermore, quantitative T1- and T2-mapping techniques have shown promise in assessing MaR.^{30–32} Validation and standardization, however, on how these

mapping techniques should be implemented on different platforms are still lacking.

It should be noted that, given similar hardware capabilities, all vendors could potentially reach similar performance with T2-STIR.

To what extent MaR assessed by CMR is affected by cardioprotection treatment has been a topic of discussion in the CMR community. Findings in the present study suggest that MaR is not affected by the adjuvant treatments in the CHILL-MI and MITOCARE studies since there was no significant difference in MaR between the treatment and placebo groups, neither for T2-STIR nor for CE-SSFP. In a recent post-conditioning cardioprotection trial, however, Thuny *et al.*³³ showed a decrease in MaR assessed by T2-STIR compared with controls. Additionally, White *et al.*³⁴ showed a decrease in MaR assessed by T2-mapping after ischaemic pre-conditioning. There are, however, differences in the methodology used in the study by White *et al.* compared with the present study. The White study used five short-axis slices and not the entire left ventricle as in the present study. Furthermore, it used the semi-automated method of Otsu, which has been shown to have limited accuracy for assessment of MaR in T2-weighted imaging.³⁵ Thus, there are still conflicting results regarding the accuracy of T2-weighted imaging for determination of MaR in cardioprotection trials.

Recent experimental data suggest a bimodal pattern of oedema after ischaemia/reperfusion injury as measured with T2-STIR and T2-mapping, suggesting that the oedema is pronounced immediately after reperfusion then decreases over the first day and slowly increases again over the first week.³⁶ The clinical data from the current study do not support such a bimodal pattern either in size, quality of MaR images, or in ability to detect culprit artery.

The findings in the present study have implications for designing clinical cardioprotection trials using MSI as surrogate end point. If T2-STIR alone had been used for assessment of MaR in CHILL-MI and MITOCARE, approximately one-third of the patients would have been excluded due to images not being of diagnostic quality. This would increase the number of patients needed to reach statistical power, thus increasing time and costs to perform a successful cardioprotection trial. Furthermore, CE-SSFP shortens the protocol since cine SSFP images are acquired anyway for functional assessment, which means no extra scanning to determine MaR. T2w imaging requires additional imaging and thereby longer protocols.

Limitations

Only STIR black-blood T2-weighted imaging was compared with CE-SSFP. Thus, the results of this study cannot be generalized to other T2-weighted sequences (e.g. bright-blood methods or T2 mapping). Surface coil intensity correction varied between vendors and sites which may have affected the results. However, this did not seem to affect the quality for CE-SSFP images, which is a strength of this technique. No reference standard for MaR assessment was available. Thus, it is not possible to conclude that one technique is superior in correctly determining MaR. Previous studies, however, have validated both T2-STIR¹⁰ and CE-SSFP¹⁵ against myocardial perfusion SPECT, with good agreement in images of diagnostic quality.

The current difference in image quality between CE-SSFP and T2-STIR might be explained by differences in implementation of T2-STIR between vendors. The T2-STIR sequences could probably become more equal if they are further improved and standardized.

Conclusions

In images of diagnostic quality, T2-STIR and CE-SSFP provide similar estimates of MaR, were constant over the first week, and were not affected by treatment. CE-SSFP had a higher degree of diagnostic quality images compared with T2 imaging for sequences from two out of the three vendors. Therefore, CE-SSFP is currently more suitable for implementation in multicentre, multi-vendor clinical trials.

Conflict of interest: H.A. is a shareholder of Imacor. H.A., E.H., M.C., and H.E. have been part-time employees in Imacor.

Funding

The study was funded by The Swedish Heart and Lung Foundation, Region of Scania, and the Medical Faculty of Lund University. CHILL-MI was funded by Region of Skane, Philips Healthcare, Lund University and Uppsala University. MITOCARE was funded by Trophos Pharmaceutical Company and the European Commission (7th Framework, Grant Agreement HEALTH-2010-261034). Funding to pay the Open Access publication charges for this article was provided by the Medical Faculty of Lund University.

Appendix 1

- (1) Long- and short-axis slices covering the left ventricle were acquired ~15 min after injection of the gadolinium-based contrast agent. The LGE images were acquired using an inversion-recovery gradient-recalled echo sequence, with or without phase-sensitive reconstruction (PSIR), with a slice thickness of 8 mm with no slice gap. In-plane resolution was typically 1.5 × 1.5 mm. Inversion time was adjusted to null the signal of viable myocardium.¹¹ Infarcted myocardium was delineated from the short-axis LGE images according to a previously described method.²³

Appendix 2

T2-STIR typical imaging parameters from DICOM files

Parameter	Vendor 1	Vendor 2	Vendor 3
Pixel size X (mm)	1.5 (1.0–2.0)	2.2 (1.9–2.3)	1.5 (1.4–1.6)
Pixel size Y (mm)	1.7 (1.2–2.0)	2.5 (2.3–2.9)	2.1 (1.4–2.5)
TI (ms)	150	180	150 (150–170)
TE (ms)	73 (59–84)	100 (65–100)	47 (47–63)
ETL (n)	32 (31–32)	32 (31–33)	15 (15–15)
Bandwidth (KHz)	94 (63–125)	93 (72–138)	60 (60–61)
Slice thickness (mm)	8	8	8
TR (n of heartbeats)	2	2	2 (1–3 ^a)
Time (s)	161 (67–268)	204 (158–241)	306 (226–372)

Numbers are given as median (interquartile range).
TI, inversion time; TE, echo time; ETL, echo train length; TR, repetition time; time, time to acquire a full short-axis stack.
^aOne instance using a TR of 1 heartbeat and one instance using a TR of 3 heartbeats.

CE-SSFP typical imaging parameters from DICOM files

Parameter	Vendor 1	Vendor 2	Vendor 3
Pixel size X (mm)	1.7 (1.1–2.3)	1.3 (1.1–1.7)	0.8 (0.8–0.9)
Pixel size Y (mm)	2.3 (1.3–2.7)	1.4 (1.2–1.9)	1.2 (1.1–1.4)
α (°)	57.5 (45–70)	60 (60–60)	65 (54–71)
TE (ms)	1.6 (1.4–1.8)	1.7 (1.5–1.8)	1.3 (1.1–1.5)
VPS (n)	19 (16–24)	12 (11–16)	16 (13–23)
Bandwidth (KHz)	164 (109–219)	200 (196–200)	197 (179–227)
Slice thickness (mm)	8	8	8
TR (ms, range)	3.7 (3.2–4.0)	3.5 (3.1–3.6)	2.9 (2.6–3.5)
Time (s)	98 (90–193)	156 (107–189)	No information
Temporal resolution (ms)	30 (28–33)	21 (18–30)	51 (39–65)

Numbers are given as median (interquartile range).
α, Flip angle; TE, echo time; VPS, views per segment; TR, repetition time; time, time to acquire a full short-axis stack.

Quality control

The same protocol for quality control was used for both the CHILL-MI and the MITOCARE trials. Before inclusion began, all centres had to qualify by sending images from two patients, including LGE, T2-STIR, and CE-SSFP, which they considered to be of diagnostic quality to the core lab. The core lab then ensured that the images were of sufficient quality before a centre was accepted.

During inclusion, all studies were continuously evaluated by the core lab.

Appendix 3

The D’Agostino and Pearson test was used to test for normality. T2-STIR ($P = 0.22$) and CE-SSFP ($P = 0.07$) of diagnostic quality did not show statistically significant deviation from a Gaussian distribution, neither did controls (T2-STIR: $P = 0.29$, CE-SSFP: $P = 0.18$) or treated (T2-STIR: $P = 0.39$, CE-SSFP: $P = 0.15$) in the CHILL-MI subset nor controls (T2-STIR: $P = 0.53$, CE-SSFP: $P = 0.20$) or treated (T2-STIR: $P = 0.81$, CE-SSFP: $P = 0.09$) in the MITOCARE subset.

Appendix 4

CMR characteristics

MaR by CE-SSFP (% LV)	36 ± 10
MaR by T2-STIR (% LV)	36 ± 11
Infarct by LGE (% LV)	17 ± 10

Continued

Appendix 4 Continued

CMR characteristics

MSI (% MaR)		54 ± 18
Ejection fraction (%)		48 ± 9
Heart rate during CMR (beats/min)		68 ± 12
	CE-SSFP	T2-STIR
MaR, hypothermia treated (% LV)	36 ± 10	36 ± 12
MaR, CHILL-MI controls (% LV)	37 ± 12	37 ± 11
MaR, TRO40303 treated (% LV)	35 ± 10	37 ± 12
MaR, MITOCARE controls (% LV)	35 ± 10	36 ± 11
Image quality ‘non-diagnostic’ (n)	4	70
Image quality ‘acceptable’ (n)	52	63
Image quality ‘good’ (n)	148	67

Numbers are given as mean ± SD.
MaR, myocardium at risk; % LV, per cent of left ventricular mass; LGE, late gadolinium enhancement; CMR, cardiac magnetic resonance imaging; CE-SSFP, contrast-enhanced SSFP; T2-STIR, T2-weighted short tau inversion recovery.

Patient characteristics

Number of patients (n)	215
Complete CE-SSFP datasets (n)	204
Complete T2-STIR datasets (n)	200
Treated with hypothermia (n)	50
Treated with TRO40303 (n)	60
Culprit vessel by angiography	
LAD (n)	84
LCx (n)	25
RCA (n)	106
Peak cTnT ^a (ng/L)	12 100 ± 9300
Peak hsTnT ^b (ng/L)	7000 ± 4600
Time from pain to balloon (min)	184 ± 73
Time from ischaemic event to CMR (days)	3.8 ± 1.4
MR Day 1 (n)	2
MR Day 2 (n)	39
MR Day 3 (n)	53
MR Day 4 (n)	53
MR Day 5 (n)	40
MR Day 6 (n)	19
MR Day 7 (n)	3
MR Day 8 (n)	2
MR day unknown (n)	4

CE-SSFP, contrast-enhanced SSFP; T2-STIR, T2-weighted short tau inversion recovery; cTnT, fourth-generation cardiac troponin T; hsTnT, high-sensitivity troponin T; CMR, cardiac magnetic resonance imaging.

^aPatients in the MITOCARE trial.

^bPatients in the CHILL-MI trial.

Appendix 5

Parameter	T2-STIR		CE-SSFP	
	Figure 3A	Figure 3B	Figure 3A	Figure 3B
Pixel size X (mm)	1	1	0.80	0.80
Pixel size Y (mm)	1	1	1.20	1.20
α (°)	180	180	76	73
TE (ms)	47	47	1.12	1.12
ETL (n)	15	15	15	15
Bandwidth (KHz)	61	61	179	182
Slice thickness (mm)	8	8	8	8
TR (ms)	1756	2056	2.6	2.6
Temporal resolution (ms)	—	—	39	39
TI (ms)	170	170	—	—
Heart rate	64	69	64	69

α , Flip angle; TE, echo time; ETL, echo train length; TR, repetition time; TI, inversion time.

References

1. Reimer KA, Lowe JE, Rasmussen MM, Jennings RB. The wavefront phenomenon of ischemic cell death. 1. Myocardial infarct size vs duration of coronary occlusion in dogs. *Circulation* 1977;**56**:786–94.

2. Lowe JE, Reimer KA, Jennings RB. Experimental infarct size as a function of the amount of myocardium at risk. *Am J Pathol* 1978;**90**:363–79.

3. Lee JT, Ideker RE, Reimer KA. Myocardial infarct size and location in relation to the coronary vascular bed at risk in man. *Circulation* 1981;**64**:526–34.

4. Braunwald E, Kloner RA. Myocardial reperfusion: a double-edged sword? *J Clin Invest* 1985;**76**:1713–9.

5. Gerczuk PZ, Kloner RA. An update on cardioprotection. *J Am Coll Cardiol* 2012;**59**: 969–78.

6. Friedrich MG, Abdel-Aty H, Taylor A, Schulz-Menger J, Messroghli D, Dietz R. The salvaged area at risk in reperfused acute myocardial infarction as visualized by cardiovascular magnetic resonance. *J Am Coll Cardiol* 2008;**51**:1581–7.

7. Hedström E, Engblom H, Frogner F, Åström-Olsson K, Ohlin H, Jovinge S et al. Infarct evolution in man studied in patients with first-time coronary occlusion in comparison to different species—implications for assessment of myocardial salvage. *J Cardiovasc Magn Reson* 2009;**11**:38.

8. Simonetti OP, Kim RJ, Fieno DS, Hillenbrand HB, Wu E, Bundy JM et al. An improved MR imaging technique for the visualization of myocardial infarction. *Radiology* 2001;**218**:215–23.

9. Kim RJ, Wu E, Rafael A, Chen E-L, Parker MA, Simonetti O et al. The use of contrast-enhanced magnetic resonance imaging to identify reversible myocardial dysfunction. *N Engl J Med* 2000;**343**:1445–53.

10. Carlsson M, Ubachs JFA, Hedström E, Heiberg E, Jovinge S, Arheden H. Myocardium at risk after acute infarction in humans on cardiac magnetic resonance. *JACC Cardiovasc Imaging* 2009;**2**:569–76.

11. Aletras AH, Kelman P, Derbyshire JA, Arai AE. ACUT2E TSE-SSFP: a hybrid method for T2-weighted imaging of edema in the heart. *Magn Reson Med* 2008;**59**: 229–35.

12. Kellman P, Aletras AH, Mancini C, McVeigh ER, Arai AE. T2-prepared SSFP improves diagnostic confidence in edema imaging in acute myocardial infarction compared to turbo spin echo. *Magn Reson Med* 2007;**57**:891–7.

13. Aletras AH, Tilak GS, Natananz A, Hsu L-Y, Gonzalez FM, Hoyt RJ et al. Retrospective determination of the area at risk for reperfused acute myocardial infarction with T2-weighted cardiac magnetic resonance imaging: histopathological and displacement encoding with stimulated echoes (DENSE) functional validations. *Circulation* 2006;**113**:1865–70.

14. Ganame J, Messalli G, Dymarkowski S, Rademakers FE, Desmet W, Van De Werf F et al. Impact of myocardial haemorrhage on left ventricular function and remodeling in patients with reperfused acute myocardial infarction. *Eur Heart J* 2009;**30**: 1440–9.

15. Sörensson P, Heiberg E, Saleh N, Bouvier F, Caidahl K, Tornvall P et al. Assessment of myocardium at risk with contrast enhanced steady-state free precession cine cardiovascular magnetic resonance compared to single-photon emission computed tomography. *J Cardiovasc Magn Reson* 2010;**12**:25.

16. Ubachs JFA, Sörensson P, Engblom H, Carlsson M, Jovinge S, Pernow J et al. Myocardium at risk by magnetic resonance imaging: head-to-head comparison of T2-weighted imaging and contrast-enhanced steady-state free precession. *Eur Heart J Cardiovasc Imaging* 2012;**13**:1008–15.

17. Erlinge D, Göteborg M, Lang I, Holzer M, Noc M, Clemmensen P et al. Rapid endovascular catheter core cooling combined with cold saline as an Adjunct to Percutaneous Coronary Intervention For the Treatment of Acute Myocardial Infarction (The CHILL-MI trial). *J Am Coll Cardiol* 2014;**63**:1857–65.

18. Atar D, Arheden H, Berdeaux A, Bonnet J-L, Carlsson M, Clemmensen P et al. Effect of intravenous TRO40303 as an adjunct to primary percutaneous coronary intervention for acute ST-elevation myocardial infarction: MITOCARE study results. *Eur Heart J* 2015;**36**:112–9.

19. MITOCARE Study Group. Rationale and design of the ‘MITOCARE’ study: a Phase II, multicenter, randomized, double-blind, placebo-controlled study to assess the safety and efficacy of TRO40303 for the reduction of reperfusion injury in patients undergoing percutaneous coronary in. *Cardiology* 2012;**123**:201–7.

20. Heiberg E, Sjögren J, Ugander M, Carlsson M, Engblom H, Arheden H. Design and validation of segment—freely available software for cardiovascular image analysis. *BMC Med Imaging* 2010;**10**:1.

21. Arheden H, Saeed M, Higgins CB, Gao DW, Bremerich J, Wyttenbach R et al. Measurement of the distribution volume of gadopentetate dimeglumine at echo-planar MR imaging to quantify myocardial infarction: comparison with 99mTc-DTPA autoradiography in rats. *Radiology [Internet]* 1999;**211**:698–708. Available from: <http://www.ncbi.nlm.nih.gov/pubmed/10352594>.

22. Arheden H, Saeed M, Higgins CB, Gao DW, Ursell PC, Bremerich J et al. Reperfused rat myocardium subjected to various durations of ischemia: estimation of the distribution volume of contrast material with echo-planar MR imaging. *Radiology [Internet]* 2000;**215**:520–8. Available from: <http://www.ncbi.nlm.nih.gov/pubmed/10796935>.

23. Rohrer M, Bauer H, Mintorovitch J, Requardt M, Weinmann H-J. Comparison of magnetic properties of MRI contrast media solutions at different magnetic field strengths. *Invest Radiol [Internet]* 2005;**40**:715–24. Available from: <http://www.ncbi.nlm.nih.gov/pubmed/16230904>.

24. Bieri O, Scheffler K. Fundamentals of balanced steady state free precession MRI. *J Magn Reson Imaging* 2013;**38**:2–11.

25. Keegan J, Gatehouse PD, Prasad SK, Firmin DN. Improved turbo spin-echo imaging of the heart with motion-tracking. *J Magn Reson Imaging* 2006;**24**:563–70.

26. Persson E, Palmer J, Pettersson J, Warren SG, Borges-Neto S, Wagner GS et al. Quantification of myocardial hypoperfusion with 99m Tc-sestamibi in patients undergoing prolonged coronary artery balloon occlusion. *Nucl Med Commun* 2002;**23**:219–28.

27. Perezto-Valdés O, Candell-Riera J, Santana-Boado C, Angel J, Agudé-Bruix S, Castell-Conesa J et al. Correspondence between left ventricular 17 myocardial segments and coronary arteries. *Eur Heart J* 2005;**26**:2637–43.

28. Payne AR, Casey M, McClure J, McGeoch R, Murphy A, Woodward R et al. Bright-blood T2-weighted MRI has higher diagnostic accuracy than dark-blood short tau inversion recovery MRI for detection of acute myocardial infarction and for assessment of the ischemic area at risk and myocardial salvage. *Circ Cardiovasc Imaging* 2011;**4**:210–9.
29. Viallon M, Mewton N, Thuny F, Guehring J, O'Donnell T, Stemmer A et al. T2-weighted cardiac MR assessment of the myocardial area-at-risk and salvage area in acute reperfused myocardial infarction: comparison of state-of-the-art dark blood and bright blood T2-weighted sequences. *J Magn Reson Imaging* 2012; **35**:328–39.
30. Aletras AH. Quantitative in vivo T2 measurements differentiate both infarcted and peri-infarct from normal myocardium. *Circulation* 2007;**116**:758.
31. Ugander M, Bagi PS, Oki AJ, Chen B, Hsu L-Y, Aletras AH et al. Myocardial edema as detected by pre-contrast T1 and T2 CMR delineates area at risk associated with acute myocardial infarction. *JACC Cardiovasc Imaging* 2012;**5**:596–603.
32. Hammer-Hansen S, Ugander M, Hsu L-Y, Taylor J, Kellman P, Arai AE. Distinction of salvaged and infarcted myocardium within the ischemic area at risk with T2 mapping. *J Cardiovasc Magn Reson* 2014;**16**(Suppl. 1):P3.
33. Thuny F, Lairez O, Roubille F, Mewton N, Rioufol G, Sportouch C et al. Post-conditioning reduces infarct size and edema in patients with ST-segment elevation myocardial infarction. *J Am Coll Cardiol* 2012;**59**:2175–81.
34. White SK, Frohlich GM, Sado DM, Maestrini V, Fontana M, Treibel TA et al. Remote ischemic conditioning reduces myocardial infarct size and edema in patients with ST-segment elevation myocardial infarction. *JACC Cardiovasc Interv* 2015;**8**:178–88.
35. Sjögren J, Ubachs JF, Engblom H, Carlsson M, Arheden H, Heiberg E. Semi-automatic segmentation of myocardium at risk in T2-weighted cardiovascular magnetic resonance. *J Cardiovasc Magn Reson* 2012;**14**:10.
36. López-martín GJ, Ech T, García-ruiz JM, Molina-iracheta A, Roselló X. Myocardial edema after ischemia/reperfusion is not stable and follows a bimodal pattern. *J Am Coll Cardiol* 2015;**65**:315–23.

IMAGE FOCUS

doi:10.1093/ehjci/jev058

Online publish-ahead-of-print 3 April 2016

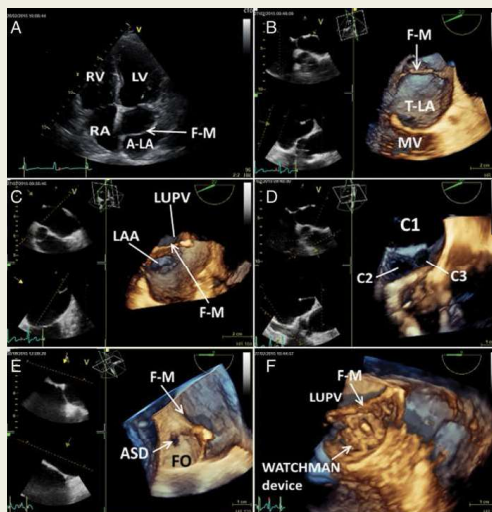
Left atrial appendage closure in a patient with cor triatriatum and ASD: the added value of 3D echocardiography

Laura Lanzoni*, Giulio Molon, Guido Canali, Stefano Bonapace, and Enrico Barbieri

Cardiology Department, Ospedale Sacro Cuore-Don Calabria, Negrar, Verona, Italy

* Corresponding author. Tel: +39 3475364340; Fax: +39 0456013925. E-mail: lanzo555@yahoo.com

A 47-year-old woman with cor triatriatum (Panel A, see Supplementary data online, Video S1 and S2) and small ostium secundum atrial septal defect (ASD) was evaluated for percutaneous closure of left atrial appendage (LAA) due to permanent AF and Cooley's disease (CHA2-DS2-VASC2;HAS-BLED4). 3D transoesophageal echocardiography shows the fibromuscular membrane (F-M) dividing the left atrium into two chambers: the accessory left atrium (A-LA) receives venous blood, whereas the true left atrium (T-LA) is in contact with mitral valve (MV), fossa ovalis (FO), and LAA (Panels B and C, see Supplementary data online, Video S3 and S4). There is one large unrestricted communication between the two chambers (C1) with mean gradient of 2 mmHg at Doppler interrogation and two smaller communications in the membrane itself (C2–C3) corresponding to Loeffler's classification type 3 (Panel D, see Supplementary online data, Video S5). A small ASD just below the membrane is also associated (Panel E, see Supplementary data online, Video S6). During the procedure, after exclusion of clots and definition of LAA anatomy, a transseptal puncture was performed



to cross the interatrial septum not through the ASD but in a more postero-inferior position below the membrane to reach easily the LAA (see Supplementary data online, Video S7). A Watchman device n.21 was implanted. The final result shows the device inside the LAA, with no interference with the membrane originating from the infold separating the LAA and left upper pulmonary vein (Panel F, see Supplementary data online, Video S8). 3D transoesophageal reconstruction is a useful tool to understand the anatomy of this rare case of congenital heart disease in detail, even more when interventional procedures are needed.

Supplementary data are available at *European Heart Journal – Cardiovascular Imaging* online.

Published on behalf of the European Society of Cardiology. All rights reserved. © The Author 2016. For permissions please email: journals.permissions@oup.com.

Paper III



Coronary Artery Disease

Extent of Myocardium at Risk for Left Anterior Descending Artery, Right Coronary Artery, and Left Circumflex Artery Occlusion Depicted by Contrast-Enhanced Steady State Free Precession and T2-Weighted Short Tau Inversion Recovery Magnetic Resonance Imaging

David Nordlund, MD; Einar Heiberg, PhD; Marcus Carlsson, MD, PhD;
Ernst-Torben Fründ, PhD; Pavel Hoffmann, MD, PhD; Sasha Koul, MD, PhD; Dan Atar, MD, PhD;
Anthony H. Aletras, PhD; David Erlinge, MD, PhD; Henrik Engblom, MD, PhD;
Håkan Arheden, MD, PhD

Background—Contrast-enhanced steady state free precession (CE-SSFP) and T2-weighted short tau inversion recovery (T2-STIR) have been clinically validated to estimate myocardium at risk (MaR) by cardiovascular magnetic resonance while using myocardial perfusion single-photon emission computed tomography as reference standard. Myocardial perfusion single-photon emission computed tomography has been used to describe the coronary perfusion territories during myocardial ischemia. Compared with myocardial perfusion single-photon emission computed tomography, cardiovascular magnetic resonance offers superior image quality and practical advantages. Therefore, the aim was to describe the main coronary perfusion territories using CE-SSFP and T2-STIR cardiovascular magnetic resonance data in patients after acute ST-segment-elevation myocardial infarction.

Methods and Results—CE-SSFP and T2-STIR data from 2 recent multicenter trials, CHILL-MI and MITOCARE (n=215), were used to assess MaR. Angiography was used to determine culprit vessel. Of 215 patients, 39% had left anterior descending artery occlusion, 49% had right coronary artery occlusion, and 12% had left circumflex artery occlusion. Mean extent of MaR using CE-SSFP was $44\pm 10\%$ for left anterior descending artery, $31\pm 7\%$ for right coronary artery, and $30\pm 9\%$ for left circumflex artery. Using T2-STIR, MaR was $44\pm 9\%$ for left anterior descending artery, $30\pm 8\%$ for right coronary artery, and $30\pm 12\%$ for left circumflex artery. MaR was visualized in polar plots, and expected overlap was found between right coronary artery and left circumflex artery. Detailed regional data are presented for use in software algorithms as a priori information on the extent of MaR.

Conclusions—For the first time, cardiovascular magnetic resonance has been used to show the main coronary perfusion territories using CE-SSFP and T2-STIR. The good agreement between CE-SSFP and T2-STIR from this study and myocardial perfusion single-photon emission computed tomography from previous studies indicates that these 3 methods depict MaR accurately in individual patients and at a group level.

Clinical Trial Registration—URL: <http://www.clinicaltrials.gov>. Unique identifiers: NCT01379261 and NCT01374321. (*Circ Cardiovasc Imaging*. 2016;9:e004376. DOI: 10.1161/CIRCIMAGING.115.004376.)

Key Words: coronary occlusion ■ coronary vessels ■ magnetic resonance imaging
■ myocardial ischemia ■ myocardium

After occlusion of a coronary artery, an area corresponding to the perfusion territory of that artery becomes ischemic and will become infarcted unless timely reperfusion occurs.¹⁻⁶ This area is known as the myocardium at risk (MaR), and it can be used to calculate myocardial salvage index,⁷ which is

See Editorial by Mangion and Berry See Clinical Perspective

currently used as an end point in at least 19 ongoing clinical trials (Appendix I in the [Data Supplement](#)).

Received December 9, 2015; accepted May 13, 2016.

From the Cardiac MR Group, Department of Clinical Physiology (D.N., E.H., M.C., A.H.A., H.E., H.A.) and Department of Cardiology (S.K., D.E.), Skåne University Hospital, Lund University, Sweden; Department of Radiology, Odense University Hospital, Denmark (E.-T.F.); Section for Interventional Cardiology, Division of Cardiovascular and Pulmonary Diseases, Department of Cardiology, Oslo University Hospital, Ullevaal, Norway (P.H.); Department of Cardiology B, Oslo University Hospital Ullevål, and Faculty of Medicine, University of Oslo, Norway (D.A.); and Laboratory of Medical Informatics, School of Medicine, Aristotle University of Thessaloniki, Greece (A.H.A.).

The Data Supplement is available at <http://circimaging.ahajournals.org/lookup/suppl/doi:10.1161/CIRCIMAGING.115.004376/-/DC1>.

Correspondence to Håkan Arheden, MD, PhD, Department of Clinical Physiology, Institution for Clinical Sciences, Lund University, S-221 85 Lund, Sweden. E-mail hakan.aheden@med.lu.se

© 2016 American Heart Association, Inc.

Circ Cardiovasc Imaging is available at <http://circimaging.ahajournals.org>

DOI: 10.1161/CIRCIMAGING.115.004376

Downloaded from <http://circimaging.ahajournals.org/> at Lund University Libraries on September 12, 2016

Earlier attempts to measure the coronary perfusion territories have relied on animal studies or anatomic studies, such as dissections and casts of the vasculature in autopsy studies.^{8,9} More recently, the advent of perfusion imaging, such as by myocardial perfusion single-photon emission computed tomography (MPS),^{10–15} and tissue characterization by cardiovascular magnetic resonance (CMR)^{7,16–19} has allowed for visualization of MaR directly. However, only 2 MPS studies with a limited number of patients have looked at the extent of perfusion territories.^{20,21} Where MPS uses injection of a radioactive perfusion tracer during occlusion to image relative perfusion, CMR imaging uses pulse sequences that are sensitive to tissue properties in postischemic myocardium, such as contrast-enhanced steady state free precession (CE-SSFP)^{18,19} and T2-weighted short tau inversion recovery (T2-STIR)^{17,18}. Although both MPS and CMR are used for imaging of MaR, CMR offers higher spatial resolution and provides an accurate anatomic representation of the heart making it ideally suited for visualization of the MaR and thus the coronary perfusion territories.

Knowledge of the perfusion territories and the size of the perfusion defect associated with different arteries is important when designing clinical trials using myocardial salvage index as end point. In addition, computer models for automatically analyzing and delineating myocardium, MaR, and infarct for CMR and MPS often use a priori information about the extent of perfusion territories.^{22,23} Such models are becoming increasingly important both for research and for clinical practice. The perfusion territories have also been of interest for electrocardiography research where effort has been made trying to predict position and extent of the myocardial injury from an ECG.^{24–26}

Thus, the aim of this study is to quantify and to visualize the extent of the perfusion territories for the 3 main coronary arteries, left anterior descending artery (LAD), left circumflex artery (LCx), and right coronary artery (RCA), using CE-SSFP and T2-STIR CMR sequences and to provide data on perfusion territories to be used for simulation and programming.

Methods

Study Population and Design

The CHILL-MI²⁷ and MITOCARE²⁸ studies were approved by the regional ethics committees, and all patients provided written informed consent to participate in the respective study. Patients from these 2 multicenter cardioprotection trials underwent CMR imaging within 2 to 6 days after being diagnosed with acute myocardial infarction and treated with primary percutaneous coronary intervention.²⁷ Inclusion and exclusion criteria for each of the clinical trials have been previously published.^{27,29} In short, all patients had clinical signs of acute myocardial infarction defined as clinical symptoms and ECG signs consistent with ST-segment–elevation myocardial infarction or new left bundle branch block, were ≥ 18 years old, and had symptom duration of <6 hours. Patients with previous infarction or history of coronary revascularization were excluded.

Coronary Angiography

For the CHILL-MI trial, the culprit lesion and Rentrop grade was estimated by an angiography core laboratory.²⁷ For the MITOCARE trial, Rentrop grade and culprit lesion was estimated and documented by the interventionalist performing the coronary intervention at the respective site using the coronary angiogram information together with clinical data, such as ECG changes.²⁹

CMR Image Acquisition

All CMR examinations were performed on a 1.5 T system from either Philips (Philips Healthcare, Best, The Netherlands), Siemens (Siemens AG, Erlangen, Germany), or General Electric (GE Healthcare, Fairfield). All subjects were placed in a supine position, and images were acquired at end-expiratory breath hold with ECG gating. Initial scout images were acquired to locate the heart. For MaR visualization, a triple inversion recovery T2-STIR black blood sequence was applied before administration of the contrast agent. In addition, a multislice multiphase SSFP sequence was applied ≈ 5 minutes after intravenous administration of a gadolinium-based extracellular contrast agent (0.2 mmol/kg). Both the T2-STIR and the contrast-enhanced SSFP images were acquired in the short-axis view covering the left ventricle (LV) from base to apex. The slice thickness was 8 mm with no slice gap, and the in-plane resolution was typically 1.5×1.5 mm. The temporal resolution of the CE-SSFP images was 20 to 30 frames per cardiac cycle.

For infarct visualization, long- and short-axis late gadolinium enhancement (LGE) images covering the LV from base to apex were

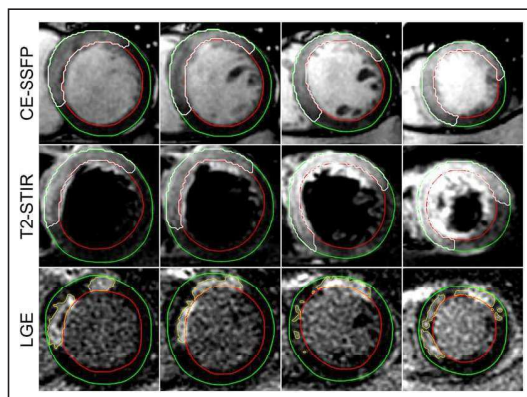


Figure 1. Cardiovascular magnetic resonance images of myocardium at risk (MaR) and infarct. The MaR by contrast-enhanced steady state free precession (CE-SSFP) and T2-weighted short tau inversion recovery (T2-STIR) are shown on the top and middle rows and infarct size by late gadolinium enhancement (LGE) on the bottom row in corresponding levels of the left ventricle. All images are from the same patient who underwent reperfusion following occlusion in the left anterior descending artery. MaR by CE-SSFP: 29% of left ventricular mass, MaR by T2-STIR: 28%, and infarct size by LGE: 7%. The epicardium is traced in green and the endocardium in red, whereas MaR is traced in white and infarct in yellow.

Table 1. Comparison of Diagnostic and Nondiagnostic T2-Weighted Short Tau Inversion Recovery

	Diagnostic Quality	Not Diagnostic Quality	P Value
Myocardium at risk, % LV	36	35	0.53
Infarct size, % LV	17	17	0.83
Myocardial salvage index, %MaR	54%	54%	0.94
LAD (n)	57	21	0.07
LCx (n)	14	9	0.14
RCA (n)	59	40	0.65

LAD indicates left anterior descending artery; LCx, left circumflex artery; LV, left ventricle; MaR, myocardium at risk; and RCA, right coronary artery.

acquired ≈ 15 minutes after injection of gadolinium. The LGE images were acquired using an inversion-recovery gradient-recalled echo sequence with a slice thickness of 8 mm with no slice gap. In-plane resolution was typically 1.5 \times 1.5 mm. Inversion time was adjusted to null the signal from viable myocardium.³⁰

CMR Analysis

All CMR images were analyzed by a core laboratory (Imacor AB, Lund, Sweden) using the software Segment, version 1.9 R3314 (<http://segment.heiberg.se>).³¹ The myocardium in each LV short-axis slice was manually analyzed by delineating the LV epicardial and endocardial borders. Regions of MaR were defined as hyperintense regions within the myocardium on the T2-STIR and CE-SSFP images and were delineated manually. CE-SSFP images were delineated in both end-diastole and end-systole as previously described.¹⁸ The size of MaR was expressed as a percentage of the total LV myocardial volume.

Infarction was delineated from the short-axis LGE images according to a previously described method that has been validated both experimentally and clinically.³² In short, the endocardial and epicardial borders

were traced manually with exclusion of the papillary muscles, and the LGE myocardium was quantified using a computer algorithm taking partial volume effects into account when estimating the amount of infarction. Manual adjustments were made when image artifacts caused misinterpretation by the computer algorithm. If present, a hypointense signal within the area of LGE (microvascular obstruction³³) was included in the analysis as 100% infarction. Finally, the myocardial infarct size was expressed as a percentage of the total LV myocardial volume. All delineations were performed by 1 observer with a second opinion with respect to the delineations in each case. In case of disagreement, differences were resolved by reaching consensus via a third expert observer.

Polar Plot Representation of Coronary Artery Distribution

Delineations of MaR from T2-STIR and CE-SSFP short-axis images and infarction from LGE short-axis images were represented as polar plots. The plots were created by resampling each stack to 20 slices, with each slice divided into 80 zones. Each zone was assigned a signal intensity proportional to how frequently MaR or infarction was present in the different patients. This was done for each culprit artery separately. The polar plots were then divided into the 17-segment model of the heart recommended by American Heart Association.³⁴ Patient images were aligned by marking the right ventricular insertion points in all short-axis slices with a visible right ventricular lumen. The LV was then rotated so that the average position of the right ventricular insertion points was aligned with the border between segments 2 and 3 of the 17-segment model.

Comparison With Previous MPS Studies

Data were compared with those from previous MPS studies published by Persson et al²⁰ and Perezot-Valdés et al.²¹ Because the ranges and SDs of extent of MaR were not published in the article by Persson et al,²⁰ the lead author was contacted and kindly supplied the data.

Statistical Analysis

The size of MaR for each vessel was presented as mean \pm SD. A linear mixed model was used to assess differences of MaR and infarct size between the different vessels and for comparing infarct size, MaR by CE-SSFP and MaR by T2-STIR. The correlation between infarct

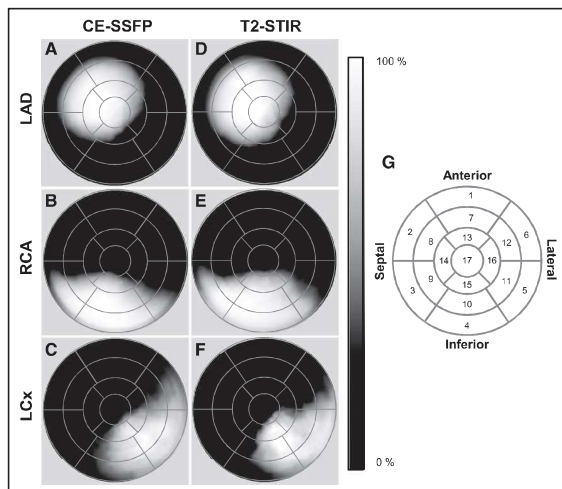


Figure 2. Polar plots of myocardium at risk (MaR). On the left are average contrast-enhanced steady state free precession (CE-SSFP) polar plots of (A) the left anterior descending artery (LAD), using 78 patients (B) the right coronary artery (RCA), using 99 patients, and (C) the left circumflex artery (LCx), using 25 patients. The polar plots on the right use T2-weighted short tau inversion recovery (T2-STIR) to show (D) the LAD, using 61 patients (E) the RCA, using 69 patients, and (F) the LCx, using 17 patients. The intensity of the plots reflect the fraction of patients with MaR in that area as shown on the bar that ranges from 0% to 100%. For reference purposes, the 17-segment model is shown in G.

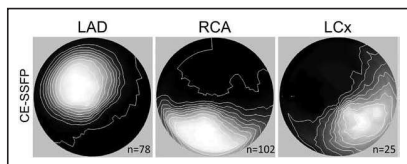


Figure 3. Polar plots of myocardium at risk (MaR) with isocontour lines. Polar plots of left anterior descending artery (LAD; 78 patients), right coronary artery (RCA; 99 patients), and left circumflex artery (LCx; 25 patients). The white lines show 10% increments proportional to the fraction of patients with MaR in that area. The most central increment represents 90% to 100%, and the most peripheral increment represents 0% to 10%.

size and MaR was assessed by using Pearson correlation coefficient. Infarct size by LGE, MaR by CE-SSFP, myocardial salvage index, and culprit vessel were compared for patients with diagnostic versus nondiagnostic T2-STIR images. Comparisons of infarct size and MaR were performed using unpaired *t* tests, and the comparison of culprit vessel was performed using Fisher's exact test. Differences with a $P < 0.05$ were considered to be statistically significant.

Results

Study Population

Of 215 patients, 39% had LAD occlusion, 49% had RCA occlusion, and 12% had LCx occlusion by angiography. As described in previous work, MR and angiography agreed in assigning culprit artery in 97% of patients by CE-SSFP and 89% by T2-STIR.³⁵ Figure 1 shows an example of CE-SSFP, T2-STIR, and LGE images taken from 1 patient. Eleven CE-SSFP data sets were excluded from MaR analysis because of incomplete image acquisition. An additional 2 CE-SSFP data sets were excluded because of inability to define MaR. Also, 86 T2-STIR data sets were excluded: 15 because of inadequate image acquisition and 71 because of inability to define MaR. Table 1 shows comparisons of patients with diagnostic versus nondiagnostic T2-STIR.

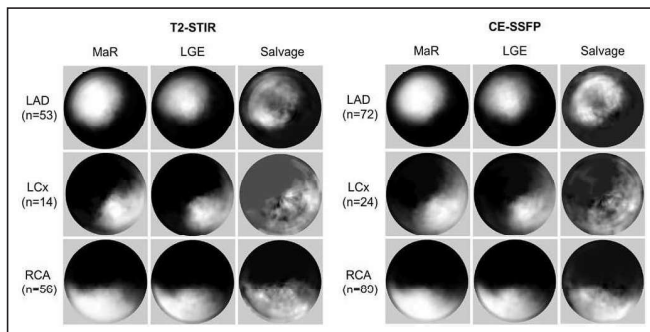


Figure 4. Polar plots of myocardium at risk (MaR), late gadolinium enhancement (LGE), and salvage in corresponding patients. The 3 columns to the left show MaR by T2-weighted short tau inversion recovery (T2-STIR), LGE, and salvage in patients with diagnostic T2-STIR and LGE. The columns to the right show MaR by contrast-enhanced steady state free precession (CE-SSFP), LGE, and salvage in patients with diagnostic CE-SSFP and LGE. Salvage is defined as the difference between MaR and LGE. The intensity of the plots reflect the fraction of patients with MaR, LGE, or salvage in that area as shown on the bar that ranges from 0% to 100%.

Distribution of MaR

The perfusion territories for each of the 3 main coronary arteries divided into the 17-segment model are shown in Figure 2, overlaid with isocontour lines in Figure 3, and compared with LGE to show myocardial salvage in Figure 4. Detailed data on the distributions are provided in Appendix II in the Data Supplement. The extent of the 3 coronary arteries together is shown in Figure 5. The overlap between perfusion territories was mainly between LCx and RCA including segments 4, 5, 10, 11, and 15. Average sizes and ranges of MaR are given in Table 2. MaR size by both CE-SSFP and T2-STIR was greater for LAD than for both RCA and LCx ($P < 0.001$). No statistically significant difference in MaR size was found between RCA and LCx by CE-SSFP ($P = 0.606$) or by T2-STIR ($P = 0.226$). There was no statistically significant difference in MaR by CE-SSFP and by T2-STIR ($P = 0.674$).

Infarct Size

Of 215 data sets, LGE was diagnostic in 190. In data sets with nondiagnostic LGE, the LGE was excluded from further analysis, whereas CE-SSFP and T2-STIR were still included (if diagnostic). The average sizes of infarctions are given in Table 2. Infarct size was greater for LAD than for both RCA and LCx ($P < 0.001$), whereas there was no statistically significant difference in infarct size between RCA and LCx ($P = 0.206$). Average infarct size was significantly smaller than MaR for all 3 vessels ($P < 0.001$) and for all vessels grouped together ($P < 0.001$). All patients had larger MaR than infarct size using CE-SSFP and all but one when using T2-STIR imaging (Figure 6).

Discussion

This is the first study to give a representative picture of the coronary perfusion territories using CMR.

Coronary Perfusion Territories

In 2008, Ortiz-Pérez et al³⁶ used LGE imaging to map the distribution of infarct in 93 patients. The present study uses MaR

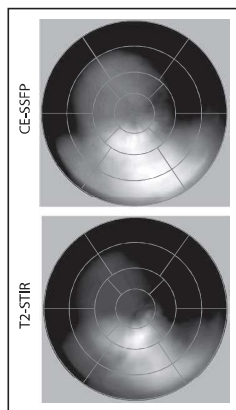


Figure 5. Combined extent of myocardium at risk (MaR). The sum of bull's-eye plots from Figure 2. Image intensity is proportional to overlap in the extent of MaR. Note the bright area representing overlap, mainly between right coronary artery and left circumflex artery territories.

instead and may, therefore, more accurately visualize the true perfusion territories of the coronary arteries. The location and spatial extent of MaR found in the present study are similar to the location and the extent of local perfusion loss found in previous studies using MPS^{20,21} (Figure 7). The overlap found between the RCA and the LCx perfusion territories (segments 4, 5, 10, 11, and 15) is similar to what was found by Pereztol-Valdés et al²¹ and Persson et al.²⁰ When comparing average size of coronary perfusion territories, however, both the RCA and the LCx sizes were smaller in the Pereztol-Valdés et al²¹ and Persson et al²⁰ MPS studies compared with both CE-SSFP and T2-STIR in the present study (Table 2). A possible explanation for this difference is that the patients in the MPS studies were treated electively for chronic coronary stenosis in contrast to the patients in the present study who all presented with first-time acute coronary occlusion. The likelihood of collateral flow influencing the results may, therefore, be less in the present study because, in cases with chronic stenosis, collaterals might have been developed that decrease the amount of myocardium affected by ischemia on occlusion. This is

Table 2. Comparison of Myocardium at Risk-Size by CMR and Extent of Hypoperfusion by Myocardial Perfusion Single-Photon Emission Computed Tomography

	LAD	RCA	LCx
CMR CE-SSFP	44±10% (23–64)	31±7% (15–45)	30±9% (15–53)
CMR T2-STIR	44±9% (24–63)	30±8% (12–52)	30±12% (16–66)
CMR infarct size	23±11% (3–47)	13±7% (2–29)	14±6% (6–44)

Values are expressed as mean±SD (min–max). CE-SSFP indicates contrast-enhanced steady state free precession; CMR, cardiovascular magnetic resonance; LAD, left anterior descending artery; LCx, left circumflex artery; RCA, right coronary artery; and T2-STIR, T2-weighted short tau inversion recovery.

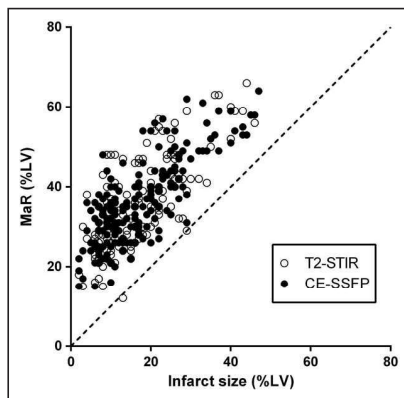


Figure 6. Myocardium at risk (MaR) vs infarct size. Linear regression plot comparing infarct size by late gadolinium enhancement imaging and MaR by contrast-enhanced steady state free precession (CE-SSFP) (●) and T2-STIR (○) imaging. The dashed line denotes the line of identity. %LV indicates percent of left ventricular mass.

reflected by the low ratio of patients with high Rentrop grade (Table 3). Another explanation may be that the plaques that tend to cause chronic stenosis have been shown to be located more distally in the coronary arteries when compared with the unstable plaques causing acute coronary occlusion.³⁷

In the present study, segments 1, 2, and 3 were only involved in MaR to a limited extent (Figure 5). Segments 1, 2, and 3 partly represent the fibrous part of the basal septum not being a part of MaR. Furthermore, segments 1 and 2 should be supplied by either the left main or the proximal LAD, and none of the patients in this study had left main occlusion.

CMR for MaR

Both T2-STIR and CE-SSFP have earlier been validated against MPS for the detection of MaR.^{17,19} In this study, the extent of the coronary perfusion territories is similar using T2-STIR, CE-SSFP, and MPS. Note that T2-STIR, CE-SSFP, and MPS use different principles for imaging MaR. MPS uses a radioactive isotope, which binds to viable mitochondria and which needs to be administered during occlusion of a coronary vessel, whereas T2-STIR and CE-SSFP are thought to be sensitive to edema generated within the MaR. The similar results obtained by 2 different mechanisms increase the confidence that these methods accurately depict MaR. Some controversy still exists around both T2-STIR imaging and CE-SSFP for depicting MaR.^{38–40} There has been some debate whether CE-SSFP and T2-STIR may actually depict infarction instead of MaR and if MaR may be overestimated using these 2 CMR techniques.⁴⁰ However, the results shown herein compare nicely with MPS findings and make it more likely that the 2 CMR techniques depict MaR accurately. Moreover, in the present study, infarct size was smaller than MaR in all data sets (except for one of the

T2-STIR images), and significant differences were found between MaR and infarct size for all 3 coronary vessel groups indicating that it is unlikely that the hyperenhanced myocardium, seen on both T2-STIR imaging and CE-SSFP, represents only infarction. The findings are consistent with previous findings on the relation between MaR by CE-SSFP and infarct size.^{18,19} Furthermore, the coronary artery overlap found in the present study occurred in parts of the myocardium congruent with previous MPS studies.^{20,21}

A significant number of data sets acquired using T2-STIR was considered to be of nondiagnostic quality, which may limit its utility in multicenter, multivendor settings as recently shown.³⁵

Limitations

The findings in the present study should be interpreted in the context of some limitations. Apart from CMR, no other method was used to estimate MaR, which means that there is no reference standard to compare with the CE-SSFP or T2-STIR imaging in the present study. Instead, reference is made to previously published studies.^{17,19} Manual delineation was used to estimate MaR both for CE-SSFP and for T2-STIR, which may introduce observer dependence in MaR quantification. However, automatic methods that rely on a fixed number of standard deviations from remote myocardium are not applicable in a multicenter setting with different signal:noise ratio in images from different centers and scanners.⁴¹ Although this study used

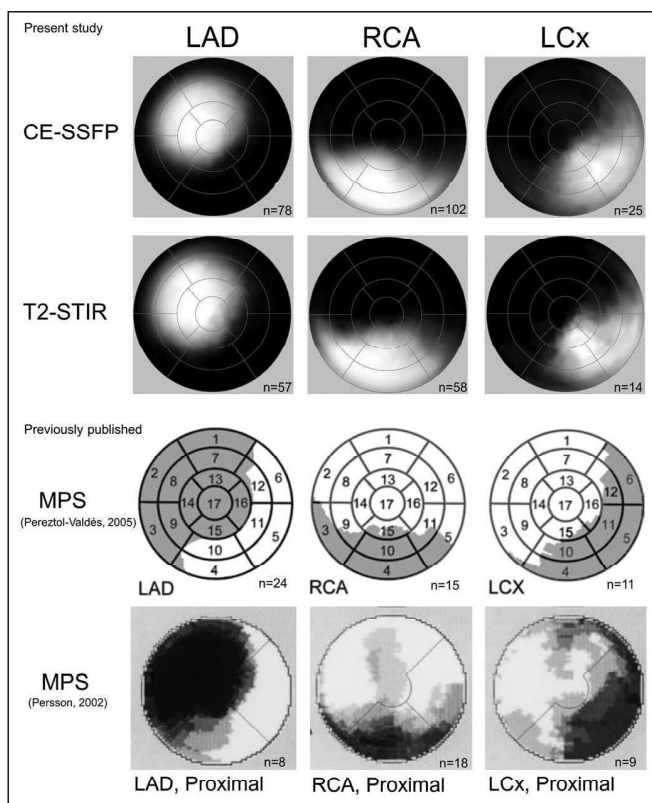


Figure 7. Polar plots, comparison between cardiovascular magnetic resonance (CMR) and myocardial perfusion single-photon emission computed tomography (MPS). The first and second rows show contrast-enhanced steady state free precession (CE-SSFP) and T2-weighted short tau inversion recovery (T2-STIR) images from the present study. The third row shows maximal extent of perfusion territories using MPS (Perezto-Valdés et al²⁰). The fourth row shows perfusion territories also using MPS (Persson et al²⁰). The left column shows left anterior descending artery (LAD), the middle column right coronary artery (RCA), and the right column left circumflex coronary artery (LCx). The intensity of the plot is proportional to the fraction of patients with myocardium at risk in that area.

Table 3. Patient Characteristics

No. of patients (n)	215
Men (n)	179
Women (n)	36
Age, y, mean±SD	60±11
Complete CE-SSFP data sets (n)	204
Complete T2-STIR data sets (n)	200
Treated with hypothermia (n)	50
Treated with TRO40303 (n)	60
Culprit vessel by angiography (n)	
LAD	84
LCx	25
RCA	106
Rentrop grade (n)	
0	127
1	40
2	24
3	2
Unknown	22
Peak cTnT,* (ng/L, mean±SD)	12100±9300
Peak hsTnT,† (ng/L, mean±SD)	7000±4600
Time from pain to balloon, min, mean±SD	184±73
Time from ischemic event to CMR, d	3.8±1.4

CE-SSFP indicates contrast-enhanced steady state free precession; CMR, cardiovascular magnetic resonance; cTnT, fourth-generation cardiac troponin T; hsTnT, high-sensitivity troponin T; LAD, left anterior descending artery; LCx, left circumflex artery; RCA, right coronary artery; and T2-STIR, T2-weighted short tau inversion recovery.

*Patients in the MITOCARE trial.

†Patients in the CHILL-MI trial.

right ventricular insertions as reference points for rotation of the heart the MPS studies by Persson et al²⁰ and Perezto-Valdés et al²¹ used an algorithm commonly applied in the MPS software.⁴² The difference in methods used is a limitation when comparing the results; however, the epicenters of MaR using CMR correspond well with those using MPS (Figure 7), which indicates that this may not be a significant limitation.

Conclusion

The present study has shown the coronary perfusion territories for the 3 main coronary arteries LAD, RCA, and LCx using CE-SSFP and T2-STIR. The agreement with MPS, which acts by a different mechanism, makes it likely that these 3 methods depict MaR accurately.

Acknowledgments

We thank Dr Eva Persson and coauthors for providing complimentary data on their study population.

Sources of Funding

Funding for the CHILL-MI trial was received from the Region of Skane, Philips Healthcare, Lund University, and Uppsala University.

The MITOCARE trial was supported by the European Union under the 7th Framework Programme for RTD—Project MITOCARE—Grant Agreement HEALTH-2010-261034.

Disclosures

Dr Arheden is a shareholder of Imacor. Drs Arheden, Heiberg, Carlsson, and Engblom consult for Imacor. Dr Heiberg is the founder and owner of the company Medviso AB, Lund, Sweden.

References

- Reimer KA, Lowe JE, Rasmussen MM, Jennings RB. The wavefront phenomenon of ischemic cell death. I. Myocardial infarct size vs duration of coronary occlusion in dogs. *Circulation*. 1977;56:786–794.
- Reimer KA, Jennings RB. The “wavefront phenomenon” of myocardial ischemic cell death. II. Transmural progression of necrosis within the framework of ischemic bed size (myocardium at risk) and collateral flow. *Lab Invest*. 1979;40:633–644.
- Lowe JE, Reimer KA, Jennings RB. Experimental infarct size as a function of the amount of myocardium at risk. *Am J Pathol*. 1978;90:363–379.
- Lee JT, Ideker RE, Reimer KA. Myocardial infarct size and location in relation to the coronary vascular bed at risk in man. *Circulation*. 1981;64:526–534.
- DeWood MA, Heit J, Spores J, Berg R Jr, Selinger SL, Rudy LW, Hensley GR, Shields JP. Anterior transmural myocardial infarction: effects of surgical coronary reperfusion on global and regional left ventricular function. *J Am Coll Cardiol*. 1983;1:1223–1234.
- Braunwald E, Kloner RA. Myocardial reperfusion: a double-edged sword? *J Clin Invest*. 1985;76:1713–1719. doi: 10.1172/JCI112160.
- Friedrich MG, Abdel-Aty H, Taylor A, Schulz-Menger J, Messroghli D, Dietz R. The salvaged area at risk in reperfused acute myocardial infarction as visualized by cardiovascular magnetic resonance. *J Am Coll Cardiol*. 2008;51:1581–1587. doi: 10.1016/j.jacc.2008.01.019.
- James TN. Anatomy of the coronary arteries in health and disease. *Circulation*. 1965;32:1020–1033.
- Reig J, Jornet A, Petit M. Coronary arterial territories of the left ventricle: extension and exclusivity. *Surg Radiol Anat*. 1994;16:281–285.
- Sinusas AJ, Trautman KA, Bergin JD, Watson DD, Ruiz M, Smith WH, Beller GA. Quantification of area at risk during coronary occlusion and degree of myocardial salvage after reperfusion with technetium-99m methoxyisobutyl isonitrite. *Circulation*. 1990;82:1424–1437.
- Gibbons RJ, Verani MS, Behrenbeck T, Pellicka PA, O'Connor MK, Mahmarian JJ, Chesebro JH, Wackers FJ. Feasibility of tomographic 99mTc-hexakis-2-methoxy-2-methylpropyl-isonitrite imaging for the assessment of myocardial area at risk and the effect of treatment in acute myocardial infarction. *Circulation*. 1989;80:1277–1286.
- Huber KC, Bresnahan JF, Bresnahan DR, Pellicka PA, Behrenbeck T, Gibbons RJ. Measurement of myocardium at risk by technetium-99m sestamibi: correlation with coronary angiography. *J Am Coll Cardiol*. 1992;19:67–73.
- Harooni HL, Remetz MS, Sinusas AJ, Baron JM, Miller HI, Cleman MW, Zaret BL, Wackers FJ. Myocardial risk area defined by technetium-99m sestamibi imaging during percutaneous transluminal coronary angioplasty: comparison with coronary angiography. *J Am Coll Cardiol*. 1993;22:1033–1043.
- De Coster PM, Wijns W, Cauwe F, Robert A, Beckers C, Melin JA. Area-at-risk determination by technetium-99m-hexakis-2-methoxyisobutyl isonitrite in experimental reperfused myocardial infarction. *Circulation*. 1990;82:2152–2162.
- Verani MS, Jeroudi MO, Mahmarian JJ, Boyce TM, Borges-Neto S, Patel B, Bolli R. Quantification of myocardial infarction during coronary occlusion and myocardial salvage after reperfusion using cardiac imaging with technetium-99m hexakis-2-methoxyisobutyl isonitrite. *J Am Coll Cardiol*. 1988;12:1573–1581.
- Aletras AH, Tilak GS, Natanzon A, Hsu LY, Gonzalez FM, Hoyt RF Jr, Arai AE. Retrospective determination of the area at risk for reperfused acute myocardial infarction with T2-weighted cardiac magnetic resonance imaging: histopathological and displacement encoding with stimulated echoes (DENSE) functional validations. *Circulation*. 2006;113:1865–1870. doi: 10.1161/CIRCULATIONAHA.105.576025.
- Carlsson M, Ubachs JF, Hedström E, Heiberg E, Jovinge S, Arheden H. Myocardium at risk after acute infarction in humans on cardiac magnetic resonance: quantitative assessment during follow-up and validation

- with single-photon emission computed tomography. *JACC Cardiovasc Imaging*. 2009;2:569–576. doi: 10.1016/j.jcmg.2008.11.018.
18. Ubachs JF, Sörensson P, Engblom H, Carlsson M, Jovinge S, Pernow J, Arheden H. Myocardium at risk by magnetic resonance imaging: head-to-head comparison of T2-weighted imaging and contrast-enhanced steady-state free precession. *Eur Heart J Cardiovasc Imaging*. 2012;13:1008–1015. doi: 10.1093/ehjci/ehj091.
 19. Sörensson P, Heiberg E, Saleh N, Bouvier F, Caidahl K, Tornvall P, Rydén L, Pernow J, Arheden H. Assessment of myocardium at risk with contrast-enhanced steady-state free precession cine cardiovascular magnetic resonance compared to single-photon emission computed tomography. *J Cardiovasc Magn Reson*. 2010;12:25. doi: 10.1186/1532-429X-12-25.
 20. Persson E, Palmer J, Pettersson J, Warren SG, Borges-Neto S, Wagner GS, Pahlm O. Quantification of myocardial hypoperfusion with 99m Tc-sestamibi in patients undergoing prolonged coronary artery balloon occlusion. *Nucl Med Commun*. 2002;23:219–228.
 21. Perezot-Valdés O, Candell-Riera J, Santana-Boado C, Angel J, Aguadé-Bruix S, Castell-Conesa J, Garcia EV, Soler-Soler J. Correspondence between left ventricular 17 myocardial segments and coronary arteries. *Eur Heart J*. 2005;26:2637–2643. doi: 10.1093/eurheartj/ehi496.
 22. Sjögren J, Ubachs JF, Engblom H, Carlsson M, Arheden H, Heiberg E. Semi-automatic segmentation of myocardium at risk in T2-weighted cardiovascular magnetic resonance. *J Cardiovasc Magn Reson*. 2012;14:10. doi: 10.1186/1532-429X-14-10.
 23. Ugander M, Sonesson H, Engblom H, van der Pals J, Erlinge D, Heiberg E, Arheden H. Quantification of myocardium at risk in myocardial perfusion SPECT by co-registration and fusion with delayed contrast-enhanced magnetic resonance imaging—an experimental ex vivo study. *Clin Physiol Funct Imaging*. 2012;32:33–38. doi: 10.1111/f.1475-097X.2011.01051.x.
 24. Andersen MP, Terkelsen CJ, Sørensen JT, Kaltoft AK, Nielsen SS, Struijk JJ, Bøtker HE. The ST injury vector: electrocardiogram-based estimation of location and extent of myocardial ischemia. *J Electrocardiol*. 2010;43:121–131. doi: 10.1016/j.jelectrocard.2009.12.001.
 25. Bacharova L, Mateasik A, Carnicky J, Ubachs JF, Hedström E, Arheden H, Engblom H. The Dipolar ElectroCARDioTopographic (DECARTO)-like method for graphic presentation of location and extent of area at risk estimated from ST-segment deviations in patients with acute myocardial infarction. *J Electrocardiol*. 2009;42:172–180. doi: 10.1016/j.jelectrocard.2008.12.005.
 26. Ubachs JF, Engblom H, Hedström E, Selvester RH, Knippenberg SA, Wagner GS, Gorgels AP, Arheden H. Location of myocardium at risk in patients with first-time ST-elevation infarction: comparison among single photon emission computed tomography, magnetic resonance imaging, and electrocardiography. *J Electrocardiol*. 2009;42:198–203. doi: 10.1016/j.jelectrocard.2008.11.003.
 27. Erlinge D, Göteborg M, Lang I, Holzer M, Noc M, Clemmensen P, Jensen U, Metzler B, James S, Bøtker HE, Omernovic E, Engblom H, Carlsson M, Arheden H, Ostlund O, Wallentin L, Harek J, Olivecrona GK. Rapid endovascular catheter core cooling combined with cold saline as an adjunct to percutaneous coronary intervention for the treatment of acute myocardial infarction. The CHILL-MI trial: a randomized controlled study of the use of central venous catheter core cooling combined with cold saline as an adjunct to percutaneous coronary intervention for the treatment of acute myocardial infarction. *J Am Coll Cardiol*. 2014;63:1857–1865. doi: 10.1016/j.jacc.2013.12.027.
 28. Atar D, Arheden H, Berdeaux A, Bonnet JL, Carlsson M, Clemmensen P, Cuvier V, Danchin N, Dubois-Randé JL, Engblom H, Erlinge D, Firat H, Halvorsen S, Hansen HS, Hauke W, Heiberg E, Koul S, Larsen AI, Le Corvoisier P, Nordrehaug JE, Paganelli F, Pruss RM, Rousseau H, Schaller S, Sonou G, Tusev T, Veys J, Vicaut E, Jensen SE. Effect of intravenous TRO40303 as an adjunct to primary percutaneous coronary intervention for acute ST-elevation myocardial infarction: MITOCARE study results. *Eur Heart J*. 2015;36:112–119. doi: 10.1093/eurheartj/ehu331.
 29. MITOCARE Study Group. Rationale and design of the MITOCARE Study: a phase II, multicenter, randomized, double-blind, placebo-controlled study to assess the safety and efficacy of TRO40303 for the reduction of reperfusion injury in patients undergoing percutaneous coronary intervention for acute myocardial infarction. *Cardiology*. 2012;123:201–207. doi: 10.1159/000342981.
 30. Simonetti OP, Kim RJ, Fieno DS, Hillenbrand HB, Wu E, Bundy JM, Finn JP, Judd RM. An improved MR imaging technique for the visualization of myocardial infarction. *Radiology*. 2001;218:215–223. doi: 10.1148/radiology.218.1.r01ja50215.
 31. Heiberg E, Sjögren J, Ugander M, Carlsson M, Engblom H, Arheden H. Design and validation of Segment—freely available software for cardiovascular image analysis. *BMC Med Imaging*. 2010;10:1. doi: 10.1186/1471-2342-10-1.
 32. Heiberg E, Ugander M, Engblom H, Göteborg M, Olivecrona GK, Erlinge D, Arheden H. Automated quantification of myocardial infarction from MR images by accounting for partial volume effects: animal, phantom, and human study. *Radiology*. 2008;246:581–588. doi: 10.1148/radiol.2461062164.
 33. Kloner RA, Ganote CE, Jennings RB. The “no-reflow” phenomenon after temporary coronary occlusion in the dog. *J Clin Invest*. 1974;54:1496–1508. doi: 10.1172/JCI107898.
 34. Cerqueira MD, Weissman NJ, Dilsizian V, Jacobs AK, Kaul S, Laskey WK, Pennell DJ, Rumberger JA, Ryan T, Verani MS; American Heart Association Writing Group on Myocardial Segmentation and Registration for Cardiac Imaging. Standardized myocardial segmentation and nomenclature for tomographic imaging of the heart. A statement for healthcare professionals from the Cardiac Imaging Committee of the Council on Clinical Cardiology of the American Heart Association. *Circulation*. 2002;105:539–542.
 35. Nordlund D, Klug G, Heiberg E, Koul S, Larsen TH, Hoffmann P, Metzler B, Erlinge D, Atar D, Aletras AH, Carlsson M, Engblom H, Arheden H. Multi-vendor, multicentre comparison of contrast-enhanced SSFP and T2-STIR CMR for determining myocardium at risk in ST-elevation myocardial infarction. *Eur Heart J Cardiovasc Imaging*. 2016;pii: jew027.
 36. Ortiz-Pérez JT, Rodríguez J, Meyers SN, Lee DC, Davidson C, Wu E. Correspondence between the 17-segment model and coronary arterial anatomy using contrast-enhanced cardiac magnetic resonance imaging. *JACC Cardiovasc Imaging*. 2008;1:282–293. doi: 10.1016/j.jcmg.2008.01.014.
 37. Sato A, Ohigashi H, Nozato T, Hikita H, Tamura M, Miyazaki S, Takahashi Y, Kuwahara T, Takahashi A, Hiroe M, Aonuma K. Coronary artery spatial distribution, morphology, and composition of nonculprit coronary plaques by 64-slice computed tomographic angiography in patients with acute myocardial infarction. *Am J Cardiol*. 2010;105:930–935. doi: 10.1016/j.amjcard.2009.11.028.
 38. Arai AE, Leung S, Kellman P. Controversies in cardiovascular MR imaging: reasons why imaging myocardial T2 has clinical and pathophysiologic value in acute myocardial infarction. *Radiology*. 2012;265:23–32. doi: 10.1148/radiol.12112491.
 39. Croisille P, Kim HW, Kim RJ. Controversies in cardiovascular MR imaging: T2-weighted imaging should not be used to delineate the area at risk in ischemic myocardial injury. *Radiology*. 2012;265:12–22. doi: 10.1148/radiol.12111769.
 40. Friedrich MG, Kim HW, Kim RJ. T2-weighted imaging to assess post-infarct myocardium at risk. *JACC Cardiovasc Imaging*. 2011;4:1014–1021. doi: 10.1016/j.jcmg.2011.07.005.
 41. McAlindon E, Pufulete M, Lawton C, Angelini GD, Bucciarelli-Ducci C. Quantification of infarct size and myocardium at risk: evaluation of different techniques and its implications. *Eur Heart J Cardiovasc Imaging*. 2015;16:738–746. doi: 10.1093/ehjci/jev001.
 42. Germano G, Kavanagh PB, Su HT, Mazzanti M, Kiat H, Hachamovich R, Van Train KF, Areeda JS, Berman DS. Automatic reorientation of three-dimensional, transaxial myocardial perfusion SPECT images. *J Nucl Med*. 1995;36:1107–1114.

CLINICAL PERSPECTIVE

This article provides data on the extent of the coronary perfusion territories for the three major coronary vessels left anterior descending artery, right coronary artery, and left circumflex artery based on quantification of myocardium at risk by contrast-enhanced steady state free precession and T2-weighted short tau inversion recovery magnetic resonance imaging in 215 patients with acute myocardial infarction. This information may be useful in the planning of cardioprotection trials, in creating computer models requiring a priori information on perfusion territories and in clinical contexts where precise knowledge on the extent of injured myocardium could guide risk evaluation.

Extent of Myocardium at Risk for Left Anterior Descending Artery, Right Coronary Artery, and Left Circumflex Artery Occlusion Depicted by Contrast-Enhanced Steady State Free Precession and T2-Weighted Short Tau Inversion Recovery Magnetic Resonance Imaging

David Nordlund, Einar Heiberg, Marcus Carlsson, Ernst-Torben Fründ, Pavel Hoffmann, Sasha Koul, Dan Atar, Anthony H. Aletras, David Erlinge, Henrik Engblom and Håkan Arheden

Circ Cardiovasc Imaging. 2016;9:

doi: 10.1161/CIRCIMAGING.115.004376

Circulation: Cardiovascular Imaging is published by the American Heart Association, 7272 Greenville Avenue, Dallas, TX 75231

Copyright © 2016 American Heart Association, Inc. All rights reserved.

Print ISSN: 1941-9651. Online ISSN: 1942-0080

The online version of this article, along with updated information and services, is located on the World Wide Web at:

<http://circimaging.ahajournals.org/content/9/7/e004376>

Data Supplement (unedited) at:

<http://circimaging.ahajournals.org/content/suppl/2016/07/13/CIRCIMAGING.115.004376.DC1.html>

Permissions: Requests for permissions to reproduce figures, tables, or portions of articles originally published in *Circulation: Cardiovascular Imaging* can be obtained via RightsLink, a service of the Copyright Clearance Center, not the Editorial Office. Once the online version of the published article for which permission is being requested is located, click Request Permissions in the middle column of the Web page under Services. Further information about this process is available in the [Permissions and Rights Question and Answer](#) document.

Reprints: Information about reprints can be found online at:

<http://www.lww.com/reprints>

Subscriptions: Information about subscribing to *Circulation: Cardiovascular Imaging* is online at:

<http://circimaging.ahajournals.org/subscriptions/>



LUND UNIVERSITY
Faculty of Medicine

Faculty of Medicine
Department of Clinical Physiology

Lund University, Faculty of Medicine
Doctoral Dissertation Series 2017:145
ISBN 978-91-7619-528-4
ISSN 1652-8220

